UC Berkeley
UC Berkeley Electronic Theses and Dissertations

Title
Progress in Xenon and Proton Relaxation Based Sensing

Permalink
https://escholarship.org/uc/item/0f13c7g6

Author
Gomes, Muller De Matos

Publication Date
2017

Peer reviewed|Thesis/dissertation

Progress in Xenon and Proton Relaxation Based Sensing

by

Muller De Matos Gomes

A dissertation submitted in partial satisfaction of the

requirements for the degree of

Doctor of Philosophy

in

Chemistry

in the

Graduate Division

of the

University of California, Berkeley

Committee in charge:

Professor Alexander Pines, Chair
Professor David E. Wemmer
Professor Jeffrey Reimer

Summer 2017

Progress in Xenon and Proton Relaxation Based Sensing

Abstract

Progress in Xenon and Proton Relaxation Based Sensing

by

Muller De Matos Gomes

Doctor of Philosophy in Chemistry

University of California, Berkeley

Professor Alexander Pines, Chair

In this dissertation, the sensitivity of xenon relaxation to changes in its environment is used to both develop new types of biosensors and also to develop new techniques that make use of xenon's intrinsic interactions with its environment. A proton based relaxation experiment is also discussed due to its similarity to relaxation experiments done with xenon biosensors.

Contrast agents are developed for xenon NMR. These agents consist of a cryptophane cage covalently attached to a DOTA chelating agent, allowing one to bring xenon close to chelated paramagnetic ions, enhancing the bulk relaxation of xenon. Both the T_1 and T_2 relaxivity of these contrast agents are tested. Adding paramagnetic metal ions seems to affect T_1 more than T_2 for most ions, possibly because the cage itself drastically affects the T_2 of xenon because of the slow exchange rate and large chemical shift difference. In general, metal ions known to have long electronic relaxation times relax xenon more efficiently than ions with shorter electronic relaxation times. Gadolinium (III) and manganese (II) have the greatest effect on the T_1 and T_2 of xenon, with gadolinium (III) affecting T_2 more and manganese (II) affecting T_1 more. Adding gadolinium (III) increases the T_1 relaxivity of M2 cages to 0.002 mM^{-1}s^{-1} from 0.0009 mM^{-1}s^{-1} and the T_2 relaxivity to 92.5 mM^{-1}s^{-1} from 26.1 mM^{-1}s^{-1} .

After testing the effect of these contrast agents, a relaxation based xenon biosensor is developed. This sensor consist of a cryptophane cage attached to a DOTA chelating agent and a biotin. The sensor works by binding to avidin, thereby increasing the rotational correlation time of the xenon inside the cage. This increases the relaxation rate of xenon inside the cage. Upon binding of a biotin-containing sensor to avidin at 1.5 µM concentration, the free xenon T_2 is reduced by a factor of 4. Changes in relaxation were more easily seen in T_2 due to the strength of the field used in this experiment. At high magnetic fields, T_1 hardly responds to changes in the rotational correlation time.

A proton based relaxation agent, developed by the IBS institute from the Republic of Korea, is discussed in this dissertation. This group developed a sensor consisting of two parts: a super

paramagnetic nanoparticle quencher and a paramagnetic metal ion enhancer. When the two are close together, the paramagnetic enhancer cannot efficiently relax water. Separating the two, done by either cleaving the bond keeping them together or by a conformational change in the linker binding them, prevents the super paramagnetic nanoparticle from quenching the enhancer, making water relaxation extremely rapid. Cleaving the bond between the quencher and enhancer increases the R_1 of water by 1.5 s^{-1}. This sensor was used to detect MMP2, an enzyme seen in certain tumors, both invitro and invivo. Concentrations as low as 15 ng per mL of MMP2 were detected invitro. This sensor is less sensitive invivo, with a lowest detected concentration of MMP2 being 450 ng per mL.

After studying many varieties of sensors developed to functionalize xenon, the direct interactions between xenon and its target were studied. Xenon interacts with many substances, including proteins, leading to rapid relaxation of the entire xenon ensemble. This is due to both nonspecific interactions with the protein surface relaxing xenon and also because many proteins have hydrophobic pockets xenon can occupy. This leads to rapid xenon relaxation, which can be perturbed by the protein binding to another ligand. Adding a ligand to a solution of protein, such as a small molecule drug, alters the relaxation of xenon in that solution. This effect was exploited in order to develop a method for measuring the binding affinity of certain drugs for albumin by monitoring their effect on the relaxation of xenon. Of the drugs studied, warfarin, tenoxicam, and sodium salicylate had the strongest effects due to their high affinity for albumin, with warfarin lowering the T_2 of xenon from 5 seconds to 2 seconds.

Para minha família,

TABLE OF CONTENTS

List of Figures

List of Tables

ACKNOWLEDGEMENTS

After five years of work, I find myself having a hard time knowing how to write this. I'll begin by thanking my advisor Alex Pines for the support he has provided. Thanks also to David Wemmer for his advice throughout the years, especially when writing papers. I am grateful to have had an opportunity to work with Alex and Dave.

There are several members of the Pines lab I would like to acknowledge. I would like to thank Phuong Dao for helping me get oriented in the lab and for teaching me how to work with xenon. Phuong also got me into the project I wrote my dissertation on, and for that I am grateful. During the difficult first years, we worked together almost every day. Chris also helped me a lot, teaching me about electronics and how to design experiments, as well as being a good friend. I would like to thank Clancy too for always being willing to give advice and review my work, including this dissertation. Jeong and Joel deserve thanks as well for synthesizing all of the biosensors I worked with over the years. Without their effors, most of the work in this dissertation would not have been possible. I'd also like to thank Ashley for all her hard work. Lastly, I'd like to thank the Pines lab as whole for helping prepare me for my qualifying exam and teaching me how to be a scientist.

During my final year in the Pines lab, I had the opportunity to work with several researchers from the IBS institute in the Republic of Korea. I would like to thank Soojin Kim, Tae-Hyun Shin, and Dongwon Yoo for telling me about their work and for allowing me to help. Doing the theoretical work on their project was a lot of fun and I'm glad to have had the opportunity to help them get their work published.

Outside of the university, I am thankful for the support of my family and friends. They have helped me during these years at Berkeley by always being willing to listen when things were difficult.

CHAPTER 1: INTRODUCTION

Xenon NMR has advanced rapidly in recent years. New biosensors have been synthesized. New pulse sequences have been developed and new molecules have been targeted. These advances have brought xenon NMR closer to becoming a routine analysis method. In this text, my contributions to this changing field are described. My dissertation begins by summarizing the theory necessary for understanding the experiments described here. The theory chapters are divided into one summarizing xenon and another summarizing relaxation.

There are many varieties of xenon NMR, too many to summarize in one chapter. So, the portions of the xenon literature necessary for putting my experiments into context are the focus of the second chapter. It begins by discussing how xenon is hyperpolarized with spin exchange optical pumping. My focus in that summary is the smaller details of a polarizer, with an explanation of why certain parameters are chosen during operation of the polarizer. It can be difficult to find such discussion in the literature. After finishing that summary, the useful properties of xenon are briefly mentioned. Xenon is not the only NMR probe one can use; it is not even the only noble gas NMR probe one can use, so choosing it over other atoms or molecules merits some discussion. After justifying choosing xenon, the actual NMR is discussed, including the experiments conducted and biosensors used with it. A few common pulse sequences used with xenon NMR are also discussed. The chapter ends with a summary of my work on relaxation based experiments.

With the introduction of relaxation in the end of the xenon chapter, it becomes necessary to discuss NMR relaxation. The theory of NMR relaxation can be subtle and most previous literature on xenon focuses on chemical shift and hyperpolarization, making the experiments discussed in later chapters difficult to understand. So, some of the vast literature on NMR relaxation is summarized in the second chapter, including a basic discussion of the dynamics responsible for it and how relaxation can be analyzed to learn about those dynamics. After that summary, the various methods for measuring relaxation rates are discussed. Choosing the correct method for measuring xenon relaxation times occupied a significant amount of my time during my dissertation, so I believe that it is important to discuss how to properly perform these measurements. After these two introductory chapters, my dissertation projects are discussed.

The body of my dissertation begins with an analysis of xenon contrast agents. These agents were the first relaxation based xenon biosensors, the foundation for the rest of my work. By attaching a cryptophane cage to a chelating agent, it became possible to bring paramagnetic metal ions very close to dissolved xenon. This, combined with the favorable dynamics of xenon inside cryptophane, drastically enhances relaxation. Trends in the relaxation of xenon in these sensors are summarized, with the implications for future projects in mind.

After discussing this preliminary xenon experiment, the main result of the dissertation is described. The fifth chapter discusses a biosensor that binds to avidin and its effect on the relaxation rate of xenon. By detecting avidin with relaxation, I hoped to show that xenon relaxometry can be used like xenon NMR, with the advantage being that relaxometry can be taken to lower fields. Unlike other xenon biosensors, the detection depends on the change in the dynamics of xenon once the sensor finds its target. There were several surprising results in this study and they are thoroughly discussed.

After summarizing this first result in xenon relaxometry, I briefly discuss a proton based biosensor. This project was pursued after a group from the IBS institute in South Korea visited the Pines lab in the fall of 2016. They were looking for someone to help them understand their results. Due to the resemblance between their work and my xenon experiments, I was able to help them with their work. Their biosensor, while differing drastically from the xenon biosensors in terms of structure, work on the same basic principle. Once the sensor finds its target, its effect on the relaxation of water changes. Like the xenon biosensors discussed in the previous chapter, these Distance dependent Magnetic Resonance Tuning (D-MRET) sensors work by changing the dynamics of the probe molecules when they encounter their targets. My contribution to this project was to determine which dynamics changed so that the experiment could by published with a sound theoretical basis. The fitting procedure for this is shown in this chapter.

After working on sensors that affect the relaxation of both xenon and water, I decided to try a different approach to relaxometry. This approach, inspired by my experience with the cryptophane based biosensors, the literature on the relaxometry of food and early work on xenon NMR before cryptophane, focuses on the direct interactions between xenon and the target, rather than the interactions mediated by the sensor. Xenon will interact with proteins without a sensor, but usually not strongly enough to yield a unique NMR peak. However, this interaction affects relaxation. Knowing this, a new method for probing ligand protein interactions with xenon relaxometry is summarized. In this final chapter, I offer an early explanation for the effect of proteins on xenon relaxation, and how this effect is perturbed by proteins binding to ligands. An early application for this method, finding the binding affinity of drugs for serum albumin, is also presented in the final chapter. It ends by proposing a series of experiments that would provide a better understanding of the interactions between xenon and proteins.

With the end of the seventh chapter, the body of my dissertation comes to an end. Xenon NMR has changed over the years, with useful advances being made every year. My contribution to this work focuses on developing new methods to be used with hyperpolarized xenon, methods that allow for analyses that could not be done before. My approach differed by focusing on collecting relaxation times instead of collecting spectra. While this approach has its limitations, I believe that the new possibilities of this method make it a worthwhile subject for study.

CHAPTER 2: XENON BACKGROUND

Xenon-129 is a spin one half nucleus that can be hyperpolarized using spin exchange optical pumping[1]. Once polarized, it can be introduced into a wide variety of samples, where it will bind to any pore large enough to fit it or dissolve in a wide variety of solvents[2,3] These two properties of xenon, its solubility and affinity for cavities, allow it to be used in a variety of sensing experiments. These experiments exploit xenon's sensitivity to its environment, with small changes affecting its chemical shift and relaxation rate. The rapid exchange of this gas between different sites in its environment also allow for many unique and useful experiments that exploit these changes in chemical shift and relaxation.

2.1 Optical Pumping of Rubidium

While the nuclear spin states of a sample of xenon-129 will gradually align with an external magnetic field, this alignment will always be weak at the magnetic fields currently available. The difference between the states aligned with the field versus those aligned against will never be more than a few atoms per million. However, it is possible to go beyond this thermal polarization. It is possible to hyperpolarize the nuclear spin states of xenon-129 with spin exchange optical pumping.

This discussion of xenon NMR will begin with a summary of spin exchange optical pumping. In order to polarize xenon, it is first necessary to polarize rubidium. Rubidium metal is placed inside a glass cell and then heated, producing rubidium vapor. This vapor is optically pumped with a laser to polarize the valence electron of rubidium.

Rubidium can be optically pumped by exciting its single valence electron with a circularly polarized laser[4]. This valence electron has a spin 1/2 because it is unpaired. If the rubidium cell is placed in a magnetic field, the valence atomic orbitals will split because of the spin of the rubidium's outermost unpaired electron. This unpaired electron can be excited from its ground state, an S orbital, to an excited state, a P orbital. The P orbitals are split into two sets of states: one set with a total angular momentum of 1/2 and the other with a total angular momentum of 3/2. The wavelength of the transition between S 1/2 and P 1/2, known as the D1 transition, is 795 nanometers. This transition is generally used for hyper polarizing xenon because it is the most efficient for hyper polarizing rubidium.

By exciting the rubidium valence electron with a circularly polarized laser tuned to the D1 transition, one polarizes the electronic spin states of the rubidium vapor. Circularly polarized light has angular momentum, which it transfers to the rubidium electron upon excitation. The fact that the light used for excitation has angular momentum creates some new restrictions on absorption since the rubidium valence electron must absorb the angular momentum too. Since the photon will have an angular momentum of 1, this means that the excited state that the electron goes to must be one unit of angular momentum higher than its ground state. In the case of rubidium atoms, there are two spin states in the ground state and excited state, each with a difference in angular momentum equal to one. This means that an electron in the S -1/2

state can only be excited to the P +1/2 state by a circularly polarized photon, assuming that it has an angular momentum of +1. If the photon has an angular momentum of -1, it cannot excite the S -1/2 electron. The P orbital excited state would need to have an angular momentum of -3/2 in order to accept the electron. While there are such P orbitals, accessing them requires that the laser be tuned to a lower wavelength than 795 nanometers.

There is therefore another requirement added to for an electron to be excited by a photon. The photon must be resonant and also in the correct spin state. This means that only portion of the ground state electrons can be excited by the laser. Once there, its spin states can change due to collisions with other gases in the cell. This can bring some of the electrons from one spin state to another. One consequence of this is that the populations of the excited states quickly become the same. After a while, the excited electrons will relax back down to the ground state with the same spin angular momentum. But, some of the excited electrons will relax to a ground state that cannot be excited by the laser. Over time the electrons in this state will relax to the other state, but this process is slow compared to the relaxation of the excited state electrons and the excitation by the laser. By selectively exciting one ground state, that state can be gradually depopulated, until all the rubidium electrons are in the one ground spin state. This process is summarized in figure 2.1.
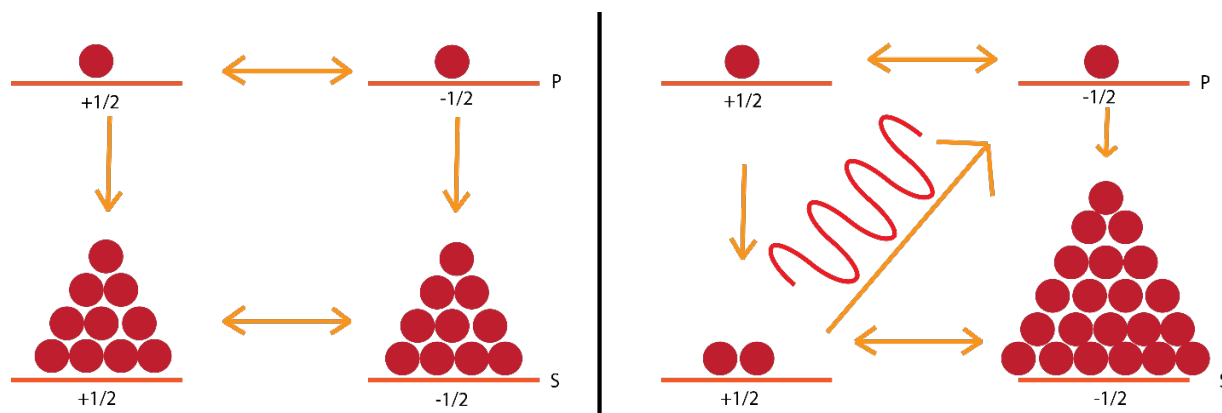
Figure 2.1: *Schematic of optical pumping. This figure shows the various relaxation pathways of the rubidium electron and how the introduction of circularly polarized light affects the population of each energy level. The valence electrons are excited with a circularly polarized laser. Once excited, the electrons populate both excited states due to collisions between the rubidium and the gases around it. The circularly polarized laser excites only one of the S ground states. By exciting only one of the S states, the other state becomes depopulated. This results in a hyperpolarized ensemble of electron spins.*

There are some details to spin exchange optical pumping that need to be discussed. As mentioned before, the rubidium cell must be filled with inert gases like helium and nitrogen for this experiment to work. These inert gases, referred to in the rubidium polarization literature as buffer gases, perform several functions. They improve the rubidium's absorption of the circularly polarized laser; they prevent the rubidium from relaxing to thermal equilibrium and they protect the rubidium from gases that react with the alkali metal[5]. Without these gases, it becomes extremely difficult to hyperpolarize rubidium.

Rubidium must absorb the laser light to become hyperpolarized. While it is trivial to make the center frequency of the laser resonant to the D1 transition frequency, doing so leaves most of the laser light unabsorbed. No laser source is truly monochromatic; the laser's output is distributed about its center frequency. In the case of rubidium, this distribution is much broader than the width of frequencies that can induce a D1 transition. This means that much of the laser light is wasted, a shame because the rate of rubidium polarization depends on the amount of light absorbed. If too little light is absorbed by the alkali metal, then the relaxation rate of the rubidium electron might be greater than the rate of polarization, resulting in a thermally polarized rubidium cell. This problem can be easily circumvented by introducing inert gases into the rubidium cell. The higher the pressure inside the rubidium cell, the broader the rubidium absorption cross section. By broadening the cross section, more laser light can be absorbed, resulting in a higher rubidium polarization rate.

Unfortunately, the polarization rate is not the only rate to consider when trying to polarize rubidium. It is also necessary to minimize the rate of rubidium relaxation. Once an ensemble of rubidium is polarized, it will immediately begin to relax. The balance between the rate of this relaxation and the rate of polarization determines what polarization the rubidium cell will ultimately reach. By choosing the right buffer gases and using a strong laser, it is possible to bring the polarization of rubidium very close to one hundred percent. The two gases mentioned before, helium and nitrogen, are the most commonly used buffer gases. The polarizer used in the experiments described in this dissertation uses a gas mixture that is 88 percent helium and 10 percent nitrogen, with the rest of the gas mixture being xenon. The two gases that make up the majority of the mixture decrease the relaxation rate of the rubidium electron spin. They do so in two ways. The first and most obvious is that they prevent the rubidium from colliding with the wall, which can depolarize the rubidium valence electrons. The presence of these gases in the cell, at concentrations much higher than that of the rubidium vapor, prevents the rubidium from diffusing very far before colliding with a buffer gas. This makes collision with glass wall of the cell much less likely. It is necessary to limit the contact between the rubidium and the walls of its cell as much as possible because collisions between the cell and rubidium frequently result in the rubidium being depolarized.

Any inert gas will prevent the rubidium from interacting the cell walls, but not all gases will do so without depolarizing the rubidium themselves. The interaction between a buffer gas and a rubidium atom can be depolarizing too. Each gas has rubidium spin destruction cross section, a value that determines its tendency to depolarize rubidium. This spin destruction cross section varies from gas to gas. For example, the spin destruction cross section of helium is about five orders of magnitude smaller than that of xenon. The extremely small spin destruction cross section of helium is why it is often used as a buffer gas in rubidium polarizers.

Nitrogen also has a small spin destruction cross section, but that is not why it is included in the gas mixture. After the rubidium is excited by the laser, it will inevitably relax back down to its ground state. When it relaxes, it can release a photon, a photon with a random polarization. This randomly polarized photon can then excite another rubidium atom in the ensemble, resulting in electron spins being excited randomly to the +1/2 states. These atoms, with electronic spins aligned in random directions, will then also release randomly polarized

photons, depolarizing even more rubidium. In order to stop the release of randomly polarized photons by excited rubidium, it is necessary to introduce a gas with vibrational energy levels into the gas mixture, like nitrogen. Doing so decreases this type of relaxation. When the rubidium collides with a gas with these energy levels, it can relax back to its ground state without emitting a photon. With a small fraction of nitrogen present, the emission of photons by excited rubidium can be quenched.

Besides increasing the absorption cross section and decreasing the relaxation rate, the buffer gases also contribute to the polarization of rubidium by helping keep the atmospheric gases out. Atomic rubidium is a very reactive metal, second only to cesium among the alkali metals in its sensitivity to water and oxygen. Any contact between rubidium and oxygen or water will result in the rubidium losing its valence electron. Without the electron, the rubidium cannot be polarized. Furthermore, the rubidium oxide created by this reaction can coat the interior of the cell, preventing laser light from getting in. As oxygen enters the cell, more of the cell becomes coated with rubidium oxide, resulting in worse polarization over time. If water gets inside the cell, the reaction is violent enough to immediately coat the cell in a black residue. There are many ways to keep these gases away from rubidium. The connections between the cell and the tubing needed for the operation of the polarizer can be made resistant to leaks, but no setup can be made truly leak proof. By making the pressure of the buffer gas inside the cell greater than atmospheric pressure, the polarizer can at least be made to leak out instead of in. This decreases the amount of oxygen and water that enters the cell. By carefully choosing the buffer gases used and by operating at a high pressure, about 70 psi, one can keep a polarizer running for about 6 months before needing to replace the rubidium in the cell.

2.2 Xenon Hyperpolarization

With the rubidium vapor polarized, it becomes possible to hyperpolarize other gases, such as xenon. Xenon can be introduced into the cell containing the rubidium vapor, where it will then collide with the metal vapor. During the collision, the xenon nucleus and the rubidium valence electron are coupled. A cartoon of this collision is shown in figure 2.2. This coupling, called the Fermi contact interaction, allows the rubidium electron to transfer its angular momentum to the xenon nucleus. The depolarized rubidium is then repolarized by the circularly polarized laser light.
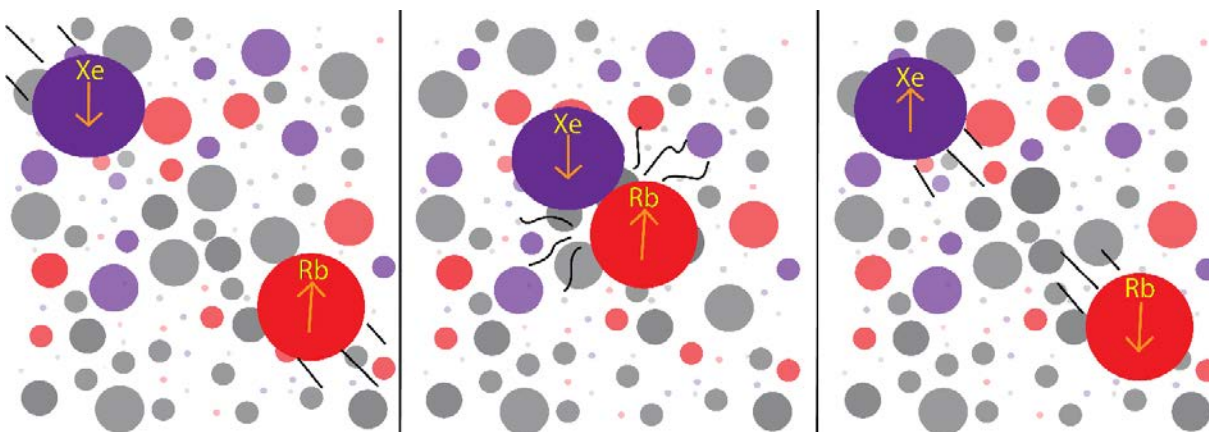
Figure 2.2: *Inside the rubidium cells used by this lab, there are four gases: xenon, rubidium and two buffer gases. This gas mixture is irradiated by a circularly polarized laser, polarizing the rubidium electrons. This rubidium collides with xenon in the cell. During this collision, the xenon nucleus and the rubidium valence electron exchange spin angular momentum. The rubidium that exchanged its angular momentum is then repolarized by the laser. It is also possible for the xenon and rubidium to form relatively long lived associations due to van der Waal interactions. These interactions bring the xenon and rubidium together for nanoseconds at a time, much more time than the picoseconds spent together during a collision. Unfortunately, these van der Waal molecules require that the rubidium cell be kept at very low pressures to form at significant concentrations, pressures that are not practical for most xenon NMR experiments.*

If the rate of xenon polarization is greater than the rate of xenon relaxation, then it will gradually build up polarization. This polarization will be many times greater than the thermal polarization from the energy splitting of the xenon nuclear spin states in a magnetic field. The polarization from the Zeeman splitting, the splitting induced by an external magnetic field, will be in the parts per million, while the polarization induced by spin exchange optical pumping can be well over ten percent[6]. This greatly increases the available xenon signal. Once hyperpolarized, xenon can be made to flow from the rubidium cell into a sample and then measured using a conventional NMR spectrometer.

While it may be tempting to introduce as much xenon into the cell as possible, it is necessary to keep the xenon fraction low when operating the polarizer. It is obvious that the magnitude of the xenon signal in an NMR experiment depends on the amount of xenon present. This means that the fraction of xenon in the gas mixture introduced into the cell should be as high as possible. Unfortunately, xenon also has a very high rubidium spin destruction cross section. What this means is that xenon will rapidly relax any rubidium it comes into contact with. When xenon and rubidium collide, spin exchange is not the only possible outcome. This spin destruction decreases the polarization of rubidium and therefore the polarization of the xenon. There is a tradeoff in the concentration of xenon and the polarization of xenon. Depending on the experiment, it may be better to opt for more polarization or more xenon. It is also possible to circumvent this tradeoff entirely by separating the xenon from the other gases after polarization. This can be done by simply condensing the xenon with a liquid nitrogen trap. The

pure xenon mixture can then brought to whatever pressure is needed, while keeping the pressure inside the cell low enough to get good polarization. In this case, the only limit is the relaxation time of the xenon one has decided to store. This relaxation time can be made very long by either freezing the xenon or by placing it in a gas storage bag in a homogenous field.

2.3 Properties of Xenon

Xenon has many properties besides being hyperpolarizable that make it a good choice for sensing experiments. It is soluble in a wide variety of solvents and it is sensitive to changes in these solvents[7,8]. Each solvent alters the xenon NMR signal in many ways. In fact, xenon is generally responsive to its environment, making it a good probe. Xenon will also enter many small cavities. While in a cavity, xenon will sometimes yield a unique signal tied to that cavity, making it useful for probing porous structures[3,9,10]. Xenon is also much more common than helium 3, the other noble spin 1/2 gas that can be hyperpolarized[11]. All of these properties make xenon an attractive probe atom for NMR.

Due to its extremely polarizable electron cloud, xenon gas will dissolve in a wide variety of solvents. While xenon is a noble gas, and therefore mostly inert, it is still soluble in many solvents, even polar ones like water[12,13]. This is because its valence electrons are far from the atom's nucleus, making them loosely held. Being loosely held, it is easy to change the distribution of the outermost electrons. These transient polarizations of the electron cloud around the nucleus allow xenon to dissolve in many solvents, with water being the most important one. While xenon is orders of magnitude more soluble in oily solvents like cyclohexane, it still dissolves in water easily enough to yield a large dissolved xenon signal. This allows one to use hyperpolarized xenon in biological experiments, which must be done in water.

Xenon gas will also enter many cavities, allowing one to use it to probe porous materials and proteins. Because of this property, xenon has been used to characterize metal organic frameworks and other porous samples[3,9]. While inside a metal organic framework, xenon gas will bind to a specific site and exchange slowly enough to yield a resonance separate from the free xenon gas peak. Many other substances will also yield separate peaks for the xenon binding site. In the case where xenon exchanges out of the binding pocket too quickly or the resonance inside to pocket is too close to the resonance outside, it is still possible to confirm that xenon is bound. Proteins are a good example of this. Some proteins have binding pockets that can accommodate xenon. But, xenon will usually exchange out of these pockets too quickly to yield a separate bound xenon peak. Instead, the binding will change the offset of the bulk xenon. This fast exchange will also alter the relaxation rate of the entire xenon population.

Xenon is not the only gas that can be hyperpolarized using the spin exchange optical pumping procedure mentioned above. Helium-3 can be polarized in this way. Like xenon 129, helium 3 is a spin one half nucleus. Its gyromagnetic ratio is three times that of xenon 129, making it seem like an attractive choice for NMR. However, helium-3 is an extremely rare isotope. Its natural abundance is 0.000137%, orders of magnitude less than xenon 129's abundance. Because of its rarity, collecting helium 3 from natural helium stocks is impractical. There are other problems

with this isotope. It is much less soluble in water than xenon, making it difficult to use in biological experiments. This lack of solubility also eliminates the advantages of having a higher gyromagnetic ratio. It is pointless to have three times more signal because of a high gyromagnetic ratio if helium is 10 times less soluble in water than xenon[14]. While hyperpolarized helium 3 has many uses in ultrasensitive physics experiments, it is not as useful as xenon for biosensing and material characterization.

Once the xenon has been hyperpolarized, it can be used in many simple NMR experiments. The gas can be bubbled into liquid samples or simply mixed with a porous solid. The simplest experiment one can do on such samples is collect a one dimensional spectrum. This alone can be very useful because the chemical shift range of xenon is extremely wide. The xenon atom alone has a 200 ppm chemical shift range. The range extends to 7500 ppm when xenon molecules are considered[15]. Unfortunately, there are few xenon molecules and the conditions needed to produce them are exotic. This limits the chemical shift range in most experiments to about 200 ppm.

2.4 Functionalized Xenon
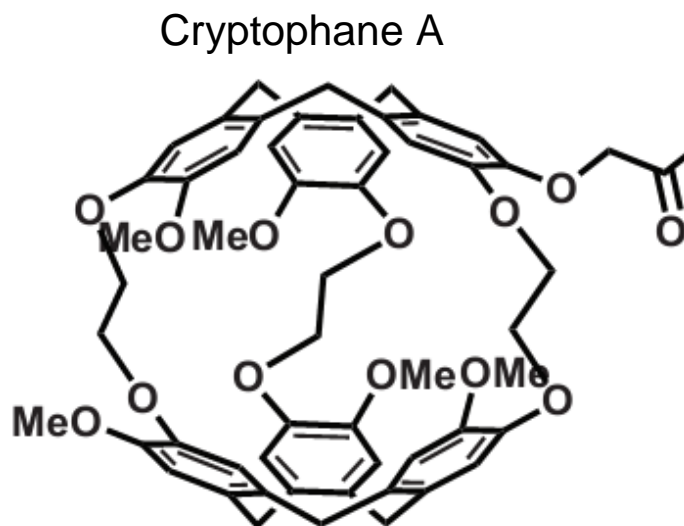
Cryptophane A

Figure 2.3: *This is the structure of cryptophane A. One of the methoxy groups on the end has been modified to include a ketone. This allows this molecule to be modified in a variety of ways. There are many varieties of cryptophane besides cryptophane A. They differ in the volume available and in the chemical structure of the groups pointing out. All biosensor experiments performed in this dissertation used sensors derived from cryptophane A.*

Many experiments are possible within the chemical shift range of atomic xenon. The most important of all of them are experiments using molecules designed to trap xenon atoms. Once inside the molecule, the chemical shift of the encapsulated xenon atom will differ from the shift outside it. For example, the chemical shift of xenon gas is 0 ppm but the chemical shift of xenon

gas inside certain metal organic frameworks can vary from 300 to 0 ppm, depending on the structure of the MOF[3]. Something similar can also be done with liquid samples. When dissolved in water, xenon has a chemical shift of about 200 ppm. If the dissolved xenon is captured by a cryptophane A molecule, structure shown in figure 2.3, modified to dissolve in water, its chemical shift changes to about 60 ppm[2]. A simulated xenon spectrum of a solution containing cryptophane A is shown in figure 2.4. It is clear that the chemical shift of xenon is highly dependent on its chemical environment. The focus of xenon research has been on how to best use these cages to develop new varieties of sensors.
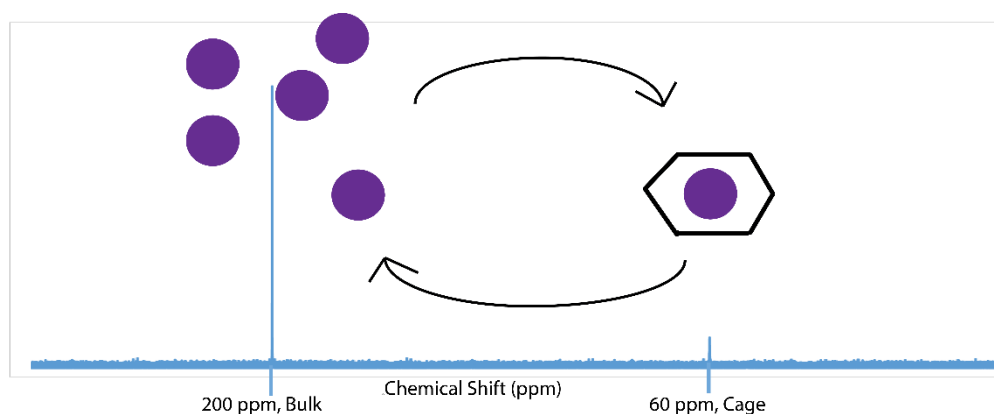
Figure 2.4: *A simulated 1D xenon spectrum. The xenon water resonance is about 200 ppm and the xenon inside cryptophane is about 60 ppm. The exact shift depends on the type of cryptophane used. There is usually much more xenon outside the cage than inside, which is why the xenon solvent peak is much larger than the cage peak. It is possible to indirectly detect the xenon inside the cage by pulsing on the encapsulated xenon and then letting it exchange with the bulk population.*

When dealing with spins exchanging from two sites with different chemical shifts, it is important to consider how the exchange affects the lines observed. Depending on the rate of exchange, the two resonances might both be sharp and easily noticed, broadened but present or coalesced into a single resonance. The equation below shows the cross over point, the point at which the two resonances merge. As the exchange rate slows down, the two peaks become more distinguishable. They also begin to get narrower. Likewise, as the exchange rate goes beyond the cross over point, the coalesced peak becomes narrower. The same phenomena will be observed if the exchange rate is kept constant and the frequency difference is changed instead by altering the magnitude of the external magnetic field. This can make it difficult to distinguish exchanging resonances at lower fields[16].

$$k_{ex} = \frac{\Delta \omega}{2\pi}$$

$$k_{ex} \text{ is the exchange rate in } \frac{1}{s}$$

$$\Delta \omega \text{ is the difference in chemical shift in radians per second}$$

Once captured, a xenon atom will respond to changes in the molecule holding it. This response is most easily seen in the chemical shift of the encapsulated xenon. This response can be functionalized by adding a targeting moiety to the cage molecule. For example, cryptophane can be modified by attaching to it a peptide chain modified to bind to specific proteins. An example of functionalized cryptophane is shown in figure 2.5. If the protein that binds to the peptide chain is introduced into the sample, it will bind to the peptide and therefore also to the cryptophane cage. This binding affects the chemical shift of the encapsulated xenon. Unfortunately, the change in chemical shift upon binding tends to be small. For example, the xenon inside a sensor comprised of cryptophane A, a peptide chain and biotin only changes its chemical shift by about 1 ppm when the biotin of the sensor binds to avidin[17]. This change can be made much larger if the distance between the cage and the biotin is made shorter. This allows the cage to get much closer to the avidin, resulting in larger changes to its structure and therefore also the chemical shift of the xenon inside. Unfortunately, getting closer to the protein also broadens the xenon cage resonance, resulting in both a more difficult detection of the cage peak and also a more difficult detection of the change in the frequency of the cage peak[18].
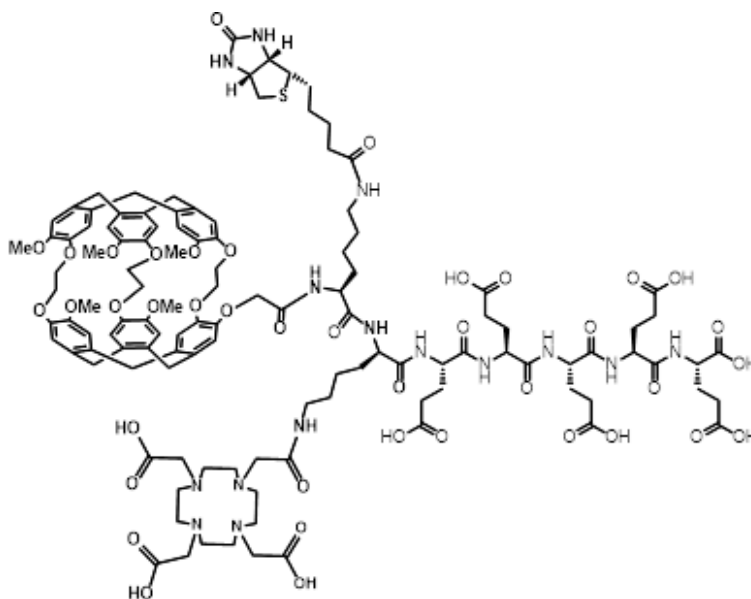
Figure 2.5: *An example of a xenon biosensor based on cryptophane A. A cryptophane A containing a single modifiable group is attached to a peptide chain. This peptide chain is further modified with a biotin and a DOTA chelating agent. The biotin allows this molecule to bind to avidin and the DOTA allows this molecule to bind to metal ions. Many xenon biosensors resemble this one. They contain a cage molecule to trap the xenon, a peptide chain to solubilize the cage and a molecule that allows the sensor to bind to its target.*

By monitoring changes in the chemical shift of the encapsulated xenon, one can detect the presence of molecules in solution by designing a cage molecule that binds to them. This allows one to use hyperpolarized xenon to detect the presence of certain solutes in solution. While xenon NMR can be used to detect changes in the bulk solution, it cannot be used to detect the

presence of dilute solutes without using these cage molecules. These cage molecules act as sensors of the solutes that bind to them.

2.5 Experiments with Functionalized Xenon

While it is possible to detect the encapsulated xenon directly by simply taking a one dimensional NMR spectrum, it can be difficult to do so in practice. The concentration of the solute one wants to detect can be low which means that the concentration of the sensor will need to be low as well. Otherwise, most of the sensor will not be bound to the solute. In that case, the resonance belonging to the xenon inside the unbound sensor can easily overwhelm the resonance belonging to the bound sensor.

If the concentration of the sensor is low, the signal to noise ratio of the xenon inside the sensor is low. This can make direct detection of the encapsulated xenon difficult. Several methods have been developed to overcome this limitation. These methods require that one understands that the xenon trapped inside the sensor does not remain there forever. The population of xenon trapped inside the sensor is always exchanging with the population of xenon outside the sensor. This exchange can be used to detect the trapped xenon indirectly.

Trapped xenon can be detected indirectly in two ways: through saturation and through repopulation. Both of these methods rely on there being much more xenon outside the sensor than inside. If this condition is not met, then neither of these methods will work.

It is possible to detect the presence of trapped xenon by selectively saturating the resonance associated with that population. This saturation quickly relaxes the fraction of the xenon population inside the sensors, while leaving the free xenon polarized. This depolarized, trapped population will then exchange with the polarized, free population, decreasing the intensity of the free xenon resonance. The polarized xenon that replaces the depolarized xenon inside the sensor can then be saturated as well. This cycle can be repeated many times, decreasing the intensity of the free xenon resonance with each saturation. This will only work if the sensor is present; otherwise, there will be no xenon at the frequency offset associated with the sensor and therefore no xenon will be relaxed by the saturation pulse. This allows for indirect detection of trapped xenon by monitoring the decay of the free xenon peak as a function of the frequency offset of the saturation pulse. This experiment is shown in figure 2.6.

This procedure, called HyperCEST (Chemical Exchange Saturation Transfer), yields a plot called a Z spectrum[19]. A Z spectrum is a plot showing the change in free xenon intensity as a function of saturation pulse offset. If the saturation pulse at a certain frequency affects the overall polarization of xenon, then the Z spectrum will have a dip at that frequency. This plot is used instead of an ordinary one dimensional NMR spectrum but it contains the same information. More information on the details of HyperCEST can be found in the literature.
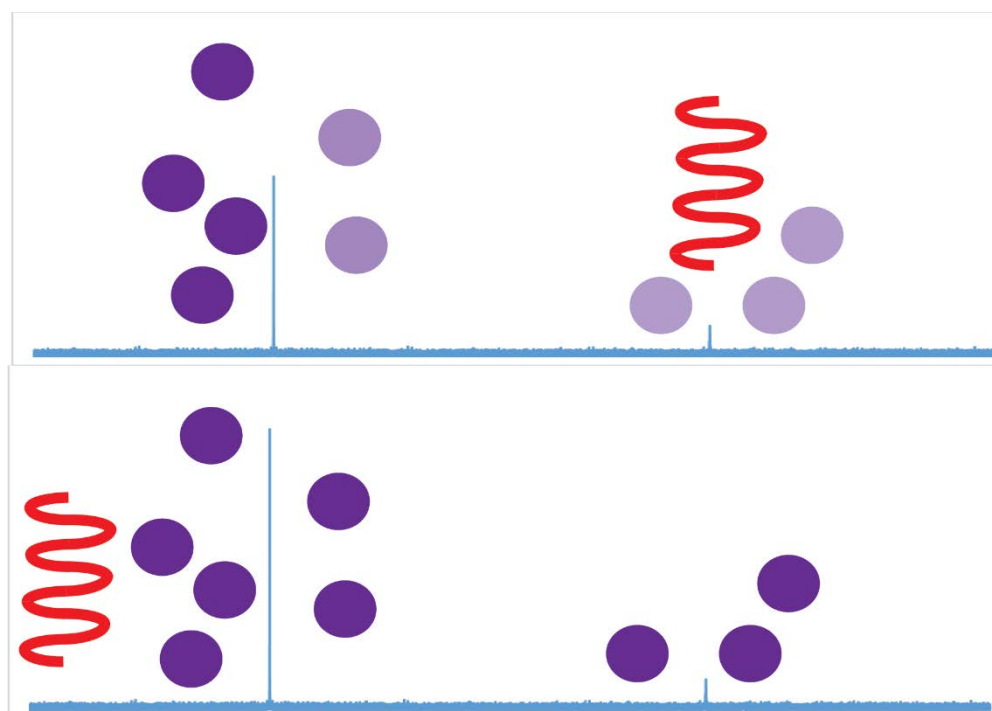
Figure 2.6: *The small cage peak can be detected indirectly by selectively saturating it and then monitoring the solvent peak. If no xenon is present at a particular frequency, then the xenon dissolved in water will decay at its normal rate. This process is shown in this cartoon. The two parts of this figure show what happens to the solvent peak when the saturation pulse is swept. When the pulse is on resonance with the cage, shown in the top part, the cage xenon is depolarized and the solvent xenon is partially depolarized due to exchange. When the pulse is not resonant, as shown in the bottom part of the figure, then no xenon is saturated.*

Collecting a Z-spectrum can be time consuming because a full one dimensional spectrum of xenon must be collected for every frequency used for saturation. If the frequency offset of the trapped xenon is already known, then this is not a problem. Only one point along the Z spectrum needs to be collected because the chemical shift of the xenon in the sensor is already known. A control point can then be collected by saturating at a frequency where no xenon is present. However, if the full xenon spectrum is needed because the sensor chemical shift is unknown or more than one sensor is present, then the experiment can take a long time. It is possible to avoid these long experiment with clever pulse sequences based on the methods developed by Lucio Frydman for quickly collecting two dimensional NMR spectra.

The method for quickly collecting Z-spectra uses the same principle as Frydman's ultrafast two dimensional pulse sequences[20]. The second dimension is encoded in real space using a magnetic field gradient. An ultrafast Z spectrum is collected with the following pulse sequence[21]. The pulses uses are the same as those used in a conventional HyperCEST experiment. After introducing xenon into the solution, the sample is saturated for a few seconds. The remaining magnetization is then excited and its spectrum then collected. To make

this pulse sequence ultrafast, a magnetic field gradient is applied during the saturation and then during the FID acquisition. By applying a gradient during the saturation pulse, the frequency of the pulse is swept by changing the resonance frequency of the cage peak.

If the saturation pulse is kept between the cage and solvent resonances, then the gradient will move the peak into the saturation pulse offset. For example, in a sample containing water and cryptophane A, the two resonances will be 200 ppm for xenon inside water and 60 ppm for xenon inside cryptophane. If the saturation pulse is set to 120 ppm, then none of the xenon will be saturated. If a gradient is turned on during the saturation pulse, then no xenon will be saturated in the center of the sample. At the edges of the sample, the frequency offset of the cage and solvent will have changed but the frequency of the saturation pulse will have remained the same. The gradient moves the resonance of the cage or solvent to the frequency of the saturation pulse. The pulse then creates regions in the sample containing depolarized xenon. These regions of depolarized xenon can then be imaged by applying a gradient during the acquisition period. The physical position of these dark regions corresponds to the NMR spectrum of the sample.

There are some limitations to this ultrafast experiment. The first is that the xenon signal is distributed along a wide frequency range by the imaging gradients. Without the gradients, it is common for the xenon solvent resonance to be around 2 Hertz wide in the middle. The signal of the solvent resonance is broadened by several hundred Hertz by the gradient in these ultrafast experiments. Therefore, this experiment requires a high signal to noise ratio because it reduces the SNR of the solvent line. If the sample size is small or the polarization of the xenon is low, then it will be necessary to signal average in order to get an ultrafast Z-spectrum.

There are other ways to rapidly collect xenon spectra while also compensating for the low sensitivity of the cage. Instead of saturating the cage peak and then acquiring a one dimensional spectrum, one can acquire multiple FIDS per sample[22]. This pulse sequence works by bubbling xenon into a sample and then selectively exciting the cage peak. An FID is then immediately collected and is then followed by a short delay of a few milliseconds. This delay allows the xenon not excited by the pulse to replace the encapsulated xenon. The sample is then excited again, without bubbling in new xenon. This cycle is repeated multiple times, acquiring multiple FIDS per bubbling, allowing one to rapidly signal average by avoiding the slowest part of a xenon experiment, the bubbling. The pulsing portion is usually done in a second or two, but the bubbling portion can last thirty seconds. If multiple FIDS can be collected per bubbling, then the acquisition of xenon spectra can be greatly accelerated. The amount of FIDS one can collect per bubbling will depend on the concentration of cage used and the relaxation rate of xenon in the sample.

This pulse sequence has some limitations. The most serious one is that some knowledge of the cage peak is required before the experiment can proceed. The selective pulse can be made wide enough to cover most possible cage molecules, but the wider the pulse, the more dissolved xenon is accidentally excited. This means that there is less polarized xenon available to replace the xenon in the cage, meaning that less transients can be collected per bubbling. This can slow down the experiment. Therefore, it is best to keep the selective pulse as narrow

as possible. Another problem is that the dissolved xenon is relaxing during the pulse sequence. This limits the amount of FIDs one can collect per bubbling. Depending on the acquisition time and the time between pulses, there might not be much polarized xenon at the end of the experiment. Lastly, some xenon experiments require that the solvent peak be present as a reference. If this experiment is done correctly, there should not be a solvent peak in the final spectrum. It is possible to regain the solvent peak by designing the selective pulse to excite a tiny amount of solvent xenon. This allows a little bit of solvent xenon signal to accumulate, introducing a small solvent peak to use as a reference. This workaround unfortunately has the same problems as a too broad selective pulse. The little bit of solvent xenon used as a reference cannot be used to replace the xenon in the cage. This reduces to the signal to noise ratio of the xenon cage resonance.

It can be difficult to observe the resonance of the encapsulated xenon either directly or indirectly. This is especially true at lower magnetic fields where the frequency difference between free and bound xenon is smaller. This limits xenon NMR because a strong, super conducting magnet is needed to keep the frequency difference between the free and bound xenon large. If lower fields are desired, then something besides chemical shift needs to be measured. Monitoring changes in the bulk relaxation rate of xenon can be an alternative to chemical shift based xenon NMR. While frequency differences decrease as the field decreases, relaxation rate differences remain the same or even increase, depending on the dynamics of the free and bound xenon.

The cages used to change the chemical shift of xenon also affect the relaxation dynamics of the entire xenon population. Once inside a cryptophane cage, the relaxation dynamics of the bound xenon change dramatically. The change is great enough to affect the relaxation dynamics of the free xenon too. The relaxation of xenon inside cage molecules can also be changed by altering the cage. If the cage binds to a large molecule or paramagnetic ion, then the relaxation rate of the bound xenon will increase. This increase in relaxation will affect the relaxation rate of all the xenon in the sample because of the rapid exchange between the bound and free xenon[23]. These changes in the relaxation rate of bulk xenon can be used for biosensing.

2.6 Bibliography

1.   Goodson, B. M. Nuclear magnetic resonance of laser-polarized noble gases in molecules, materials, and organisms. *J. Magn. Reson.* **155,** 157–216 (2002).

2.   Huber, G. *et al.* Water soluble cryptophanes showing unprecedented affinity for xenon: candidates as NMR-based biosensors. *J. Am. Chem. Soc.* **128,** 6239–46 (2006).

3.   Ooms, K. J. & Wasylishen, R. E. 129Xe NMR study of xenon in iso-reticular metal-organic frameworks. *Microporous Mesoporous Mater.* **103,** 341–351 (2007).

4.   Happer, William. Optical Pumping. *Rev. Mod. Phys.* **44,** 169–250 (1972).

5.   Seltzer, S. J. Developments in Alkali-Metal Atomic Magnetometry. (2008).

6.   Nikolaou, P. *et al.* Near-unity nuclear polarization with an open-source 129Xe

hyperpolarizer for NMR and MRI. *Proc. Natl. Acad. Sci. U. S. A.* **110,** 14150–5 (2013).

7.   Morgado, P., Bonifácio, R., Martins, L. F. G. & Filipe, E. J. M. Probing the structure of liquids with 129Xe NMR spectroscopy: N -Alkanes, cycloalkanes, and branched alkanes. *J. Phys. Chem. B* **117,** 9014–9024 (2013).

8.   Miller, K. W. *et al.* Xenon NMR: Chemical shifts of a general anesthetic in common solvents, proteins, and membranes. *Biophysics (Oxf).* **78,** 4946–4949 (1981).

9.   Fraissard, J. & Ito, T. 129Xe n.m.r. study of adsorbed xenon: A new method for studying zeolites and metal-zeolites. *Zeolites* **8,** 350–361 (1988).

10.   Kunth, M., Witte, C., Hennig, A. & Schröder, L. Identification, classification, and signal amplification capabilities of high-turnover gas binding hosts in ultra-sensitive NMR. *Chem. Sci.* (2015). doi:10.1039/C5SC01400J

11.   Aldrich, L. T. & Nier, A. O. The occurrence of 3He in natural sources of helium. *Phys. Rev.* **74,** 1590–1594 (1948).

12.   Pollack, G. L. & Himm, J. F. Solubility of Xenon in Liquid N-Alkanes - Temperature-Dependence and Thermodynamic Functions. *J. Chem. Phys.* **77,** 3221–3229 (1982).

13.   Ladefoged, J. & Andersen, a M. Solubility of Xenon-133 at 37C in Water, Saline, Olive Oil, Liquid Paraffin, Solutions of Albumin, and Blood. *Phys. Med. Biol.* **12,** 353–358 (2002).

14.   Weiss, R. F. Solubility of helium and neon in water and seawater. *J. Chem. Eng. Data* **16,** 235–241 (1971).

15.   Bagno, A. & Saielli, G. DFT Study of the NMR Properties of Xenon in Covalent Compounds and van der Waals Complexes – Implications for the Use of 129 Xe as a Molecular. 1486–1495 (2003).

16.   Levitt, M. H. & Wiley, J. *Spin Dynamics Second edition*.

17.   Spence, M. M. *et al.* Development of a functionalized xenon biosensor. *J. Am. Chem. Soc.* **126,** 15287–94 (2004).

18.   Lowery, T. J. *et al.* Optimization of xenon biosensors for detection of protein interactions. *Chembiochem* **7,** 65–73 (2006).

19.   Schröder, L. *et al.* Xenon biosensors for multi-purpose molecular imaging. in *IFMBE Proceedings* **25,** 176–179 (2009).

20.   Frydman, L., Scherf, T. & Lupulescu, A. The acquisition of multidimensional NMR spectra within a single scan. *Proc. Natl. Acad. Sci.* **99,** 15858–15862 (2002).

21.   Boutin, C., Léonce, E., Brotin, T., Jerschow, A. & Berthault, P. Ultrafast Z-spectroscopy for 129Xe NMR-based sensors. *J. Phys. Chem. Lett.* **4,** 4172–4176 (2013).

22.   Truxal, A. E. *et al.* Nondisruptive Dissolution of Hyperpolarized [129] Xe into Viscous Aqueous and Organic Liquid Crystalline Environments. *Angew. Chemie Int. Ed.* **55,** 4666–4670 (2016).

23.   Gomes, M. D. *et al.* 129Xe NMR Relaxation-Based Macromolecular Sensing. *J. Am. Chem. Soc.* **138,** 9747–9750 (2016).

CHAPTER 3: RELAXATION

There are many ways to use xenon-129 to detect analytes and understand samples. The conventional methods exploit the wide chemical shift range of xenon to detect changes in one sample by monitoring changes in its spectra. However, this dissertation explores a new xenon sensing approach based on monitoring changes in the bulk relaxation of xenon. This new approach has several advantages when compared to other xenon sensing techniques, among them applicability at low fields and no need of a cryptophane sensor. This new relaxation technique offers many new advantages and is therefore worth pursing and understanding. Before xenon relaxometry can be discussed, it is necessary to review the theory of NMR relaxation. Relaxation can be a subtle phenomenon, affected by many things. Having a good grip on the basics makes understanding xenon relaxation much easier.

3.1 General Relaxation Theory

In the previous chapter, the hyperpolarization of xenon was discussed. This hyperpolarization allows for xenon NMR spectra to be collected in a reasonable amount of time. Without spin exchange optical pumping, one would need to wait for a xenon sample to build up thermal polarization. This thermal polarization would then be used up upon excitation, requiring that one wait some time for the polarization to build up again. This return to thermal equilibrium is the focus of relaxation theory and will be discussed before moving on to the mechanism for this relaxation.

When an ensemble of spins is placed in an external magnetic field, the ensemble will gradually align with or against the external field. Not all spins in the ensemble will align; instead, there will be slightly more spins aligned with the field than against it or vice versa, resulting in a net spin alignment. The difference between spins aligned against the field and those aligned with it equals a net magnetization. This process is summarized in figure 3.1. This population difference depends on the strength of the external magnetic field, the strength of the magnetic moments of the spins, and the temperature of the sample. The spin ensemble will reach a stable population difference depending on those parameters known as thermal equilibrium. A spin ensemble will return to thermal equilibrium if it is placed in a state different from its equilibrium. This process is known as relaxation. The rate of this relaxation depends on many parameters. By monitoring the changes in the rate of relaxation, one can monitor the changes in the parameters that affect it.
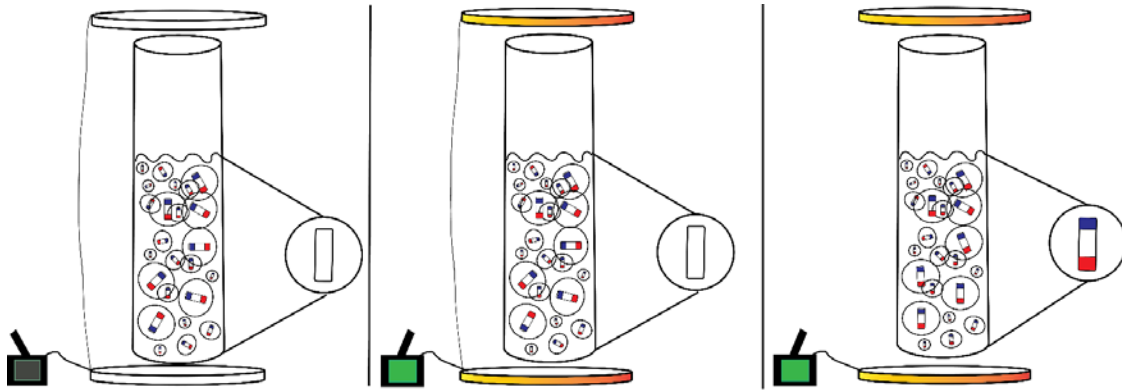
Figure 3.1: *This cartoon shows how an ensemble of spins builds up polarization when placed in a magnetic field. An ensemble of spins when not placed in a magnetic field will not build up polarization, as shown in the first part of the figure. The nuclear magnetic dipoles point in random directions, adding up to nothing. Then, the current source connected to the coils is turned on. This places the spin ensemble in a magnetic field. However, this does not mean that the spins are aligned with it. It takes time for the spins to begin to align with the external field, as seen in the third part of the figure. The time it takes to reach thermal equilibrium depends on many things, such as the motion of the spins and the strength of the external magnetic field. While many spins still point away from the external field, there is a small net alignment of the nuclear dipoles with the field. These spins add up to a net dipole.*

An expression for the thermal polarization of a spin 1/2 system is derived below. The derivation begins with the expressions for the probability of being in one state versus the other. These expressions come from the partition function of a spin 1/2 system.

$$p_\alpha = \frac{e^{\frac{E_\alpha}{k_b T}}}{e^{\frac{E_\alpha}{k_b T}} + e^{\frac{E_\beta}{k_b T}}}$$

$$p_\beta = \frac{e^{\frac{E_\beta}{k_b T}}}{e^{\frac{E_\alpha}{k_b T}} + e^{\frac{E_\beta}{k_b T}}}$$

$$E_{\alpha,\beta} = Energy\ of\ the\ energy\ levels\ in\ Joules$$

$$k_b = Boltzmann\ constant\ in\ Joules\ per\ Kelvin$$

$$T = Temperature\ in\ Kelvin$$

$$p_{\alpha,\beta} = Fraction\ of\ the\ spins\ in\ state\ \alpha\ or\ \beta$$

With the expressions for the probabilities of being in a state known, one can now calculate the difference in the probability of being in one state versus the other. This difference will be the polarization.

$$Polarization = \; p_\alpha - p_\beta$$

$$Polarization = \frac{e^{\frac{E_\alpha}{k_bT}} - e^{\frac{E_\beta}{k_bT}}}{e^{\frac{E_\alpha}{k_bT}} + e^{\frac{E_\beta}{k_bT}}}$$

This expression can be simplified by noting that the energy of the two states in a spin 1/2 are opposite one another.

$$Spin\frac{1}{2}system: E_\alpha = -E_\beta$$

$$Polarization = \frac{e^{\frac{E}{k_bT}} - e^{\frac{-E}{k_bT}}}{e^{\frac{E}{k_bT}} + e^{\frac{-E}{k_bT}}}$$

Using this relation, the numerator and the denominator can be converted into hyperbolic functions.

$$Polarization = \frac{2\sinh(\frac{E}{k_bT})}{2\cosh(\frac{E}{k_bT})}$$

$$Polarization = \tanh(\frac{E}{k_bT})$$

By converting the exponentials into hyperbolic functions and then also writing an expression for E, a final expression for the polarization can be written down. This expression for polarization is handy for understanding the relationship between polarization and the parameters that affect it. For example, polarization is a roughly linear function of the external magnetic field B at low polarizations. However, as the field increases, the polarization will asymptotically approach one, as seen in figure 3.2.

$$E = \frac{1}{2}\gamma Bh$$

$$Polarization = \tanh(\frac{\gamma Bh}{2k_bT})$$
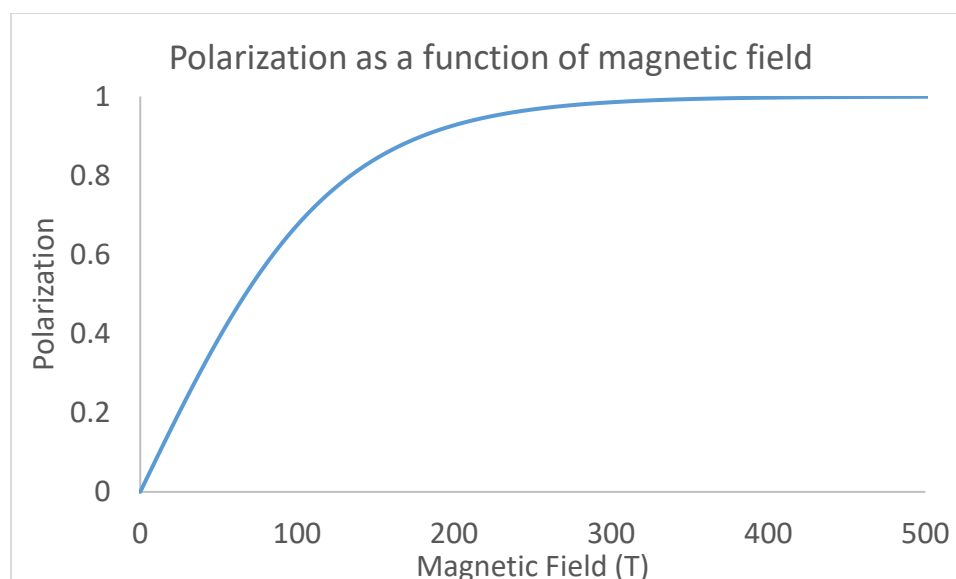
Figure 3.2: *This is a plot of the polarization of an ensemble of electron spins at liquid nitrogen temperatures as a function of the external magnetic field strength. The polarization is a roughly linear function of the external field strength up until it reaches 0.7 or so. After that, the polarization begins to asymptotically approach 1. It's important to note that even at very low temperatures with an unpaired electron, the polarization is far below one for most accessible magnetic field strengths.*

If the net magnetization produced by the net alignment is perturbed, then it will relax back to its thermodynamically determined orientation and magnitude. Unlike the relaxation seen in optical spectroscopy, NMR relaxation is not dominated by spontaneous emission. Instead, fluctuations in local magnetic fields are responsible for relaxation. A spin is exposed to the magnetic fields produced by neighboring spins with dipole moments. The dipolar coupling between these two or more spins creates local fields, fields which are randomly oscillating because of the motion of the spins. This exposes a spin to several fluctuating magnetic fields. Like the fluctuating magnetic fields used to rotate bulk magnetization, these local oscillating fields can rotate the magnetic moment of the spin. However, these local fluctuations are random and therefore must be described using a correlation function.
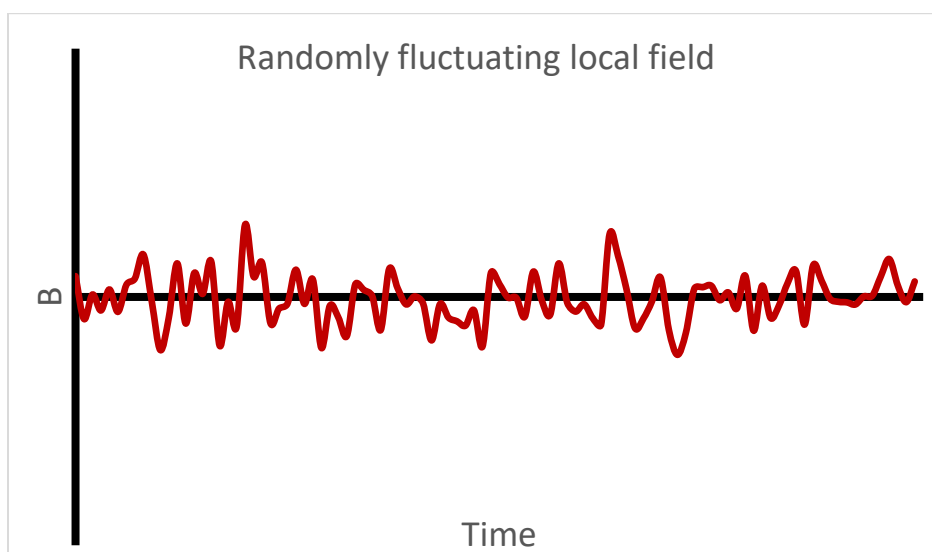
Figure 3.3: The dipolar coupling between two spins fluctuates due to the random motion of the two interacting spins. This dipolar coupling creates a local magnetic field that oscillates randomly. These random oscillations in the local dipolar field can lead to relaxation.

A correlation function can be used to describe how the random motions of nearby atoms affect a spin. These functions describe how a particular motion becomes interrupted by nearby particles. This means that if a local field is oscillating at a particular frequency, that oscillation will eventually decay. No frequency is assumed to be likelier than any other, so the correlation function does not contain a resonant component. Instead, the function assumes that any particular movement will exponentially decay back to thermal equilibrium, resulting in a randomly changing field, as seen in figure 3.3. The rate of this decay is called the correlation time, a key variable for describing the relaxation of spins.

This correlation time describes the frequency spectrum of the local fluctuations. Like a coherent pulse, local fluctuations are more efficient at rotating a spin if they are resonant to the spin's Larmor frequency. To get the frequency spectrum of the random fluctuations in the local field, one takes the Fourier transform of the correlation function. Since the correlation function is an exponential decay with no coherent phase, the Fourier transform will be a Lorentzian centered at zero Hertz. This Lorentzian is known as a spectral density function. The amount of energy at a particular frequency is known as a spectral density.

What correlation function one uses depends on the physical system being studied. For this chapter, the function used below will be used as the correlation function. It assumes that a motion will exponentially decay with a characteristic decay time constant. This time is called the rotational correlation time. Its derivation can be found in the literature[1].

$$G(t) = G(0)e^{\frac{-t}{\tau_r}}$$

$$\tau_r = The\ correlation\ time\ of\ the\ interaction\ in\ seconds$$

It is difficult to understand how the correlation time affects relaxation so long as this function remains in the time domain. Taking the Fourier transform of the correlation function makes it easier to understand the significance of the correlation time. This Lorentzian is called the spectral density function. It describes the amount of power present at a given frequency.

$$J(\omega) = 2\frac{\tau_c}{1 + \omega^2 \tau_c^2}$$

With this formalism, where a spin's relaxation is induced by the motions of nearby spins, it becomes possible to predict how local motions affect relaxation. If a random motion is described by a correlation function and the Fourier transform of this function describes how this random motion affects relaxation, then the correlation time becomes the key variable to describe relaxation. As mentioned before, the correlation function is an exponential decay with the correlation time being the decay time for that exponential decay function. The faster the correlation function decays, the shorter the correlation time. This also affects the spectral density function. As the correlation function becomes narrower in the time domain, the spectral density function becomes broader in the frequency domain. The inverse of that statement is true as well. This means that a long correlation time will result in a spectral density function narrowly contained about zero Hertz. These changes in the shape of the spectral density functions affect NMR relaxation in many tricky ways. Figure 3.4 shows how a change in the rotational correlation time affects the shape of a Lorentzian function and how this change might affect relaxation.
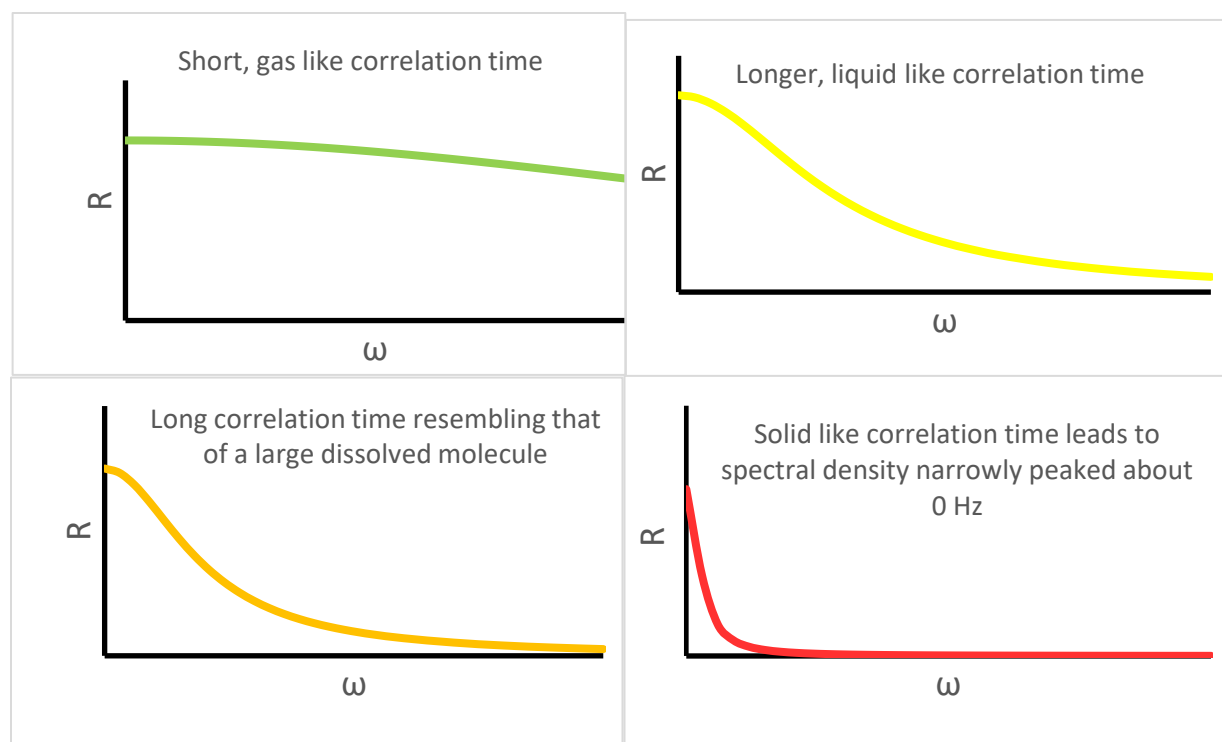
Figure 3.4: *These four Lorentzian functions show how changes in the correlation time can affect relaxation. As the correlation time increases, the spectral density function narrows. The effect of this on relaxation depends on the Larmor frequency of the spin being considered. At very high frequencies, any increase in rotational correlation time will also decrease the relaxation rate. However, at some lower fields, increasing the rotational correlation time brings more spectral density to the spins Larmor frequency, increasing the relaxation rate. Eventually, the spectral density available at the Larmor frequency reaches a point where further increases in the rotational correlation time once again lead to a decrease in the relaxation rate.*

If the shape of the spectral density function changes then the power present at the Larmor frequency of the spin of interest will change. This ties NMR relaxation to molecular dynamics. This also makes relaxation strongly dependent on the external magnetic field[2]. These two facts allow a researcher to learn a lot about the dynamics of a molecule by studying its NMR relaxation at various fields. If the motion governing relaxation is slow, then T_1 relaxation will be inefficient until the Larmor frequency approaches zero. If the motion is fast, then the relaxation may be inefficient at all fields or it may become suddenly fast, depending on the field and motion. This formalism explains why the relaxation of gases and solids tend to be slow and why the relaxation of liquids tends to be fast at higher fields. If the correlation time is extremely short, as in the case of gases, then the spectral density is distributed almost evenly across all frequencies. This means that there is very little spectral density at any frequency, making relaxation inefficient. The opposite holds for solids. Almost all of the spectral density is contained about zero Hertz, with very little left for the Larmor frequency. This also slows down relaxation. Liquids are somewhere in between where the spectral density function has broadened enough to bring some power to the Larmor frequency but is still narrow enough to not be evenly distributed among all frequencies. With this formalism, the relaxation time of

nuclear spins aligned with the external field, called T_1, can be described. The response of T_1 to changes in the rotational correlation time are shown in figure 3.5 for high field systems and figure 3.6 for low field systems.
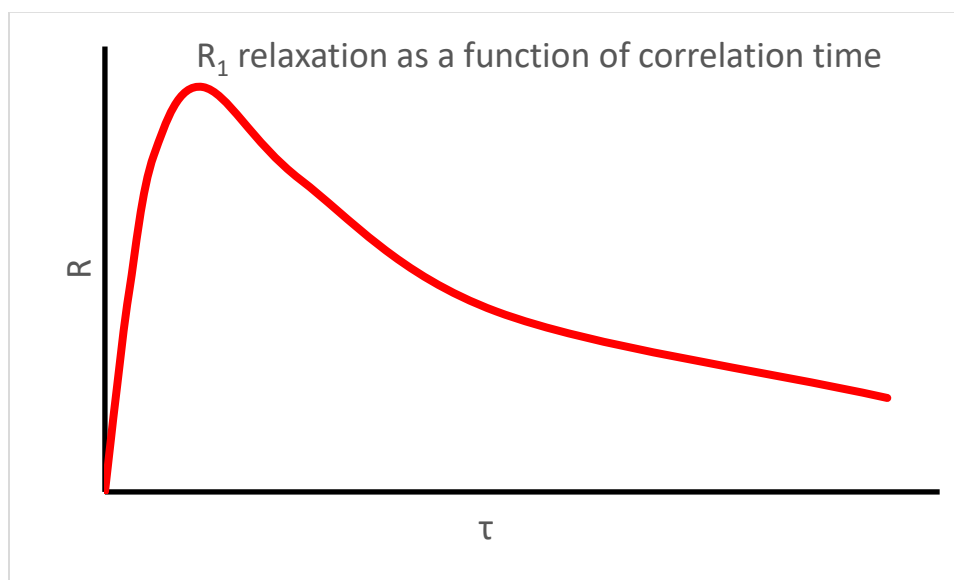
Figure 3.5: This figure shows how R_1, the inverse of T_1, is affected by changes in the rotational correlation time at high field. The longitudinal relaxation rate increases with the rotational correlation time, reaches a maximum, and then decreases. The correlation time at that maximum will change if the external magnetic field changes. At low field, the longitudinal relaxation rate responds to changes in the rotational correlation time like the transverse relaxation rate.

Here is a term that describes the longitudinal relaxation of a spin coupled to an unlike spin. The second spin is decoupled from the first, which simplifies the term. This equation is derived from the Solomon equations[3]. The details of this derivation are shown in the literature. At high magnetic fields, this function yields a function that resembles figure 3.5. At lower magnetic fields, the frequency components in the denominator go to zero, and R_1 becomes proportional to the rotational correlation time. As for the term in front of the spectral density functions, b, it represents the magnitude of the coupling that is modulated by the correlation time. In this case, b is the dipolar coupling between the two unlike spins. Other types of contributions to T_1, such as quadrupole coupling or chemical shift anisotropy, have similar forms. In the equation below, b is the amplitude of the interaction responsible for this contribution to relaxation. It will have very different forms depending on the interaction being considered[4].

$$R_1 = b^2 * \left(\frac{\tau_c}{1 + (\omega_S - \omega_I)^2 \tau_c^2} + \frac{3\tau_c}{1 + \omega_I^2 \tau_c^2} + \frac{6\tau_c}{1 + (\omega_S + \omega_I)^2 \tau_c^2} \right)$$

$$\omega_S = Larmor\ Frequency\ of\ spin\ coupled\ to\ spin\ of\ interest\ in \frac{radians}{s}$$

$$\omega_I = Larmor\ Frequency\ of\ spin\ of\ interest\ in \frac{radians}{s}$$

$$\tau_c = Overall\ rotational\ correlation\ time\ in\ seconds$$

$$b^2 = Magnitude\ of\ the\ interation\ between\ spin\ S\ and\ I\ in\ Hertz$$

Like the spectral density case mentioned above, the width of a resonance in an NMR spectrum is related to the lifetime of the free induction decay responsible for the signal. A signal with a long lifetime will have a narrow peak. However, this is not seen in actual experiments. Many substances with long lifetimes can have extremely broad spectra. If a spectrum is taken of a solid, liquid and gas in a homogenous magnetic field, only the liquid and the gas will yield a narrow line, but the gas line would be broader than the liquid line. This implies that there is another type of relaxation that needs to be considered, the relaxation of spins placed in a coherent superposition. This relaxation will determine the linewidth of an NMR sample.

The previous discussion assumed that the only relevant lifetime was the time a spin spent in a particular state. This assumption ignores that the signal collected by the NMR spectrometer is created by a precessing ensemble of spins coherently placed in a superposition state. The relaxation time for the ensemble of spins placed in the plane orthogonal to the external field is T_2, which determines the width of the peak in the spectrum. It is also possible for the width of the sample resonance to be affected by differences in the phase of the precessing spins. If phase differences accumulate between the spins, then the magnitude of collective magnetic moment in the transverse plane decreases. This decreases the intensity of the signal collected. It is necessary to examine how transverse relaxation differs from longitudinal relaxation to understand why samples differ in linewidths.

This type of relaxation can also be understood using the spectral density function formalism. Non-resonant perturbations affect the precession of spins. In addition to the spectral density at the Larmor frequency, the spectral density at zero Hertz contributes to transverse relaxation. This means that transverse relaxation has a drastically different response to changes in the rotational correlation time. This response is shown in figure 3.6. At all fields, an increase in the rotational correlation time will increase the transverse relaxation rate. The more flexible the molecule, the narrower the resonance because less of the spectral density is around 0 Hertz or the Larmor frequency. With this addition to the relaxation theory, the relaxation induced by local fields can be explained. With this theory, a flexible molecule is predicted to have a narrow peak and an inflexible molecule is predicted to have a broad peak.

R$_2$ relaxation as a function of correlation time
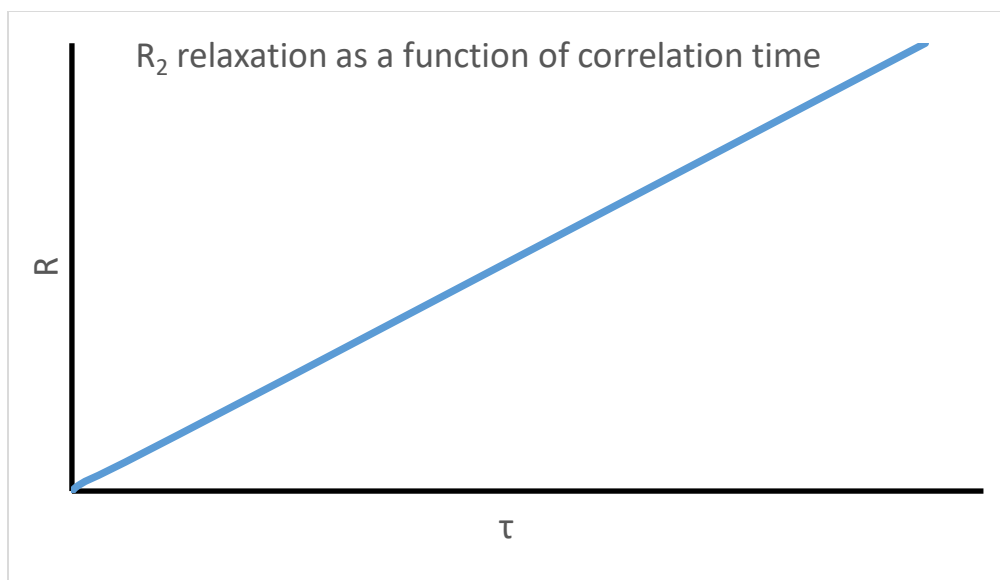
Figure 3.6: *Unlike T$_1$, T$_2$ is affected by the spectral density at zero Hertz. This means that an increase in the rotational correlation time will always shorten T$_2$. It is important to note that at very low magnetic fields, this figure also shows how T$_1$ is affected by changes in the rotational correlation time.*

This is the function that describes the transverse relaxation of a spin coupled to an unlike spin. Like the previous function, this one was derived from the Solomon equations. Notice that this function contains many of the same parts as the function for R$_1$. The main differences are the inclusion of a high frequency spectral density and a 0 Hertz spectral density. That last addition is key. Because R$_2$ always has a zero field component, it is almost a linear function of the rotational correlation time. The zero field spectral density dwarfs the higher frequency contributions[4].

$$R_2 = 0.5 * b^2 * (\frac{\tau_c}{1 + (\omega_S - \omega_I)^2 \tau_c^2} + \frac{3\tau_c}{1 + \omega_I^2\,\tau_c^2} + \frac{6\tau_c}{1 + (\omega_S + \omega_I)^2 \tau_c^2} + \frac{6\tau_c}{1 + \omega_S^2\,\tau_c^2} + 4\tau_c)$$

While this approach explains why a solid sample would have a broader resonance than a liquid sample, it fails to explain why a gas sample would have one too. The rotational correlation time of a gas is extremely short, implying that a gas resonance should be extremely narrow. This predicted long relaxation time is the intrinsic T$_2$. To explain why liquid samples tend to be narrower than gas samples, one must consider the inhomogeneity of the external magnetic field and how quickly a sample diffuses through this field. When an ensemble of spins begin to precess in an external magnetic field, differences in that field across that sample will result in slightly different precession frequencies across the sample. These differences in frequencies mean that an ensemble of spins that were once aligned along a single direction begin point in slightly different directions over time. This difference in the phase of different parts of the spin ensemble gradually eliminates the initial coherence of the sample. This inhomogeneity will therefore also decrease the life time of the signal and therefore broaden the sample resonance. In fact, the line width of a sample may be primarily determined by the inhomogeneity of the

external field, masking the contribution from dipolar coupling entirely. The overall transverse relaxation time, including intrinsic relaxation from local fields and relaxation from the inhomogeneity of the external field, is known as T_2^*. The effect of field inhomogeneities can be seen in figure 3.7. This loss of phase coherence leads to rapid decrease in the intensity of the free induction decay, despite the ensemble of spins remaining in the xy plane.
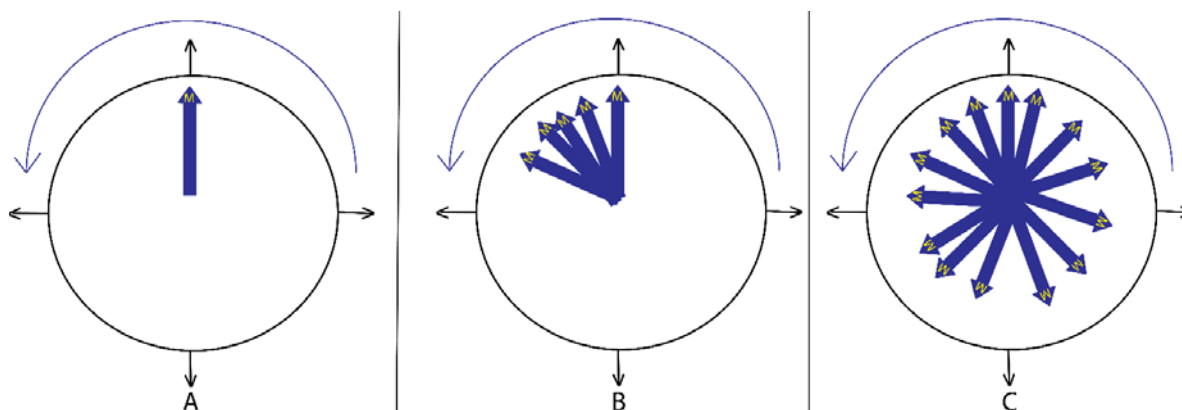
Figure 3.7: A spin ensemble will lose coherence in an inhomogeneous field. Each arrow represents magnetization. In part A, the spins across the sample are pointing in the same direction after just being excited. The spins will begin to precess in the direction indicated by the curved arrow. In part B, the spins have begun to dephase. Some are precessing faster than the others, so the spins are no longer all pointing in the same direction. Over time, the spins will point in all directions, with no net magnetization, as shown in part C.

The other major T_2 relaxation contribution besides local field fluctuations and external field inhomogeneity is chemical exchange. This contribution to relaxation is especially important for xenon relaxometry because of the wide chemical shift range and slow exchange of many xenon systems. Many chemical systems can exchange between different places or conformations. Xenon exchanging into and out of cryptophane A is one example. These different places or conformations might have different chemical shifts or they may coalesce into a single resonance. When the sample's magnetization is kept along the external field, this exchange does not affect relaxation unless the intrinsic relaxation rates of the two states differ. If the exchange affects relaxation, it does so by mixing two sample populations with different relaxation rates. The exchange its self does not contribute to T_1. The same is not true for T_2. If there is a chemical shift difference between the sites that the sample is exchanging from, then this exchange will relax the spins in the transverse plane. The combination of exchange and chemical shift creates a time dependent randomly modulating field along the longitudinal axis, leading to relaxation of spins perpendicular to this axis. The magnitude of this relaxation depends on the square of the difference in frequency between the exchange sites, making this type of relaxation more important at high magnetic fields. The correlation time describing this randomly oscillating field is the exchange time between the different sites.

There are many terms for the exchange contribution to T_2. Which term one uses depends on the relative relaxation rates of the two sites, as well as the chemical shift difference between

them. As an example, the exchange contribution to R_2 in the fast exchange case is presented below. This equation shows the field dependence of exchange relaxation[5].

$$R_{2,ex} = \frac{p_a p_b \tau_a \tau_b}{\tau_a + \tau_b} (2\,\Delta\,\omega)^2$$

$$p_{\alpha,\beta} = Population\ of\ sample\ in\ state\ \alpha\ or\ \beta$$

$$\tau_{\alpha,\beta} = Exchange\ time\ of\ each\ state\ in\ seconds$$

$$\Delta\,\omega = Chemical\ shift\ difference\ between\ \alpha\ and\ \beta\ in\ radians\ per\ second$$

Exchange relaxation can also be affected by spin echoes if the transverse magnetization is inverted at a rate comparable to the exchange rate. As the refocusing pulses get closer together in time, the exchange contribution to R_2 goes to zero. A similar effect can occur for the dipolar contributions to R_2, provided that the motions responsible for relaxation are slow relative to the repetition rate of the spin echo[6].

$$R_{2,ex} = p_a p_b \frac{2\,\Delta\,\omega^2}{k_{ex}} [1 - \frac{1}{k_{ex}\tau_{cp}} \tanh(k_{ex}\tau_{cp})]$$

$$k_{ex} = Exchange\ frequency\ between\ \alpha\ and\ \beta\ in\ Hertz$$

$$\tau_{cp} = Time\ between\ 180\ pulses\ in\ a\ CPMG\ in\ seconds$$

It is possible to introduce a field into the transverse plane, changing the frequency requirements for relaxation and therefore changing the exchange contribution to relaxation. After excitation, it is possible to apply a field parallel to the excited magnetization. This is known as a spin locking field. With a spin locking field applied, the frequency in the spectral density of the chemical exchange that contributes to relaxation changes from zero to the resonant frequency of the spins in the spin locking field. This is known as $T_{1\rho}$ relaxation, ρ for T_1 in the rotating frame. These spin locking experiments are performed because $T_{1\rho}$ changes as the strength of the spinlocking field changes. By performing many such spinlocking experiments, the exchange rate between different chemical sites can be estimated.

The equation describing the exchange contribution to $R_{1\rho}$ is shown below. It resembles the equations for the exchange contribution to R_2. In fact, when the spin locking field is set to zero, this equation becomes identical to the R_{2ex}. By collecting $R_{1\rho}$ at multiple spin locking fields, it is possible to find the exchange time by fitting the results to this equation. There is one subtlety to consider before performing such an experiment. The dipolar contribution to relaxation can also be changed by spin locking the sample. The sample, by being quantized along a transverse pulse, now requires fluctuations equal to the spin locking field strength to efficiently relax. If the sample has a short correlation time, then this dipolar relaxation in the rotating frame is equal to R_1. Slowly rotating samples, however, will relax at different rates and will therefore complicate the fitting procedure, making it difficult to find the exchange time[7],[8].

$$R_{1\rho,ex} = p_a p_b (2\,\Delta\,\omega)^2 \frac{\tau_{ex}}{1 + \tau_{ex}^2 \omega_{sl}^2}$$

$$\omega_{sl} = Spinlocking\ pulse\ strength\ in\ rads\ per\ second.$$
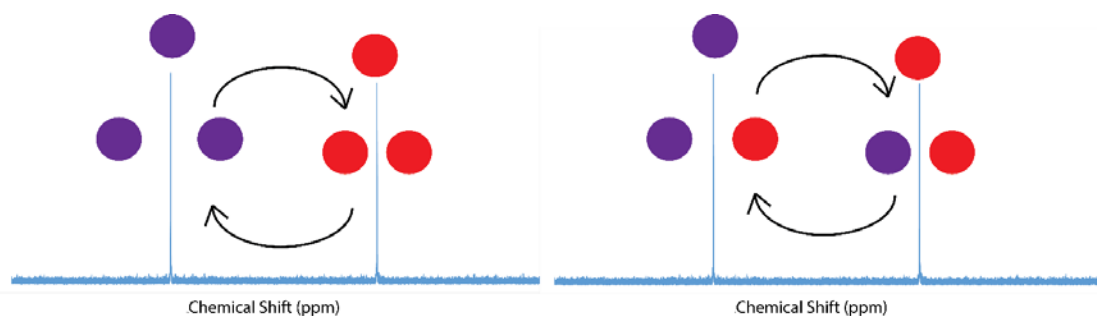
Figure 3.8: Schematic of chemical exchange. Many chemicals undergo various types of reversible exchange. They might exchange between different conformations, binding sites, or even structures. These different conformers, sites and structures can have different chemical shifts. The exchange between these different chemical shifts can result in rapid T_2 relaxation of the entire spin population. This contribution to T_2 can be diminished by reducing the external magnetic field or spin locking the sample after excitation.

Unpaired electrons can rapidly relax a nuclear spin. The formalism used to describe this type of relaxation is similar to the one used for relaxation caused by other nuclear spins. The electron spin couples to the nuclear spins in the same way a nuclear spin would. However, the gyromagnetic ratio of an electron is about a thousand times greater than that of a nuclear spin, making the dipolar coupling between an electronic and nuclear spin much stronger than coupling between nuclear spins. This makes the relaxation caused by unpaired electrons much more rapid than other varieties of relaxation. Besides the difference in magnitude, paramagnetic relaxation is also affected by slightly different local dynamics.

While the dipolar coupling between electronic and nuclear spins is modulated by rotational diffusion, it can also be affected by the relaxation of the electronic spin. In some samples, the electronic T_1 can be as short as nanoseconds, making it as short as some rotational correlation times. This means that electronic relaxation can affect the dipolar coupling between the electronic and nuclear spins. Under certain conditions, it can be the main correlation time.

There are many ways to introduce unpaired electrons into a sample. The most common sources of unpaired electrons are paramagnetic ions and radical electrons. In liquid state experiments, paramagnetic ions tend to be used because of their stability. These ions are usually transition metals and lanthanides, with manganese (II) and gadolinium (III) being two popular examples used for enhancing image contrast in MRI and for decreasing repetition time in NMR. These metal ions are better choices because of their relatively long electronic relaxation time and high number of unpaired electrons[9,10,11]. There are five unpaired electrons on a manganese (II) ion and seven on a gadolinium (III) ion. A paramagnetic ion will more effectively relax nuclear spins if it has a greater number of unpaired electrons. Their longer electronic relaxation times also

enhances their relaxivity, their tendency to relax other spins, provided that the external field is not too high. If the electronic T_1 is long enough to quench relaxation by making the spectral density function narrow, leaving little spectral density at the nuclei's Larmor frequency, it is probably too long to contribute to the overall correlation time of the electronic nuclear dipole coupling. This makes these ions close to ideal for increasing the relaxation rate of nuclear spins.

The equations below explain how paramagnetic contrast agents affect T_1 relaxation. These equations show that the effect of the paramagnetic ion depends on the amount of unpaired electrons and on the overall correlation time[4].

$$R_{1\ bound\ proton} = \frac{2}{15} * S(S+1) * b^2 * \left(\frac{\tau_{c2}}{1+(\omega_S - \omega_I)^2 \tau_{c2}^2} + \frac{3\tau_{c1}}{1+\omega_I^2\ \tau_{c1}^2} + \frac{6\tau_{c2}}{1+(\omega_S+\omega_I)^2\tau_{c2}^2}\right)$$

$$\omega_s = Larmor\ Frequency\ of\ electron\ in\ \frac{rad}{s}$$

$$\omega_I = Larmor\ Frequency\ of\ proton\ in\ \frac{rad}{s}$$

$$\frac{1}{\tau_{c1,2}} = Summed\ Correlation\ rates\ in\ Hz.$$

$$\frac{1}{\tau_{c1,2}} = \frac{1}{T_{1,2e}} + \frac{1}{\tau_m} + \frac{1}{\tau_r}$$

$$\tau_m = proton\ exchange\ time\ when\ bound\ to\ Gd\ ion$$

$$\tau_r = proton\ rotational\ correlation\ time\ when\ bound\ to\ Gd\ ion$$

$$T_{1,2e} = Electronic\ relaxation\ time\ in\ seconds$$

Notice how the correlation rate is a sum of the electronic relaxation time, the exchange time and finally the rotational correlation time of the metal-ligand complex. In many common systems, like Gd-DOTA in water, the exchange time is usually much longer than the other terms. Therefore, the two times to consider are the rotations of the complex and the electronic relaxation time.

This final equation shows one of the finer points when considering paramagnetic relaxation enhancement. While the exchange time is usually too long to affect the overall rotational correlation time of the ion ligand complex, it can nevertheless alter the observed relaxation change by affecting how quickly the rapidly relaxing bound population exchanges with the slowly relaxing free population.

$$\frac{1}{T_{1,bulk\ proton}} = \frac{p_m}{\tau_m + T_{1,bound\ proton}}$$

$$p_m = Fraction\ of\ bulk\ water\ bound\ to\ metal\ ion.$$

3.2 Methods for measuring relaxation times

There are many ways to measure relaxation times, each with its own little considerations. There are broadly two types of approaches: those which require that the entire relaxation experiment be done in one scan and those that do not. While it is generally preferable to wait for samples to return to thermal equilibrium before repeating a measurement, this cannot be done when working with hyperpolarized samples.

To calculate the T_1 or T_2 of a sample, it is necessary to measure the amplitude of the signal at different points along its return to thermal equilibrium. This can be done by simply collecting different spectra at each point along the decay curve. A simple relaxation time measurement experiment begins by placing the sample magnetization in a non-equilibrium state. The sample is allowed to relax for some time and is then made observable. A spectrum is then collected and the sample is allowed to return to thermal equilibrium. The procedure is then repeated with more time for the sample to relax before being observed until additional time no longer affects the signal collected.

A good example of this general procedure is the inversion recovery pulse sequence, shown in figure 3.9, a sequence used to measure T_1. The experiment begins with a sample at thermal equilibrium. Most liquid samples will achieve thermal equilibrium within a minute of being placed inside the magnet but some solids and gases can take hours to achieve equilibrium. The magnetization of the sample is inverted using a resonant 180 degree pulse. If the T_1 of resonances are being measured simultaneously, then special care must be taken to make sure that the flip angle is 180 degrees along the entire spectrum. After inverting the peak, the sample is allowed to relax for some time and is then excited with a 90 degree pulse. A free induction decay is immediately collected. After collecting the FID, the instrument waits for a delay equal to five times the T_1 of the longest T_1 that one hopes to measure. The inversion delay and excitation procedure is repeated with a longer delay between the inversion and excitation. This procedure is repeated until the sample reaches thermal equilibrium between the inversion and excitation pulse.
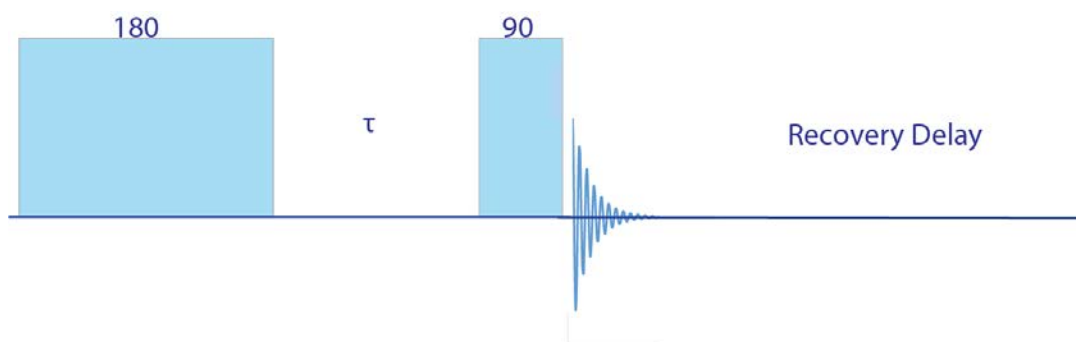
Figure 3.9: *Pulse sequence for an inversion recovery. The spin magnetization is first inverted with a 180 degree pulse. This inversion pulse brings the magnetization from point with the field to pointing against it. This inversion takes the spins away from thermal equilibrium, resulting in relaxation during time tau.*

After relaxing for some time, the magnetization along the z axis is excited by a 90 degree pulse. After collecting an FID, the spins are allowed to return to thermal equilibrium before another inversion recovery is performed with a different tau. This experiment is repeated until enough points along the exponential decay are collected for an acceptable fit. It is very important that the recovery delay is set such that the magnetization before the 180 pulse is always the same.

This procedure has several obvious problems. The first is that some knowledge of the T_1 is needed before one can begin this experiment. It is necessary to wait five times the T_1 before collecting the next point along the decay curve because each point must begin with the same initial magnetization. If less time is spent waiting between samples, then the initial magnetization will differ. This means that there will be a lot of trial and error before the T_1 of a sample can be measured. This will also be a lengthy experiment for almost any samples except some liquids because each experiment must be separated by five times the T_1. It can take days to measure the T_1 of some solid samples. Nevertheless, this procedure offers the most accurate T_1 out of all the alternatives with only saturation recovery offering similar results.

Saturation recovery is very similar to inversion recovery. Instead of inverting the spins and seeing how long they take to return to their previous alignment, the spins are instead saturated. Saturation is a process where the population difference between the Zeeman states are equalized and where any coherence created is eliminated. There should be no net magnetization along the transverse plane after saturation. Once saturated, the sample is allowed to relax for some time. Then, the sample is excited and its FID is collected. This is then repeated with more time between the saturation pulse and the excitation pulse until additional time no longer affects the FID collected.

To measure T_2, it is necessary to remove the inhomogeneous broadening from the sample. This can be done with a spin echo, shown in figure 3.10. A spin echo pulse sequence contains the following: a 90 degree excitation pulse, a delay, a 180 degree pulse, and another delay equal in length to the first delay and then an acquisition. This pulse sequence allows the sample to precess and decay at a rate the inhomogeneous external magnetic field. The spin echo does this by refocusing the contribution of the frequency offset. At the end of the second delay, the phase accumulated during the first delay is refocused. By arraying the total length of spin echo delay, T_2 can measured.
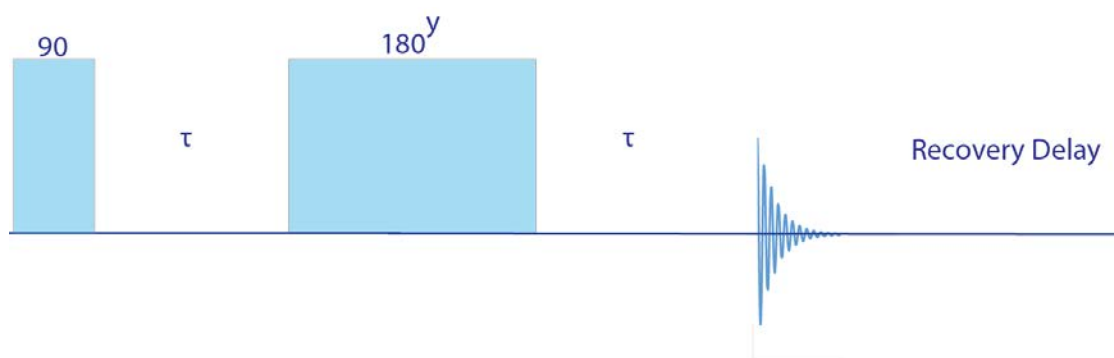
Figure 3.10: *This is a spin echo pulse sequence. The spins are excited by a 90 degree pulse. These spins then precess for a while before being inverted by a 180 pulse. After this inversion, the phase accumulated during the first delay time tau is refocused during the second delay. After the sample has completely recovered, an FID is acquired. This procedure is repeated several times with either different taus or with multiple echoes between the 90 degree pulse and the signal acquisition steps. It is not necessary for the phase of the excitation pulse to 90 degrees out of phase with the refocusing pulse. Keeping it this way just makes it so that the spins are pointing in the same direction at the end of the second tau as they are in the beginning of the first tau. If the two pulses are along the same axis, then the magnetization at the beginning of the first tau and the end of the second tau will point in opposite directions.*

A spin echo only refocuses the offset if the sample does not change frequency during the echo. For example, if the molecule diffuses to a region with a slightly different field during the echo, then the offset will not be refocused. This means that the spin echo pulse sequence can fail to remove the inhomogeneity from the sample if there is significant diffusion during the spin echo. This can become a problem as the delay length is increased. This problem can be removed with a simple change in pulse sequence.

Instead of increasing the delay length to collect the points on the T_2 decay curve, one can instead keep the delay length fixed and instead increase the number of echoes. If the delay lengths are kept short, then the change in offset induced by diffusion can be reduced or even removed. This allows one to collect the entire T_2 decay without any contribution from diffusion. However, this procedure requires a homogenous refocusing pulse. If the pulse flip angle deviates slightly from 180 degrees, then the offset will fail to completely refocus. If the number of echoes are kept small, then the pulse imperfection contribution to T_2 might not be significant. This introduces a tradeoff into this pulse sequence. By keeping the delays short, the contribution to T_2 can be reduced or removed. However, more echoes are needed to allow the sample to decay to thermal equilibrium. This requires many more refocusing pulses, increasing the pulse flip angle error contribution to T_2. This contribution to T_2 can be reduced by increasing the delay, decreasing the amount of echoes needed to let the sample reach thermal equilibrium. Of course, this increases the diffusion contribution to T_2.

While these methods allow one to accurately measure T_1 or T_2, they are all time consuming. It is necessary to wait many times T_1 between each point on the decay curve in order to begin with the same magnetization every time. If the T_1 is long, then these pulse sequences might take too much time. These methods are especially difficult when used on hyperpolarized samples. In this

case, it is no longer possible to wait for samples to return to thermal equilibrium. Instead, more hyperpolarized spins must be introduced before continuing with the experiment. Without hyperpolarization, one's sample might be undetectable. Hyperpolarized samples might not be consistent between experiments. Each sample begins in a non-equilibrium state with an initial magnetization that could easily change every time. This introduces shot noise into the decay. It might also take a long time to introduce the hyperpolarized sample to the magnet. It is therefore necessary to collect the entire decay curve at once, without acquiring new magnetization by waiting for the sample to relax or introducing a new hyperpolarized sample.

There are many ways to collect the entire decay curve without having to wait for new magnetization. Both T_2 and T_1 can both be measured in this way, albeit with some artifacts and instrumentation challenges. The pulse sequence used to measure T_2 is the simplest so it will be explained first.

By making a few modifications to the T_2 pulse sequence, one can collect the entire T_2 decay curve without waiting for the sample to return to thermal equilibrium between scans. This CPMG sequence begins with a sample either at thermal equilibrium or in some hyperpolarized state[12]. The pulse sequence for a CPMG is shown in figure 3.11. It is then excited using a 90 degree pulse and the FID is acquired immediately. Then the phase accumulated during the acquisition period is refocused with a 180 degree pulse and a delay equal to the acquisition period. This is repeated until the sample decays to nothing, with an FID collected every time. This minor change allows one to collect the entire decay curve with some minor downsides.
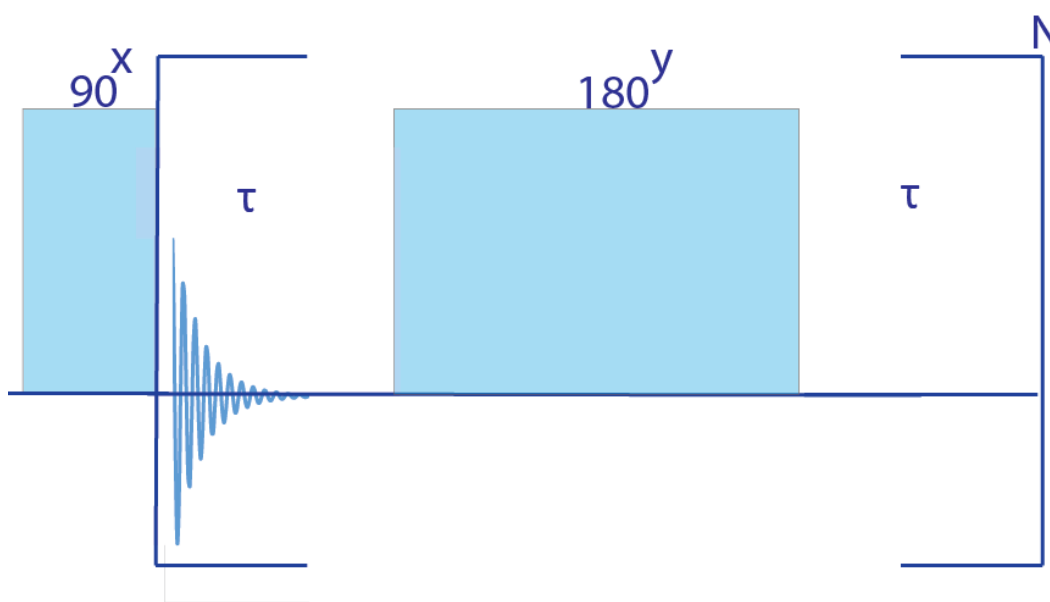
Figure 3.11: *This is the pulse sequence for a CPMG. Unlike the previous spin echo pulse sequence, this sequence collects the entire decay curve in with a single initial magnetization, making this sequence ideal for hyperpolarized samples. Unfortunately, the rapid switching between pulsing and acquiring can be difficult for the spectrometer. The value t_{cp} mentioned in an equation earlier in this chapter is equal to 2τ.*

This fast spin echo pulse sequence has some problems that are not obvious. The first problem is that the acquisition time length is also the echo delay. These two times have fundamentally different requirements. The echo delay needs to be kept as short as possible to remove the diffusion contribution to T_2. This means that the acquisition period needs to be kept short too. If the sample does not decay much during the acquisition period, then the FID is truncated. This will introduce significant ringing and broadening to the spectrum. This therefore introduces another tradeoff into the pulse sequence. It becomes necessary to keep the acquisition period long enough to allow the sample to decay a bit, enough not to ruin the spectrum. However, it can be impossible to allow the FID to decay without introducing diffusion into T_2. There are also some hardware limitations that affect this pulse sequence. Time is needed to switch the acquisition channel on and off and this time must be added to the refocusing delay after the 180 degree pulse. It is important to remember that this switching delay might not be visible in the pulse programming interface. While this delay is usually small, on the order of a few microseconds, if it isn't taken into account, it can lead to large phase accumulations after many imperfectly timed echoes. This will make T_2 seem shorter than it is.

While quickly measuring T_2 is straightforward, collecting the data to find T_1 is trickier. There are many schemes used to quickly measure T_1 without waiting for new magnetization. Among them, the most straightforward involves periodically exciting the relaxing sample with a small flip angle pulse. This is known as a Look Locker pulse sequence, shown in figure 3.12[13]. The pulse allows one to sample the decaying magnetization without putting it all in the transverse plane. This method obviously makes T_1 seem shorter than it is because magnetization is lost both because of T_1 decay and also because of the pulse. However, if the small flip angle is well known, then it is possible to calculate the real T_1. Another method involves exciting the decaying magnetization with a 90 degree pulse but then refocusing it after acquiring the FID and then placing it back onto the z axis. The sample is then allowed to decay for some time before being sampled again. While this method doesn't distort T_1 by periodically removing magnetization with small flip angle pulses, it does mix T_2 with T_1. If T_2 is extremely short and many FIDS are collected, than this pulse sequence could yield artificially shortened T_1 decays.
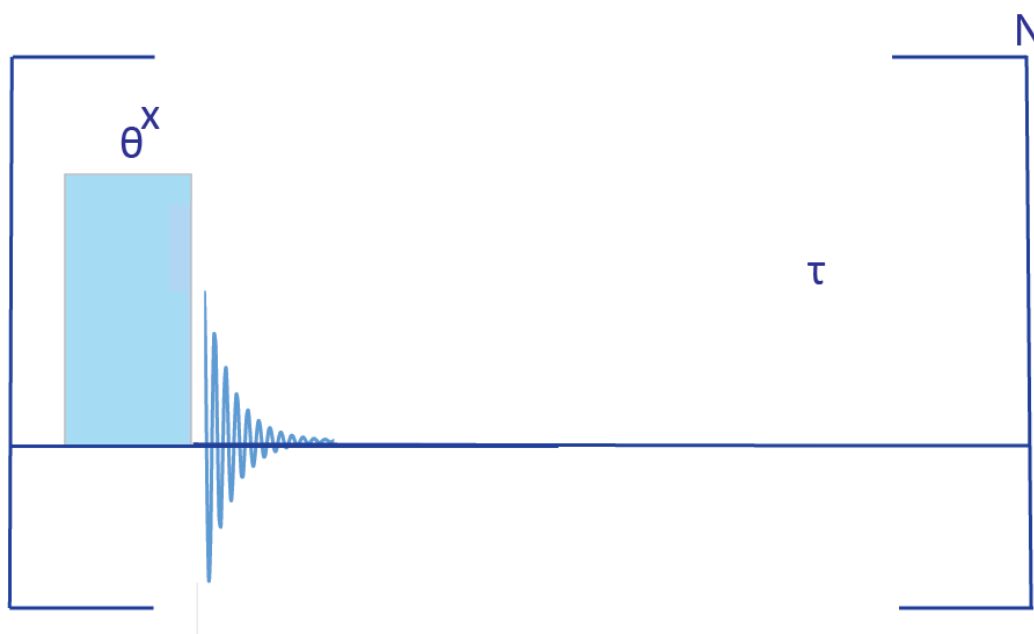
Figure 3.12: This is a Look-Locker pulse sequence. The initial magnetization is kept along z and is sampled many times by a small flip angle pulse. It is important to keep the amount of points along the decay curve small because a small of amount of magnetization is lost every time an FID is collected. The lost in signal due to oversampling can very easily overwhelm the loss in signal due to T_1 relaxation. It is also necessary to make tau long enough to prevent there still being signal present during the next small flip angle excitation. In practice, the inhomogeneity of the external magnetic field is sufficient to dephase the signal. If not, a gradient can be turned on during tau to eliminate any remaining transverse magnetization.

Both the T_1 and T_2 of hyperpolarized xenon were measured. All T_2 measurements were done with a fast spin echo pulse sequence and all T_1 measurements were done with a small flip angle pulse sequence. Because xenon tends to chemically exchange from magnetically inequivalent sites at a rapid rate, its T_2 is much shorter than its T_1.

3.3 Bibliography

1.   Hubbard, P. S. Quantum-mechanical and semiclassical forms of the density operator theory of relaxation. *Rev. Mod. Phys.* **33,** 249–264 (1961).

2.   Gore, J. C. & Anderson, A. W. The Physics of Relaxation. *eMagRes* **1,** 67–78 (2013).

3.   Solomon, I. Relaxation Processes in a System of Two Spins. *Phys. Rev.* **99,** 559–567 (1955).

4.   Kowalewski, Jozef, Maler, L. *Nuclear Spin Relaxation in Liquids: Theory, Experiments, and Applications*. (Taylor and Francis Group, 2006).

5.   McLaughlin, A. C. & Leigh, J. S. Relaxation times in systems with chemical exchange: Approximate solutions for the nondilute case. *J. Magn. Reson.* **9,** 296–304 (1973).

6.   Traaseth, N. J. & Veglia, G. Probing excited states and activation energy for the integral membrane protein phospholamban by NMR CPMG relaxation dispersion experiments. *Biochim. Biophys. Acta - Biomembr.* **1798,** 77–81 (2010).

7.   Deverell, C., Morgan, R. E. & Strange, J. H. Studies of chemical exchange by nuclear magnetic relaxation in the rotating frame. *Mol. Phys.* **18,** 553–559 (1970).

8.   Wang, Y. Sen. NMR rotating frame relaxation measurements of conformational exchanges on the microsecond time scale. Part I: Theory. *Concepts Magn. Reson.* **4,** 327–337 (1992).

9.   Chemistry, B. Molecular Dynamics of Gd (III) Complexes in Aqueous Solution by HF EPR Alain Borel , Lothar Helm and Andre E . Merbach. 207–247 (2004).

10.   Benmelouka, M., Borel, A., Moriggi, L., Helm, L. & Merbach, A. E. Design of Gd(III)-based magnetic resonance imaging contrast agents: Static and transient zero-field splitting contributions to the electronic relaxation and their impact on relaxivity. *J. Phys. Chem. B* **111,** 832–840 (2007).

11.   Aime, S. *et al.* Relaxometric evaluation of novel manganese(II) complexes for application as contrast agents in magnetic resonance imaging. *J. Biol. Inorg. Chem.* **7,** 58–67 (2002).

12.   Meiboom, S. & Gill, D. Modified spin-echo method for measuring nuclear relaxation times. *Rev. Sci. Instrum.* **29,** 688–691 (1958).

13.   Look, D. C. Time Saving in Measurement of NMR and EPR Relaxation Times. *Rev. Sci. Instrum.* **41,** 250 (1970).

CHAPTER 4: XENON CONTRAST AGENTS

4.1 Overview of Xenon Contrast Agents

Several xenon contrast agents were studied before any xenon relaxometry experiments were conducted. These contrast agents were tested in order to be used as parts of future biosensors. Several varieties of sensors and metal ions were studied in these experiments in order to get some understanding of how the paramagnetic ions affected relaxation. The experiments conducted on these sensors allow one to get a sense of how much one can expect the paramagnetic ion to affect relaxation. This lays the foundation for future work where a xenon biosensor based on paramagnetic relaxation enhancement is used for detecting a wide variety of targets.

A mono-acid cryptophane A cage was covalently attached to 1, 4, 7, 10-tetraazacyclododecane-1, 4, 7, 10-tetraacetic acid, DOTA, and a solubilizing peptide chain consisting of five glutamic acids. (Figure 4.1). These constructs form stable complexes with several well-known paramagnetic MRI contrast agents such as Mn^{2+} and Gd^{3+} as well as some diamagnetic metal ions (Ca^{2+} and Ag^{1+}). Several varieties of these cage molecules were synthesized with the main difference between them being the position of the DOTA chelating agent. The sensors studied are shown in figure 4.1. T_2 times were measured with a CPMG and T_1 times were measured with a Look Locker pulse sequence.
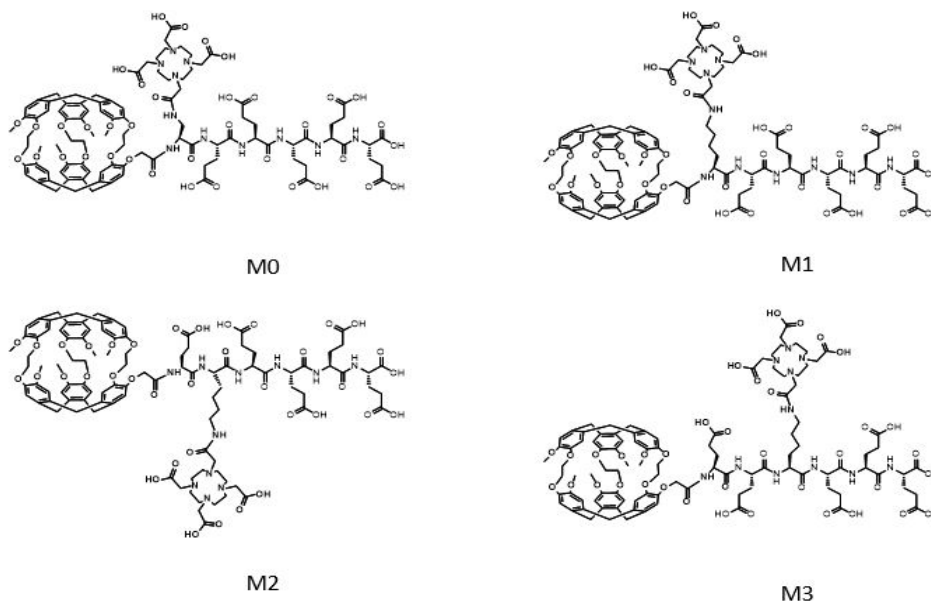
Figure 4.1: *Four different sensors were studied. Cages M1 to M3 use lysine to attach DOTA to the overall sensor, while cage M0 uses diamino propionic acid.*

The M1 cage was used to test the paramagnetic relaxation enhancement of different metal ions. These ions affected the T_1 and T_2 of xenon in many different ways, with each one having a unique effect on the measured relaxation times. Manganese (II) and gadolinium (III) were the most effective relaxation agents. This result was expected because these two ions are also the most efficient at relaxing water. Their efficient relaxation comes from their relatively long electronic relaxation times[1,2]. Unlike many other metal ions, the valence orbitals of Mn (II) and Gd (III) are symmetric. This is because their outmost orbitals are all occupied by a single electron, making the static and transient zero field splitting of the electrons much smaller[3]. The other paramagnetic metal ions studied, like nickel (II) or dysprosium (III) were much less efficient relaxation agents because of their much shorter electronic relaxation times[4]. Short electronic relaxation times quench paramagnetic relaxation enhancement. Several diamagnetic ions were also studied and they, predictably, had little effect on the T_1 and T_2 of xenon. Some of them even, such as silver (I) and calcium (II), even increased the xenon relaxation times.

4.2 Results from Xenon Contrast Agent Experiments

These ions had a stronger effect on T_1 than T_2, beyond even the effect of the sensor alone. These results are summarized in figure 4.2. Changes in T_1 were more drastic than T_2. Adding gadolinium (III), the most effective T_2 relaxation agent, only shortened the T_2 of xenon to 5 seconds from 10 seconds. Some ions, like silver (I) and calcium (II), even increased T_2. T_1 ranged from 100 seconds in the sensor without an ion, essentially the T_1 of xenon dissolved in pure water, to about 20 seconds, the T_1 of xenon in a solution with a cage and manganese (II). There

are three broad categories of ions seen in these experiments. Manganese and gadolinium are out alone on the left of the figure 4.2, due to their long electronic relaxation times and therefore efficient paramagnetic relaxation enhancement. Then, there are a few ions clustered together in the middle of the T_1 line. These are nickel (II), dysprosium (III), copper (II), europium (III), and tellurium (III). These ions have T_2 times that range from 5 to 10 seconds and T_1 times that range from 60 to 80 seconds. Due to their rapid electronic relaxation, these ions were only able to lower T_1 effectively. The last cluster is comprised of the diamagnetic cages in the far right. These cages have T_1 times in the 90 to 100 seconds and T_2 times that range from 20 to 10 seconds. Their T_2 is similar to the other clusters, except in the case of silver and calcium. These two ions increased the T_2. This is a surprising result, suggesting that these ions might also affect the exchange time of the xenon. These changes in T_1 would become much more drastic at lower magnetic fields because most of the spectral density of the xenon electron dipolar coupling is at lower frequencies. Seeing how these metal ions differed at lower fields would be the next step to using them as biosensors.

T_2 contrast is worse than T_1 contrast in this case because the dipolar coupling between the unpaired electrons and the xenon inside the cage must compete with T_2 relaxation from chemical exchange. As has been discussed before, the chemical shift difference between xenon inside the cage and xenon outside the cage is very large, about 140 ppm. At the fields used in this experiment, 9.4 Tesla, this translates to a frequency difference of about 15 KHz, a huge frequency offset. Combine this shift, with the relatively slow exchange between the free and bound xenon, and one gets a gigantic chemical exchange contribution to relaxation. T_2 times can be as short as ten seconds from exchange relaxation alone, assuming an exchange time of 1 millisecond and a binding affinity of about 1000 M^{-1}. By contrast, T_1 is only affected by dipolar coupling and chemical shift anisotropy. Adding a paramagnetic ion to a cage therefore alters longitudinal relaxation more drastically because the dipolar coupling between the ion and xenon only has to compete with the dipolar coupling between the cage protons and xenon. Transverse relaxation must compete with those two mechanisms and chemical exchange.
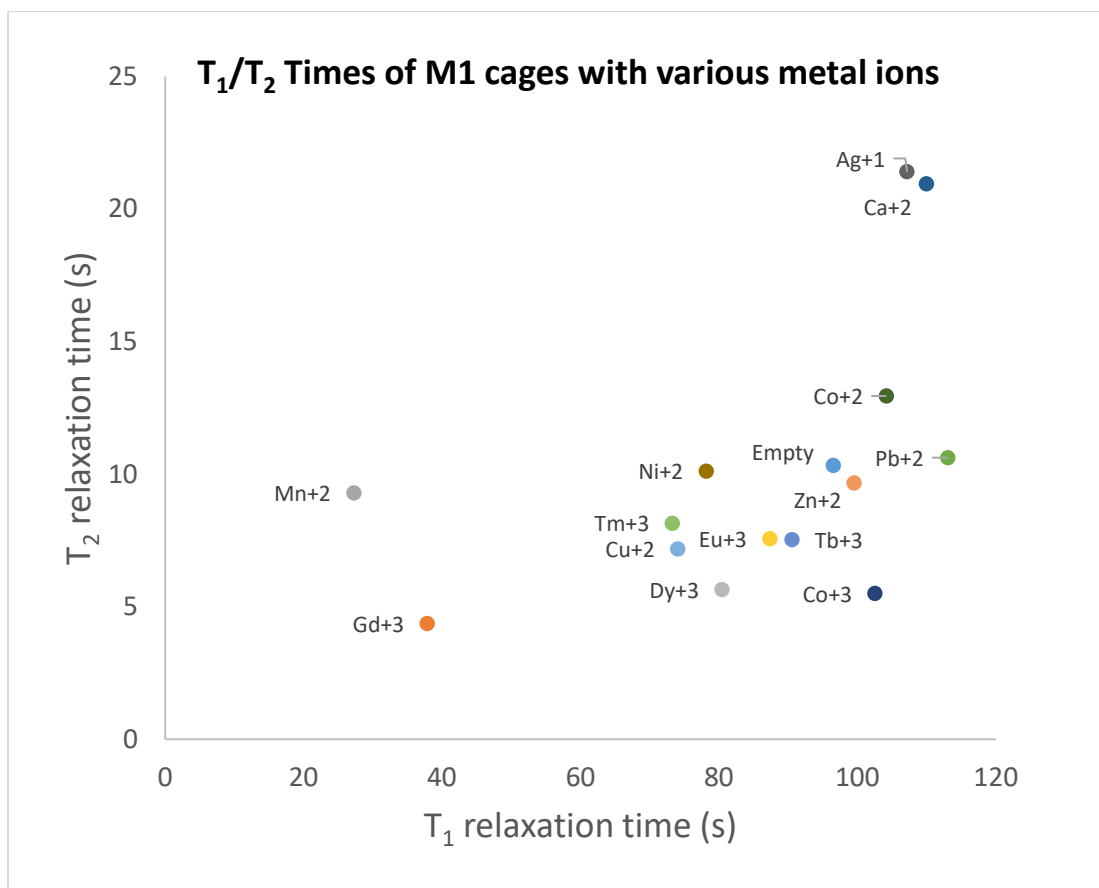
Figure 4.2: *2d plot of 10 micromolar M1 metal complexes. Each paramagnetic metal yields a unique T_1/T_2 signal. T_2 tends to be unaffected by the addition of a relaxation agent except in the case of silver, calcium and gadolinium.*
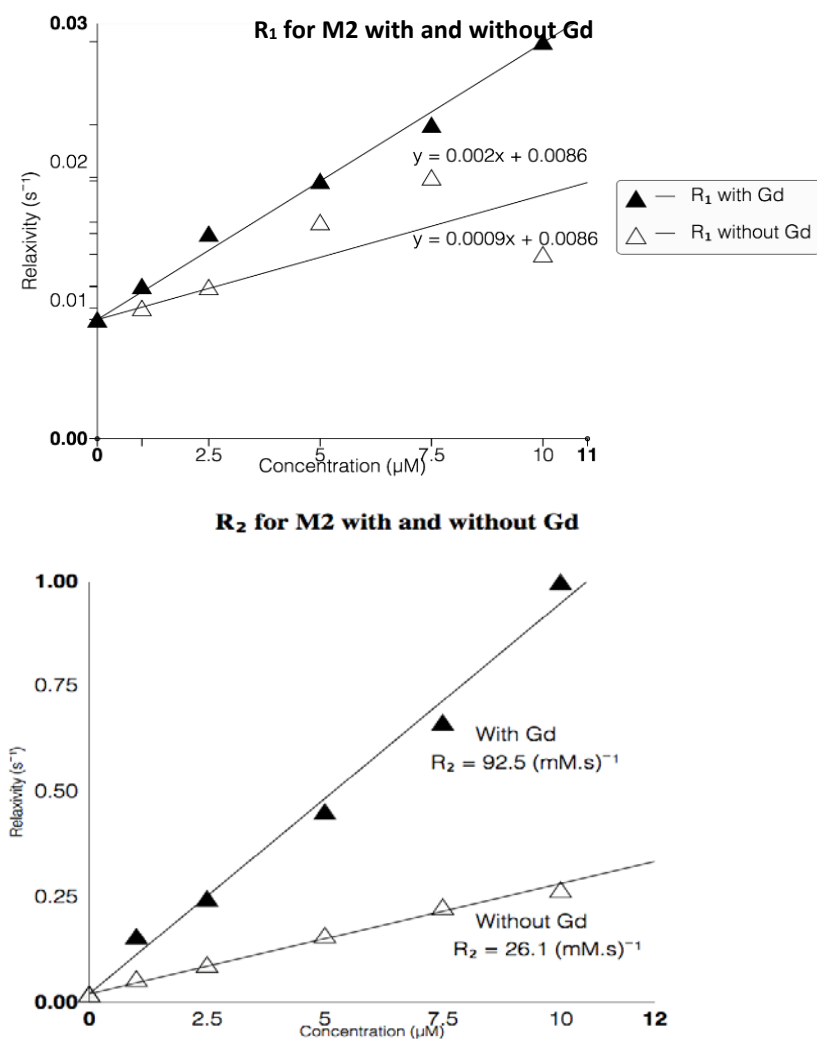
Figure 4.3: *Plot of transverse and longitudinal relaxation rate versus concentration for the M2 cage. Adding the metal increases the relaxivity (rate per concentration) by an order of magnitude, demonstrating how paramagnetic relaxation enhancement can be used to increase xenon relaxation.*

After measuring the paramagnetic relaxation enhancement of different metal ions, the relaxivity of the sensor with and without gadolinium (III) was measured. This ion was chosen because it had the strongest effect on the T_2 of bulk xenon. Figure 4.3 shows how the addition of gadolinium (III) drastically increases the T_1 and T_2 relaxivity of the M2 sensor. While this was expected in the case of T_1, the fact that the metal ion would help decrease the T_2 of xenon was not clear. In the slow exchange limit, the limit of this experiment, the T_2 of the bound xenon should not affect the bulk T_2 measured. Only the exchange rate would affect the T_2 measured[5,6]. But, these metal ion experiments have shown that changing the T_2 of the bound xenon can affect the T_2 of the entire xenon population, despite the xenon cage system being in the slow exchange limit. Nevertheless, these metal ion experiments have shown that it is possible to use changes in the relaxation rate of bound xenon to detect changes in solution, in this case the presence of metal ions. This result is then used to detect avidin in a relaxation based biosensing experiment.

4.3 Bibliography

1.   Aime, S. *et al.* Relaxometric evaluation of novel manganese(II) complexes for application as contrast agents in magnetic resonance imaging. *J. Biol. Inorg. Chem.* **7,** 58–67 (2002).

2.   Borel, A., Helm, L. & Merbach, A. *Molecular Dynamics of Gd (III) Complexes in Aqueous Solution*. (2004).3.   Krzystek, J., Ozarowski, a & Telser, J. Multi-frequency, high-field EPR as a powerful tool to accurately determine zero-field splitting in high-spin transition metal coordination complexes. *Coord. Chem. Rev.* **250,** 2308–2324 (2006).

4.   Alsaadi, B. B. M., Rossotti, C., Williams, R. J. P. & Road, S. P. Electronic Relaxation Rates of Lanthanide Aquo-cations. *Dalt. Transcations* 2147–2150 (1980).

5.   Swift, T. J. & Connick, R. E. NMR-Relaxation Mechanisms of O17 in Aqueous Solutions of Paramagnetic Cations and the Lifetime of Water Molecules in the First Coordination Sphere. *J. Chem. Phys.* **37,** 307 (1962).

6.   McLaughlin, A. C. & Leigh, J. S. Relaxation times in systems with chemical exchange: Approximate solutions for the nondilute case. *J. Magn. Reson.* **9,** 296–304 (1973).

CHAPTER 5: XENON RELAXOMETRY

5.1 Introduction to Relaxometry and its application to Xenon NMR

Relaxometry is an NMR technique where changes in relaxation rates, usually the relaxation rates of water, are monitored in order to gain chemical and physical information about a sample[1]. This technique is extended to hyperpolarized xenon in this chapter. In this example of xenon relaxometry, a cryptophane cage covalently attached to a peptide chain is used as a sensor. While cryptophane biosensors have generally depended on changes in chemical shift as a way to detect protein targets, the sensors discussed in this chapter instead exploit the change in the dynamics of xenon as a sensing method[2,3,4]. These changes in dynamics alter the relaxation of xenon inside the cage and, by rapid exchange with the dissolved bulk of xenon, the relaxation of the entire xenon ensemble. To enable sensing of a specific target we developed molecular sensors that combine a xenon binding cage, cryptophane-A, with a target-binding element. The details of this new technique are discussed in the body of this chapter, including how it may be extended into new targets and made more sensitive.

Conventional xenon NMR requires that the cage peak be resolved from the bulk xenon peak. Even at moderately high fields, resolving the peaks is not a problem, because the cryptophane-associated shift is about 120 ppm from the bulk dissolved xenon. Discriminating free and target-bound sensor is more challenging, because binding-induced shifts are a few parts per million[5]. Since the magnetization from hyperpolarization is independent of field, an alternative sensor was developed that would remove the need to resolve peaks. To this end, a new sensor was prepared for studies of binding induced xenon relaxation, M2B1 (Figure 5.1 and 5.2) that combines cryptophane for binding xenon, a targeting element, and a DOTA chelator to allow introduction of paramagnetic metals.

NMR relaxation rates are sensitive to the magnitude of magnetic interactions of the spins studied (e.g. dipole moments of other spins nearby and chemical shift anisotropy), and also their time dependence, arising from molecular tumbling in solution. The difference in tumbling correlation time between a free sensor and one that is bound to a high molecular weight target was exploited for biosensing[4,6,7,8]. Relaxed xenon in the cage is exchanged into solution at a rate much higher than the relaxation rate of bulk xenon and, hence, affects the bulk xenon relaxation as well. Detection of the target is achieved by determining the change in relaxation rates of the bulk xenon, a form of relaxometry.

It is shown in this chapter that there are significant differences in the relaxation rate for xenon in solution with the sensor alone and xenon in solution with the sensor bound to a macromolecular target, like avidin. The changes are sufficiently large to allow use of relaxation rates to detect the association of the sensor with the target, and hence the presence of the target in the sample. Avidin has been used as a model system, but this sensing principle can be extended to a wide variety of possible targets. The only requirement is that the target is

sufficiently larger than the sensor (2 kDa) to alter the rotational correlation time of the cryptophane cage.

5.2 Synthesis of the sensor

Before the experiment is discussed, the characteristics of the sensor and its synthesis will be briefly summarized. The sensor used in this experiment resembles the ones used before in the literature, with the DOTA chelating agent being the only major change. This sensor was synthesized and purified by the Francis group at UC Berkeley.

Mono-acid cryptophane-A cage was covalently attached to the N-terminus of a seven amino acid peptide chain (KKEEEEE) that was further derivatized with 1, 4, 7, 10-tetraazacyclododecane-1, 4, 7, 10-tetraacetic acid, DOTA, and biotin through the lysine amino groups (Figure 5.1). For binding studies with avidin, which is a tetramer with four biotin sites, the sensor was added to avidin in a 4:1 ratio. DOTA forms very stable complexes with most metals; both metal-free and Gd^{3+}-bound forms were studied.
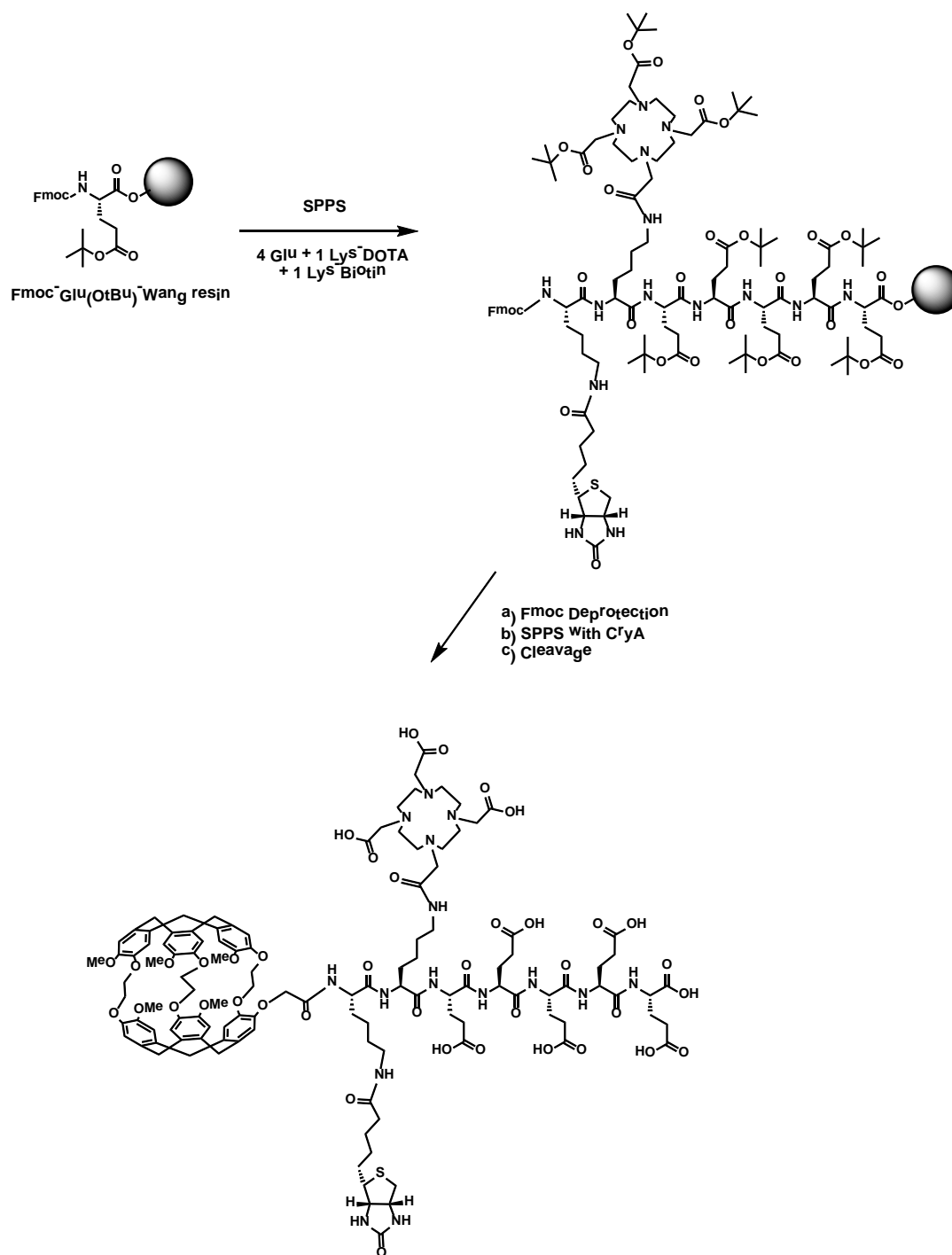
Figure 5.1: *CryA-Biotin-DOTA synthesis scheme.*

The synthesis is shown schematically in Figure 5.1. Fmoc Glutamic acid Wang resin (50 mg, ~ 25 µmol) was prepared for solid phase peptide synthesis (SPPS, purchased from AnaSpec company). After deprotecting fmoc with 20% piperidine 80% DMF (dimethylene formamide) solution (30 min., room temperature), fmoc Glutamic acid (5 equiv.) was added with HCTU (5 equiv.) in DMF for 5 hours. The full attaching was checked with a Kaiser test. Three additional glutamic acids were attached on the resin and cleaved. Fmoc-Lys-mono-amide-DOTA (purchased from Macrocyclics company) and fmoc-Lys(biotin)-acid (purchased from AnaSpec company) were attached by using the same reaction condition except using 2 equivalents of each compound. After cleaving fmoc, 2 fold excess of Cryptophane cage acid (supplied by Kang Zhao, Tianjin University in China) was attached with the same activating compounds for 24 hours. The sample was cleaved using TFA: water: triisopropylsilane (95:2.5:2.5) for 4 hours. A white salt precipitated after adding diethyl ether. The solid was dissolved in water mixed with sodium hydroxide. The dissolved compound was purified by reverse phage HPLC (~1mg). ESI-HRMS ($C_{118}H_{153}N_{15}O_{40}S_1$+2H) calculated for 2454.0120 Found 2454.0240.
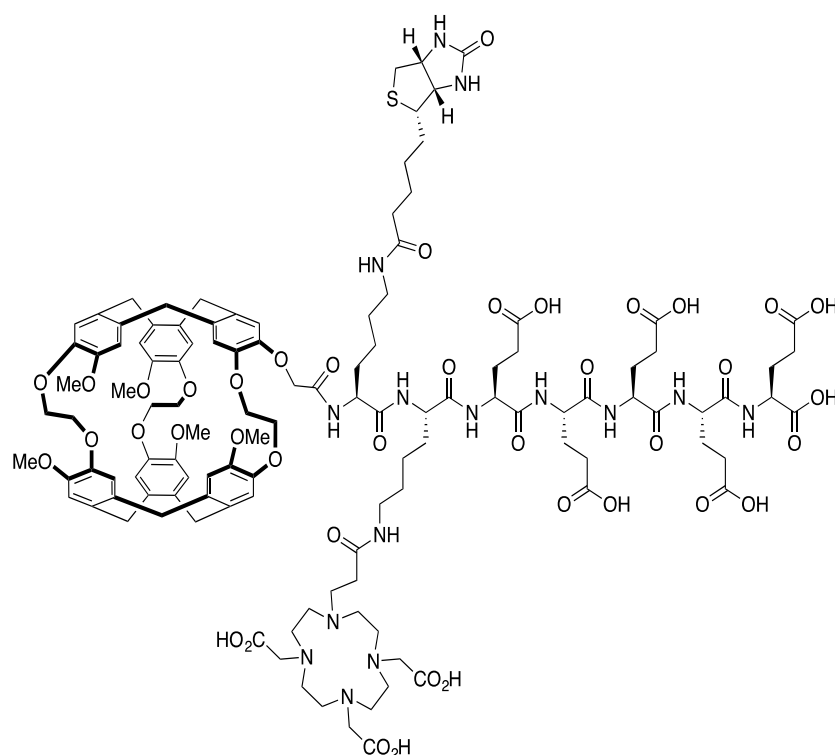
Figure 5.2: *The relaxation sensor, M2B1, consists of a cryptophane cage modified with a DOTA for metal ion chelation, a biotin for avidin binding, and glutamate residues for solubilization. The designation, M2B1, refers to the placement of the metal-binding moiety at position 2 and biotin at position 1 of the peptide chain.*

5.3 Experimental Conditions

It is necessary to carefully list the experimental parameters used for this experiment because relaxation times can be sensitive to small changes in the procedure. For all experiments, the sensors and controls were dissolved in 10 mM PBS (pH 7). Each sample was pressurized to 50 psi with a mixture of 2% natural isotopic abundance xenon gas, 10% nitrogen and 88% helium gas mixture (natural abundance of ^{129}Xe is 26%). ^{129}Xe in this mixture was hyperpolarized using a homebuilt SEOP xenon polarizer and then bubbled into the sample at a flow rate of 0.4 standard L/min. Bubbling was stopped before acquisition to allow bubbles to dissipate. T_2 relaxation times of the bulk xenon resonance were measured with a standard CPMG pulse sequence[9]. The echo time used in this experiment's CPMG sequence was kept short in order to eliminate the diffusion contribution to T_2. T_1 relaxation times of the bulk xenon resonance were measured by means of a single-shot decay signal using a Look-Locker pulse sequence[10]. The flip angle used in the Look-Locker pulse sequence was 20 degrees, small enough not to take too much signal from the z axis but large enough to rotate a detectable amount of xenon into the transverse plane. This sequence minimizes the shot noise of each measurement and reduces the measurement time. Relaxation times for a solution containing stoichiometric amounts of sensor added to avidin were also measured. All data were collected on a 9.4 T Varian Inova NMR spectrometer at 293 K.

5.4 T_2 Xenon Relaxometry

The relaxation of xenon in water is known to be very slow, because fluctuations of the water around xenon are very rapid (see Table 5.1). The addition of M2B1 to the solution decreases the T_2. The broadening of bulk xenon due to exchange in and out of the cage is quite small (less than 1% of xenon is bound, and the exchange rate is $\approx$ 20 s^{-1}), consistent with a modest decrease in relaxation time[11]. The addition of avidin alone to the xenon solution causes exchange broadening, but the process is near the fast exchange limit reflecting transient binding of the xenon. Similar weak binding and broadening of xenon has been seen for many proteins[12]. Adding biotin to a solution of avidin increased the T_2 of xenon, because the biotin-binding pockets of the protein are no longer open to xenon. When M2B1 and avidin are both added to the solution, the biotin on the sensor binds to avidin, and the cryptophane cage is substantially immobilized. The sensor also interacts nonspecifically with avidin which decreases the bulk T_2 of xenon.
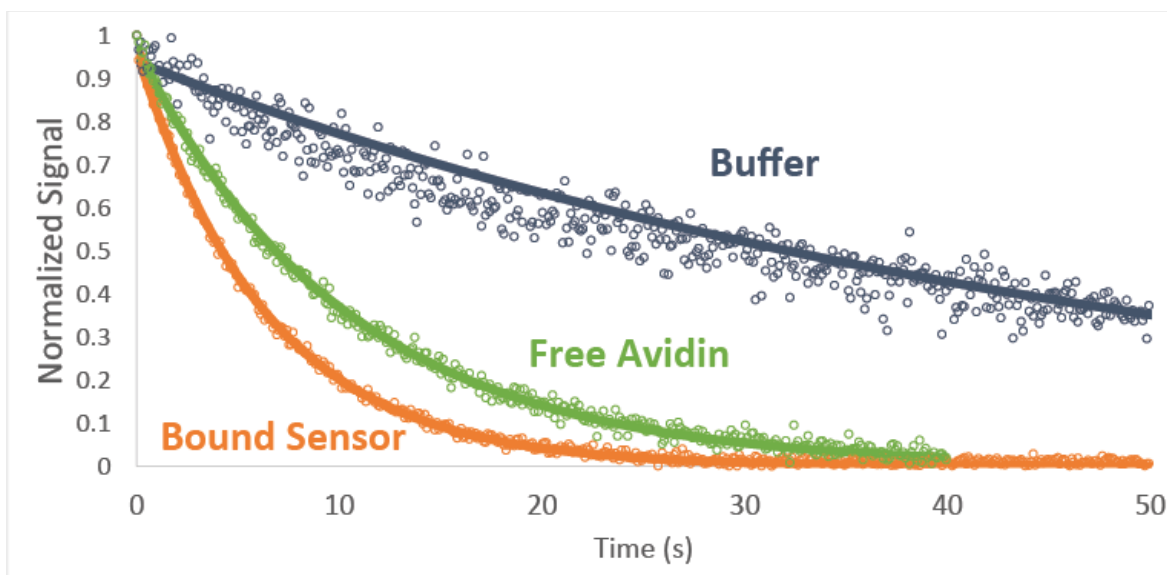
Figure 5.3: *Plot of T_2 relaxation curves of xenon in buffer, xenon with avidin, and xenon with sensor bound to avidin showing dramatic enhancement of relaxation in the complex. In the case of the buffer, relaxation is dominated by the rapid motions of xenon dissolved in water. The correlation time characterizing this motion is very short, resulting in very slow relaxation due to the dipolar coupling between dissolved xenon and water. The avidin and bound sensor cases show how drastically T_2 can be altered by a sample. The addition of these two samples introduces several new ways for xenon to relax. The motion of the gas can be drastically slowed by binding or it can rapidly exchange between sites with different chemical shifts, drastically shortening T_2 in either case.*

Sample	$T_2(s)$
1x PBS buffer	56.4 ± 0.6
5 µM M2B1	28.3±0.4
1.5 µM avidin	11.2±0.2
Biotin saturated 1.5 µM avidin	17.6±0.2
5 µM M2B1 added to 1.5 µM biotin-saturated avidin	7.32±0.08
5 µM M2B1 with 1.5 µM avidin	6.40±0.03
5 µM M2B1 with 130 nM avidin	26.9±0.6

Table 5.1: *Relaxation times of xenon in solutions of sensor and target given as an average and standard deviation of 10 T_2 times collected on the same sample. Each avidin tetramer binds four biotins and may also bind nonspecifically to the sensor.*

Many different interactions between xenon, avidin and the sensor contribute to the relaxation times measured in this chapter. For example, a 1.5 µM solution of avidin (Fig 5.4 A) has a relaxation time of 11 seconds, implying that the xenon has some association with the protein even without the cryptophane sensor. Adding biotin to the avidin solution increased the relaxation time to 17.6 s (Fig 5.4 B) suggesting that part of this interaction included the biotin binding pocket of avidin. Blocking this pocket with biotin keeps xenon from binding to this part of avidin and therefore also increases the bulk T_2. Compare these relaxation times to those of a solution containing the sensor at the concentrations used in this experiment. A 5 µM solution of the cage yields a 28 s relaxation time, longer than even the blocked avidin.

These nonspecific interactions between xenon and the protein are dwarfed by those mediated by the sensor. Mixing the sensor with avidin (Fig 5.4C) reduces the xenon relaxation time to 6.4 s.   The effectiveness of the sensor, however, also depends on nonspecific binding of the sensor to avidin, made possible by the hydrophilic peptide that solubilizes the cryptophane. The pre-mixed biotin-avidin solution (Fig 5.4 D) cannot specifically bind the sensor, so adding it to the solution would, in the absence of any interaction, result in a relaxation time of 10.9 s calculated as the sum of relaxation rates of a solution containing only the sensor and a solution containing only avidin already bound to biotin. The measured relaxation time, however, was lower (7.3 s) confirming that there is a nonspecific sensor-avidin interaction. The sensor specifically bound to avidin relaxes at a rate approximately 40% faster, but strategies to reduce the nonspecific sensor-protein interaction would increase the overall contrast upon specific binding.
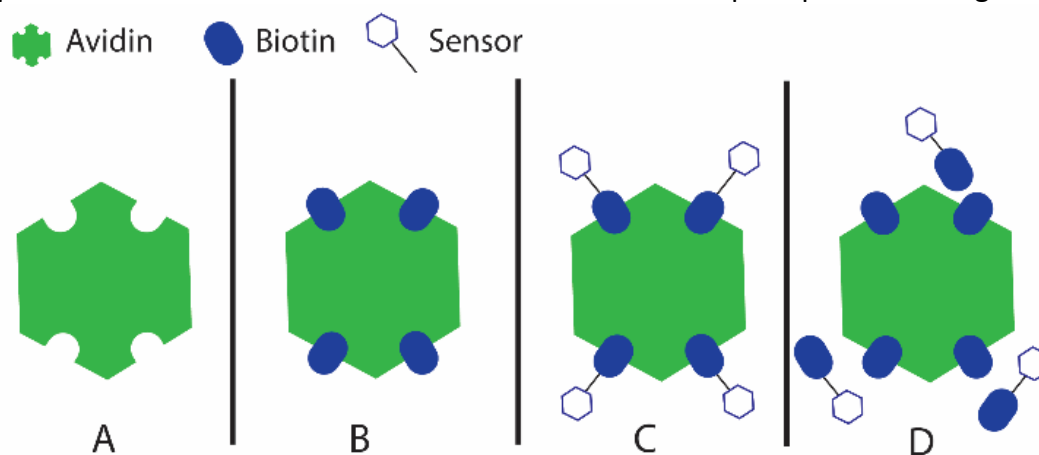
Figure 5.4: *Tested relaxation environments for specific and nonspecific binding interactions with avidin, A corresponds to nonspecific binding of xenon gas to avidin with nothing bound to it; B is the relaxation of xenon with biotin-bound avidin; C is the sensor bound to avidin with the assumption that by adding stoichiometric amounts there is minimal nonspecific binding; D is nonspecific binding of the sensor to avidin bound to biotin.*

This nonspecific interaction between the sensor and avidin is problematic, but it can be fixed with some small changes to the sensor. Due to the small amount of sensor necessary to observe relaxation contrast, shortening the solubilizing linker could significantly reduce

nonspecific interactions while not reducing solubility to the point where it would no longer be effective. The solubility of the sensor is around 300 µM, so it should be possible to shorten its peptide chain without reducing its solubility below 5 µM. It is also possible to imagine generating a solubilizing linker that acts as your targeting moiety for many systems or designing sensors that take advantage of the nonspecific binding.

To calculate the effects of bound state ^{129}Xe T_2 relaxation on the bulk ^{129}Xe, it is necessary to use the Carver Richards equation in its corrected form that treats the second-order exchange process and the effects of the Carr Purcell sequence[13,14]. The analysis shows that exchanged transferred T_2 relaxation can contribute significantly to the bulk xenon relaxation when the occupancy of the cage is significant and the cage bound T_2 relaxation is fast.
The two sites – xenon in solution and xenon in cage – have both a very large chemical shift difference and a dramatically different intrinsic relaxation rate. This makes it necessary to use an exact formulation for the bulk T_2 in a chemically exchanging system as described by Baldwin. The results from the Carver Richards equation were compared to results from Spinach[15], a spin dynamics simulation package for Matlab.

The ratio of the sensor xenon population to the solvent xenon population is less than 0.01. With a sensor concentration of 5 µM and a xenon concentration on the order of 1 mM, more than half the sensors are occupied. The large xenon: sensor concentration ratio behaves in a pseudo first-order manner, with the xenon population incorporated into one of the rate constants. This is shown below:

$$p_g = \frac{[cage]}{[cage] + [cage \bullet xenon]}$$

$$p_e = \frac{[cage \bullet xenon]}{[cage] + [cage \bullet xenon]}$$

$$k_{eg} = p_g k_{ex}$$

$$k_{eg} = p_e k_{ex}$$

$$[cage][xenon]k_{ge} = R_{ge}$$

$$[cage \bullet xenon]k_{eg} = R_{eg}$$

This system qualifies as a pseudo first-order system because the xenon concentration is effectively a constant. Therefore, we introduce a new rate $\tilde{k}_{ge}$ dependent only on cage concentration:

$$\tilde{k}_{ge} \equiv [xenon]k_{ge}$$

$$[cage]\tilde{k}_{ge} = R_{ge}$$

The populations of the ground and excited states, p_g and p_e in the above equations, refer to the fractions of unbound and bound sensors respectively. If more than half of the population is in the excited state, then the Carver Richards equation predicts that the intrinsic T_2 of the excited state will affect the bulk T_2.

These equations are valid in first order and in pseudo first order conditions. However, if most of the cages are occupied in the pseudo first order case, then the Carver Richards equation predicts that the T_2 of the bound site will affect the bulk relaxation rate. This is an exchange-transferred T_2 effect, which is different from the exchange-broadening effect. If half or more of the cages are bound, then the bulk T_2 is significantly affected by the bound T_2. The relevant terms of the Carver Richards equation are shown below, as well as a reworking of the second order binding of xenon to cryptophane to make it a pseudo first order process.

$$h_1 = 2\Delta\omega(\Delta R_2 + k_{eg} - k'_{ge})$$

$$h_2 = (\Delta R_2 + k_{eg} - k'_{ge})^2 + 4k_{eg}k'_{ge} - \Delta\omega^2$$

$$\Delta R_2 = R_{2e} - R_{2g}$$

The relevant mole fractions involve the fraction of bound and unbound cage and not xenon. Xenon is incorporated into the pseudo first order rate constant. The key terms are h_1 and h_2. The sign of the difference between $k_{eg} - k_{ge,}$ present in h_1 and h_2, is important. When k_{eg} is smaller than k_{ge}, or in other words, when p_g is smaller than p_e, the bound T_2 affects the bulk T_2. The results from this equation agree with Spinach simulations using parameters similar to those of a xenon cage experiment. With residence times in the millisecond range and chemical shifts in the 150 ppm range at 9.4 Tesla, both Spinach and these equations predict that the bulk T_2 depends on the T_2 of the excited state and that the xenon is exchanging too slowly for the echo spacing to affect the bulk T_2. Neither Spinach nor the Carver Richards equation takes diffusion through inhomogeneous fields into account, so it is possible that diffusion can contribute to the overall T_2 if the echo spacing is too long. As the bulk T_2 relaxation times of the samples tend to be short, and the external field homogeneous, the echo spacing needed for diffusion to affect T_2 is longer than the spacings used.

5.5 Paramagnetic Contribution to Xenon Relaxometry

A DOTA chelating agent was added to the sensor to investigate using a paramagnetic ion to enhance the binding contrast. The hope was that the shape of the sensor would change upon binding to its target, therefore changing the distance between the xenon inside the cage and the gadolinium (III) inside the DOTA. A small change in this distance would lead to drastic shifts in the paramagnetic contribution to relaxation, which can then be used to detect a target. Unfortunately, these contributions were overwhelmed by other factors, as seen in table 5.2. These results show that binding gadolinium to the chelating agent does not improve the sensitivity of the sensor. The difference between the bound and unbound sensors is greater when the sensor does not contain a gadolinium ion, implying that the paramagnetic contribution when the sensor is bound to the avidin is small. This implies that the DOTA did not get much closer to the xenon inside the cage. It may have even gotten further away. Future work on this subject would require more sophisticated biosensors with better characterized shape changes. Several such molecules exist and are already used in proton NMR[16]. Combining such sensors with a cryptophane cage would allow one to use changes in the distance between xenon and gadolinium for detection.

Sample	$T_2(s)$
1x PBS buffer	56.4 ± 0.6
5 µM M2B1	28.3±0.4
1.5 µM avidin	11.2±0.2
5 µM M2B1 with 1.5 µM avidin	6.40±0.03
5 µM M2B1 with Gd^{3+}	11.2±0.5
5 µM M2B1 with Gd^{3+} and avidin	4.01±0.03
Biotin saturated 1.5 µM avidin	17.6±0.2
5 µM M2B1 added to biotin saturated 1.5 µM avidin	7.32±0.08

Table 5.2: T_2 measurements including gadolinium (III)-chelated M2B1.
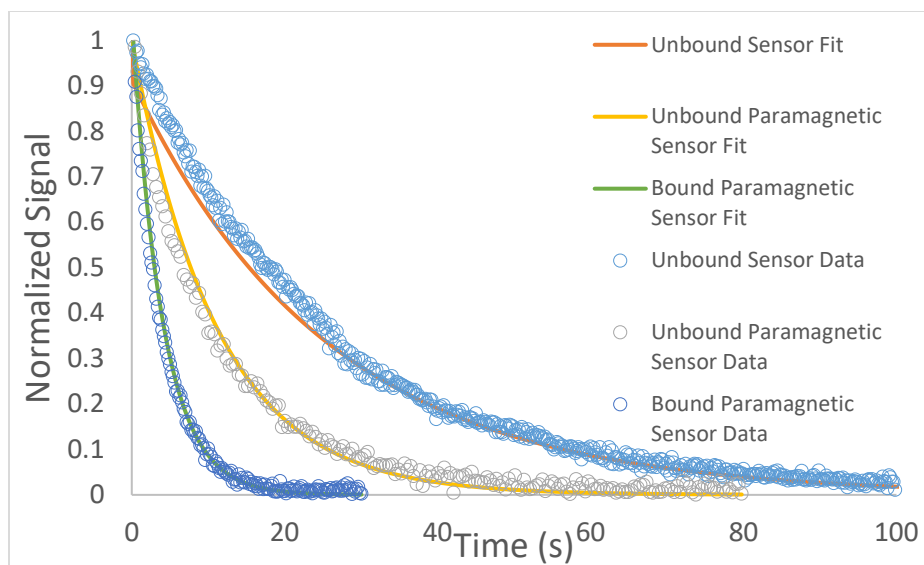
Figure 5.5: T_2 decay curves for the paramagnetic sensors as well as the unbound diamagnetic sensor. Adding gadolinium (III) to the solution lowers the T_2 of the bulk xenon by quite a bit. The T_2 of xenon is lowered even more when the paramagnetic sensor binds to avidin. The sensor still works when it has a paramagnetic metal ion on it, but it doesn't work any better than the sensor without it. This figure also has the decay curve of the sensor without a metal ion or its target. The sensor alone has a very small effect on the bulk T_2 of xenon, suggesting either that the sensor is rotating very rapidly inside the sensor or that the chemical exchange contribution to T_2 is very small.
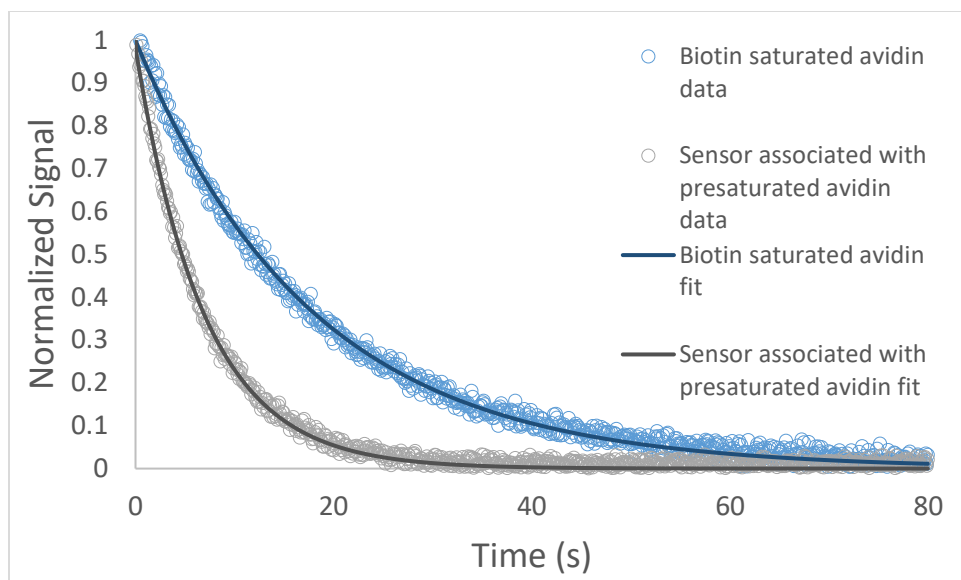
Figure 5.6: T_2 decay curves the samples where avidin was pretreated with biotin. These decay curves reveal that xenon has some affinity for the biotin binding sites of avidin because when biotin is added to a solution containing avidin and no sensor, the T_2 of the solution increases dramatically. It is important to note that the T_2 of a solution of pretreated avidin is still much shorter than the T_2 of a solution of just buffer, implying that xenon still interacts with avidin when the binding sites are blocked. The amount of interactions are just reduced. This figure also shows how the sensor still interacts with avidin even if the binding pockets are prebound with biotin. Once biotin binds with avidin, it is unlikely to leave. This means that the sensor must have another interaction with the avidin besides that of biotin binding to avidin because the T_2 of a solution of sensor and pretreated avidin is much shorter than a solution containing only one of these substances.

5.6 T$_2$ measurement parameters
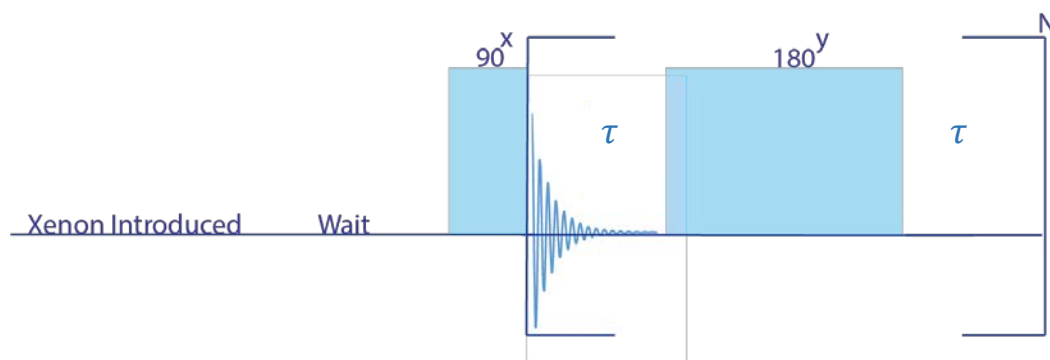
Figure 5.7: The pulse sequence used to measure the T$_2$ of xenon is a CPMG sequence with a bubbling period inserted beforehand. A wait period after the bubbling allows the solution to settle.

Measuring T$_2$ relaxation times can be difficult because of the many contributions to transverse relaxation. So, the experimental details of these experiments are summarized here. Hyperpolarized xenon was bubbled into the sample for 40 s. After waiting one second for the bubbles to dissipate, a non-selective 90 degree pulse centered at the xenon solvent resonance was applied to the sample. An FID was collected after the pulse. After collecting the FID, a non-selective 180 degree pulse, centered at the xenon solvent resonance, was applied to the sample. The 90 degree pulse was 12 μs long. Another FID was then collected after waiting for the signal to refocus. The number of FIDs collected was equal to the number of echoes. Figure 5.7 shows the pulse sequence used to collect T$_2$. The FID integrals are fit to the equation in order to extract a relaxation time:

$$y = Ae^{-t/T_2}$$

The decay curves collected and their fits are shown in figures 5.3, 5.5 and 5.6. T$_2$ is independent of the echo spacing in the slow exchange limit. Nevertheless, decreasing the echo spacing can still increase T$_2$ if there is a significant diffusion contribution to the decay.

Echo Spacing (ms)	T_2 (s)
1000	19.8 ± 0.5
500	32.0 ± 0.6
100	57.0 ± 1
50	56.4 ± 0.6

Table 5.3: *The echo spacing affects the T_2 of xenon in 1x PBS buffer. As the echo spacing increases, the contribution of diffusion to T_2 also increases.*

The table 5.3 shows the T_2 of xenon in 1x PBS buffer as the echo spacing changed. By pulsing quickly, it is possible to refocus the signal faster than the diffusion of xenon through the local gradients. To avoid diffusion, the echo spacing used in these experiments were set to 50 milliseconds.

5.7 T_1 xenon relaxometry

Changes in T_1 were also used as a way to detect the presence of avidin using the M2B1 sensor. All T_1 relaxation times were measured using a Look Locker pulse sequence. With the angle of the sampling pulse known, it is possible to calculate the T_1 of a sample using this pulse sequence. Results from the T_1 experiments are summarized in table 5.4 and the parameters used in the experiments are summarized in table 5.5. The fits to the decay curves collected are shown in figures 5.8 and 5.9. Unfortunately, changes in the T_1 of xenon were mild. The T_1 of a 5 µM solution of the sensor was 132 seconds. Introducing a stoichiometric amount of avidin to that solution only lowered the T_1 to 121 seconds. This change was detectable, which is encouraging, but it was a much smaller than the change in T_2. This makes T_1 a less desirable relaxation time to measure, but there is one advantage to it, its insensitivity to chemical exchange and weak interactions.

Besides the T_1 of the sensors, the other key relaxation time is that with avidin dissolved in buffer. The T_1 of a 1.5 µM solution of avidin is 151 seconds, well within the T_1 of a solution of the buffer alone. This suggests that the contribution of avidin alone to the bulk T_1 of xenon was negligible. Unlike T_2, T_1 is unaffected by rapid exchange between two sites with different chemical shifts. The exchange between these two sites only affects the bulk T_1 by averaging the different T_1 times of the two sites. Therefore, if the T_1 of the bound site is also long, due to the motions of xenon remaining rapid when bound, then the presence of the binding site will not affect T_1.

Sample	T_1(s)
1x PBS buffer	182±26
5 μM M2B1	132 ±3
1.5 μM avidin	151±8
5 μM M2B1 with 1.5 μM avidin	121±4
5 μM M2B1 with Gd^{+3}	126±2
5 μM M2B1 with Gd^{+3} and avidin	128±3

Table 5.4: There is a modest change in the bulk xenon T_1 when the sensor binds to the avidin. Gadolinium does not enhance the change upon binding. The contribution of the small flip angle to the bulk T_1 was removed. The T_1 values are consistent with the work of Zamberlan et al.[17], who measured a relaxivities of 0.1 and 0.416 1/(mM s) for diamagnetic and paramagnetic cryptophanes bound to DOTA. Given those relaxivities, both the diamagnetic and paramagnetic cages should have T_1 values very close to the solvent T_1.

5.8 T_1 measurement parameters:

Xenon was bubbled into the sample for 40 s. After waiting one second for the bubbles to dissipate, a non-selective 20.2 degree pulse centered at the xenon solvent resonance was applied to the sample. An FID was collected after the pulse. After collecting the FID, the signal was allowed to decay. After the signal decayed, another 20.2 degree pulse was applied to the remaining magnetization and another FID was immediately collected. This was repeated for the number of points in the decay curve. The signal was then fitted to a monoexponential decay curve:

$$y = Ae^{-\frac{t}{T_1}}$$

It's important to note that the T_1 measured with this pulse sequence will be shorter than the T_1 measured with a conventional pulse sequence. Every pulse decreases the amount of magnetization, shortening the time needed for the signal to decay to zero. However, the effect of the small flip angle pulses can be corrected for if the flip angle[18]:

$$\frac{1}{T_1} = \frac{1}{T_1^*} + \frac{\ln(\cos(\theta))}{\tau}$$

In the above equation, T_1 is the corrected T_1, while T_1^* is the measured T_1. The angle θ is the small flip angle used to sample the magnetization over time and τ is the time between samplings.

.

Sample	Flip Angle θ	Wait time τ (s)	N
1x PBS Buffer	20.2	100.5	6
5 µM Sensor No metal	20.2	100.5	7
5 µM Sensor with gadolinium	20.2	50.5	10
1.5 µM Avidin	20.2	40.5	15
5µM sensor with avidin and no gadolinium	20.2	18.5	50
5µM sensor with avidin and gadolinium	20.2	18.5	50

Table 5.5: *These are the parameters used in the Look Locker T_1 measurements. Long wait times were used to assure that all transverse magnetization decayed before the next small flip angle pulse.*
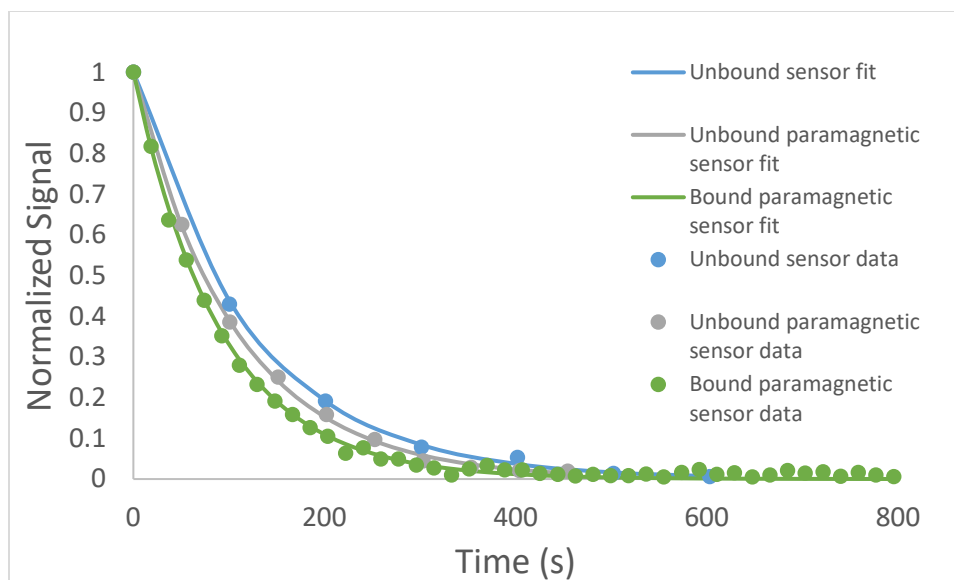
Figure 5.8: T_1 decay curves for the unbound sensor, the unbound sensor with gadolinium (III) and the sensor with gadolinium (III) bound to avidin. There is no diffusion contribution to T_1, so the curves are purely monoexponential. Note that there are much fewer points in this decay curve. This is because each point taken in a small flip angle T_1 experiment removes some signal from the Z axis, artificially shortening the T_1 of the sample. This makes it a bit difficult to measure T_1, although it is possible to back calculate the real T_1 of a sample if the flip angle used in the Look Locker experiment is known. It is also important to note that the changes in relaxation time are much smaller than the changes seen in T_2 experiments. This is because T_1 responds much less drastically to changes in the rotational correlation time at high magnetic fields.
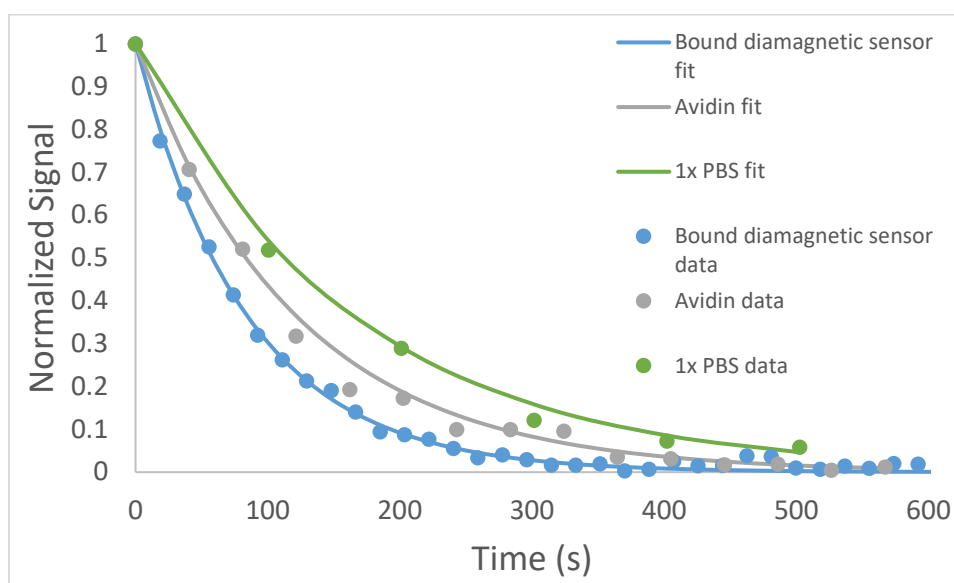
Figure 5.9: T_1 decay curves for the 1x PBS buffer, a solution of 1.5 µM avidin and the sensor bound to avidin. Binding to a diamagnetic sensor reduces the T_1 of the solution by a bit. These changes are not as

dramatic as those seen in T₂ experiments, despite the drastic changes in the rotational correlation time of the sensors upon binding.

Xenon NMR for sensing has exploited binding-induced shifts and saturation transfer for contrast generation, which both require resolution of chemically-shifted peaks. Here we demonstrate that a sensor with a xenon-binding cage can act as a relaxation agent that responds to altered correlation times upon binding a macromolecular target. Even with a moderately-sized protein target there is a dramatic enhancement of T_2 relaxation of the caged xenon, which is transferred to bulk xenon through exchange. There is also a small, but detectable change in the bulk T_1 relaxation of xenon. This effect does not require chemical shift resolution, making low field applications of this technique feasible. The relaxation effects will be increased for larger target molecules, because T_2 relaxation scales with molecular weight.

5.9 Low Field Xenon Relaxometry

This sensor based experiment should be repeated at low magnetic fields, ideally below a Tesla. Instead of measuring T_2, T_1 should be measured because it should be less affected by other factors besides changes in the rotational dynamics of xenon. Lacking the contribution of chemical exchange, T_1 based experiments should be sensitive only to the presence of the sensor and changes to the sensor's correlation time at these low magnetic fields. By measuring T_1 at low magnetic fields, one can perform these sensing experiments with greater sensitivity and selectivity, with the relaxation signal being dominated by the dynamics of the sensor.

Figures 5.10 and 5.11 show what one can expect from low field xenon relaxometry. At the fields commonly used in commercial high frequency spectrometers, the T_1 of the bound xenon is insensitive to changes in the rotational correlation time after crossing a certain threshold. At very high correlation times, the relaxation rate even begins to decrease when the xenon's motions become slower. Lowering the fields, however, changes this behavior. The correlation time that yields the maximum relaxation rate gets greater and greater. Eventually, the relaxation rate stops reaching a maximum and simply increases linearly with the correlation time, as seen in the curve for relaxation at Earth's field.
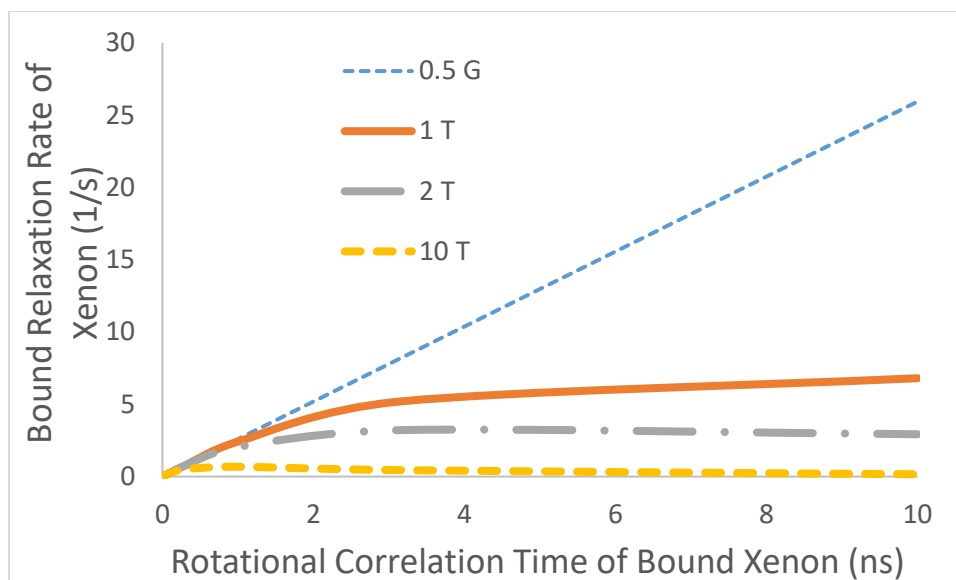
Figure 5.10: Plot of the R_1 of xenon inside the cryptophane cage. As the correlation time increases, the relaxation rate generally increases as well, except at high magnetic fields. At 10 Tesla, the relaxation rate peaks at a rotational correlation time of about 1000 picoseconds. The most important feature of this plot is that the change in relaxation rate as a function of rotational correlation time is steepest at low magnetic fields. While Earth's field is plotted here, there is a similar curve at 0.1T.
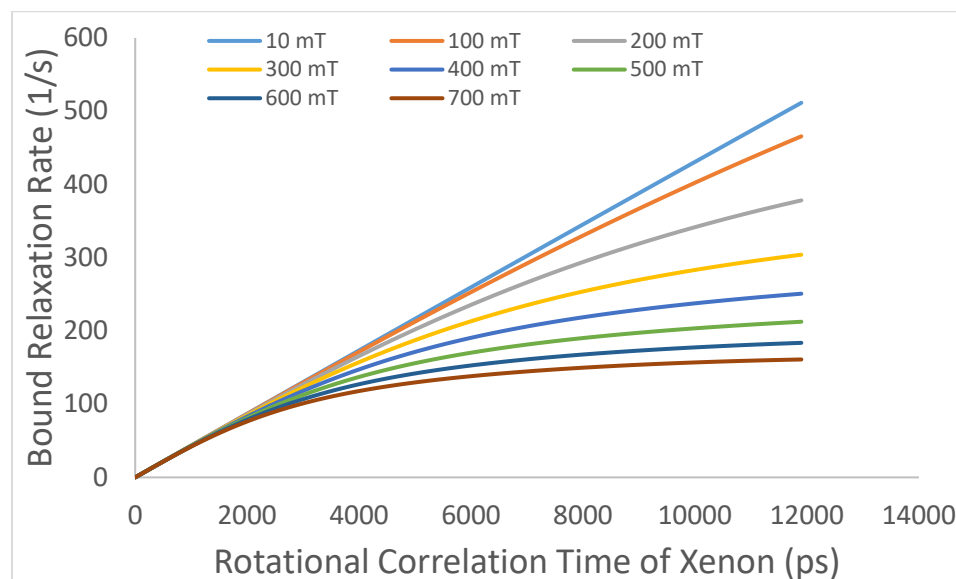
Figure 5.11: This plot takes a closer look at the effect of the external magnetic field on T_1 relaxation. The slope of R_1 as a function of relaxation reaches a maximum at about 10 mT. Below that, it tends to stay the same until the field gets well below a nanoTesla. Relaxation dynamics at those fields are not well understood.

It is necessary to go to lower fields to make R_1 more sensitive to changes in the rotational correlation time. As figure 5.11 shows, one needs to get down to about 10 mT before R_1

becomes a linear function of the rotation correlation time. This is the ideal regime to occupy because it is also where the slope of R_1 versus the rotational correlation time is greatest.

 When examining these graphs, it is important to remember that the relaxation rates plotted on them are the rates of the xenon bound to the M2B1. The rates actually measured would depend on the exchange between the xenon inside and outside the cage. The effect of this exchange on R_1 can be calculated by treating the cryptophane cage like a T_1 relaxation agent relaxing the bulk xenon population. An equation for this, taken from the relaxation chapter, is shown below. So long as the bound T_1 times are greater than the exchange time, changes in them should be noticeable in the bulk T_1.

$$\frac{1}{T_{1,bulk\ xenon}} = \frac{p_m}{\tau_m + T_{1,bound\ xenon}}$$

$$p_m = Fraction\ of\ bulk\ xenon\ bound\ to\ a\ cage.$$

Switching from measuring T_2 to T_1 requires more than altering an experiment. At high magnetic fields, T_1 barely changes when the xenon is significantly immobilized. This is both predicted by theory, and demonstrated by experiments. So, these T_1 experiments should be repeated at low magnetic fields, ideally 10 mT. That field is ideal because the slope of R_1 as a function of the correlation time stops increasing if the field is lowered past that. Working at fields below that would not make the experiment any worse, but it wouldn't make them any better either. There are two ways to perform this low field experiments, each of which will be discussed.

Field cycling is the most obvious way to measure the T_1 at low magnetic fields. It is the method of choice for measuring the T_1 of proton samples at very low magnetic fields. The principle is very simple. The sample is placed in a NMR probe inside an electromagnetic capable of rapidly altering the magnetic field it produces. The NMR probe can be tuned to a Larmor frequency that the electromagnet can induce in the sample. Once the sample is placed inside the field cycling relaxometer, the electromagnet is set to a very high magnetic field in order to polarize the sample. After building up polarization, the field is rapidly cycled down to a very low field, the field at which one wants to measure the relaxation of the protons in the sample. Once the sample has relaxed for the desired amount of time, the field is brought back up until the probe is resonant with the sample's Larmor frequency. The sample is then excited and its FID is collected. This procedure is repeated many times with the amount of time spent in the very low field increased. By plotting the amplitude of the signal as a function of time spent at the very low magnetic field, one can extract the T_1 of the sample at that field. This method is well established in the literature[19].

While this method has good sensitivity, the time spent waiting for the magnet to reach its field can be a problem. The electromagnet cannot instantaneously change its magnetic field, so some time is spent relaxing during this rise time. A similar experiment could also be done with a shuttling system. In this version of the field cycling experiment, the magnetic field is kept static. Instead, the sample is shuttled from the high field region to a low field region to relax. After relaxing, its shuttled back into the high field region for detection. Like the method based on the

electromagnet, this method suffers from the need to wait while the sample reaches its desired magnetic field.

Xenon would be well suited to either variety of field cycling experiment. The polarization step in the field cycling experiments would just be replaced by bubbling in hyperpolarized xenon. These field cycling instruments are not capable of generating very high magnetic fields. Fields of about 1 to 2 Tesla are about the best one can expect. This means that proton samples will have relatively low SNR due to relying on thermal polarization at these small fields. The same is not true for xenon. As mentioned before, xenon can be hyperpolarized, meaning that the only SNR loss expected from going to low fields comes from the lower frequency of the coil, a disadvantage shared by thermally polarized samples. Xenon also generally has a longer relaxation time than proton samples, meaning that the time spent ramping the current of the electromagnet up or down or shuttling from place to place will have less of an effect on both the measured relaxation time and also the SNR.

The main problem to consider is the shot noise of the xenon. As mentioned before, the amount of xenon introduced into a sample tends to vary, meaning that the relaxation curve should be collected all at once if possible. This means that the xenon sample, after being allowed to relax at the low field, should be excited with a small flip angle pulse when the magnet is at its detection field.

Alternatively, one could keep the magnetic field low and build a coil tuned to xenon's Larmor frequency at that field. This is more feasible with xenon than with other nuclei because the polarization will remain the same regardless of field. The sensitivity of hyperpolarized xenon is therefore only linear with regard to the external field strength instead of quadratic. At fields of about 10 mT or so, it would no longer be necessary to measure T_1 with a small flip angle pulse sequence either. Measuring T_2 with a CPMG would give one essentially T_1 because of the absence of measurable frequency differences at such low fields. Regardless of how one chooses to measure relaxation times, doing so with a field cycling relaxometer would be the most straightforward way to go about doing so.

5.10 Bibliography

1. Koenig, S. H. Dynamics of Water in Biological Systems: Inferences from Relaxometry. *Encycl. Magn. Reson.* (2007). doi:10.1002/9780470034590.emrstm0144

2. Huber, G. *et al.* Water soluble cryptophanes showing unprecedented affinity for xenon: candidates as NMR-based biosensors. *J. Am. Chem. Soc.* **128,** 6239–46 (2006).

3. Roy, V. *et al.* A cryptophane biosensor for the detection of specific nucleotide targets through xenon NMR spectroscopy. *Chemphyschem* **8,** 2082–5 (2007).

4. Lowery, T. J. *et al.* Optimization of xenon biosensors for detection of protein interactions. *Chembiochem* **7,** 65–73 (2006).

5. Garimella, P. D. *et al.* Hyperpolarized xenon-based molecular sensors for label-free detection of analytes. *J. Am. Chem. Soc.* **136,** 164–8 (2014).

6.   Hall, L. D., Evans, S. D. & Nott, K. P. Measurement of textural changes of food by MRI relaxometry. *Magn. Reson. Imaging* **16,** 485–492 (1998).

7.   Jaeger, F., Bowe, S., Van As, H. & Schaumann, G. E. Evaluation of 1H NMR relaxometry for the assessment of pore-size distribution in soil samples. *Eur. J. Soil Sci.* **60,** 1052–1064 (2009).

8.   Allsopp, K., Wright, I. Lastockin, D., Mirotchnik, K., Kantzas, A. Determination of oil and water compositions of oil / water emulsions using low field NMR relaxometry. *J. Can. Pet. Technol.* **40,** 58–61 (2005).

9.   Meiboom, S. & Gill, D. Modified spin-echo method for measuring nuclear relaxation times. *Rev. Sci. Instrum.* **29,** 688–691 (1958).

10.   Look, D. C. Time Saving in Measurement of NMR and EPR Relaxation Times. *Rev. Sci. Instrum.* **41,** 250 (1970).

11.   Spence, M. M. *et al.* Development of a functionalized xenon biosensor. *J. Am. Chem. Soc.* **126,** 15287–94 (2004).

12.   Rubin, S. M., Spence, M. M., Pines, a & Wemmer, D. E. Characterization of the effects of nonspecific xenon-protein interactions on (129)Xe chemical shifts in aqueous solution: further development of xenon as a biomolecular probe. *J. Magn. Reson.* **152,** 79–86 (2001).

13.   Carver, J. P. & Richards, R. E. A general two-site solution for the chemical exchange produced dependence of T2 upon the carr-Purcell pulse separation. *J. Magn. Reson.* **6,** 89–105 (1972).

14.   Baldwin, A. J. An exact solution for R2,eff in CPMG experiments in the case of two site chemical exchange. *J. Magn. Reson.* **244,** 114–24 (2014).

15.   Hogben, H. J., Krzystyniak, M., Charnock, G. T. P., Hore, P. J. & Kuprov, I. Spinach - A software library for simulation of spin dynamics in large spin systems. *J. Magn. Reson.* **208,** 179–194 (2011).

16.   Choi, J. *et al.* Distance-dependent magnetic resonance tuning as a versatile MRI sensing platform for biological targets. *Nat. Mater.* (2017). doi:10.1038/nmat4846

17.   Zamberlan, F. *et al.* Molecular Sensing with Hyperpolarized [129] Xe Using Switchable Chemical Exchange Relaxation Transfer. *ChemPhysChem* n/a-n/a (2015). doi:10.1002/cphc.201500367

18.   Li, W., Scheidegger, R., Wu, Y., Vu, A. & Prasad, P. V. Accuracy of T1 measurement with 3-D Look-Locker technique for dGEMRIC. *J. Magn. Reson. Imaging* **27,** 678–82 (2008).

19.   Kimmich, R. & Anoardo, E. *Field-cycling NMR relaxometry*. *Progress in Nuclear Magnetic Resonance Spectroscopy* **44,** (2004).

CHAPTER 6: DISTANCE DEPEDENT MAGNETIC RESONANCE TUNING (D-MRET)

6.1 Introduction to Quencher and Enhancer Proton Relaxation Enhancement

The principles discussed in the previous chapter on xenon relaxometry can be extended to a water based sensor as well. Like the cryptophane cage based relaxation agents, these sensors respond to the presence of a target by altering their relaxivity. This is an interesting variation in MRI contrast agent design because it means that the agent does not need to accumulate in a particular region of the body. Instead, a change in relaxation will indicate the presence of a target. These responsive sensors have tremendous potential as proton MRI contrast agents and maybe also as models for future xenon biosensors.

The proton relaxation agents discussed in this chapter rely on a novel method, called D-MRET (Distance dependent Magnetic Resonance Tuning) for changing the relaxivity of a chelated metal. These sensors are built from two components: a quencher and an enhancer. The names to of these components refer to their effect on the longitudinal relaxation rate of water. The enhancer is a chelated gadolinium (III) ion, so called because it makes water relax much more quickly[1]. The quencher is a bit different. It doesn't quench the relaxation of water on its own; in fact the quencher used in this experiment is a super paramagnetic $Zn_{0.4}Fe_{2.6}O_4$ nanoparticle, designed to drastically increase the transverse, but not the longitudinal, relaxation rate of water[2]. Instead, the quencher interferes with the enhancer's ability to relax water[3]. The closer the enhancer gets to the quencher, the slower the water relaxes. This phenomenon therefore allows one to design a biosensor based on changing the distance between the enhancer and the quencher when a target is present. Thus far, sensors have been developed that change the distance between the two by cleaving the link between them, creating a link between them, and folding the link between them. With a cleaving based sensor, the IBS institute went on to detect MMP2 (matrix metalloproteinase) an enzyme known to be present at tumors, in invitro and invivo studies[4].

6.2 Water Paramagnetic Relaxation Enhancement

To understand how this new biosensor works, it is necessary to review how paramagnetic contrast agents affect the relaxation rate of water. In MRI and NMR, paramagnetic ions and superparamagnetic nanoparticles are used to increase the relaxation rate of various samples. The unpaired electrons of these contrast agents rapidly relax the nuclear spins around them. Water is especially affected by these contrast agents because it will bind directly to them. For example, gadolinium (III) will bind nine different water molecules in solution, rapidly relaxing each one[5]. Once bound, the water will remain on the gadolinium for a long time, roughly a few microseconds. This exchange time can be much longer than the rotational correlation time of the water gadolinium complex and the relaxation time of the electron spin[6].
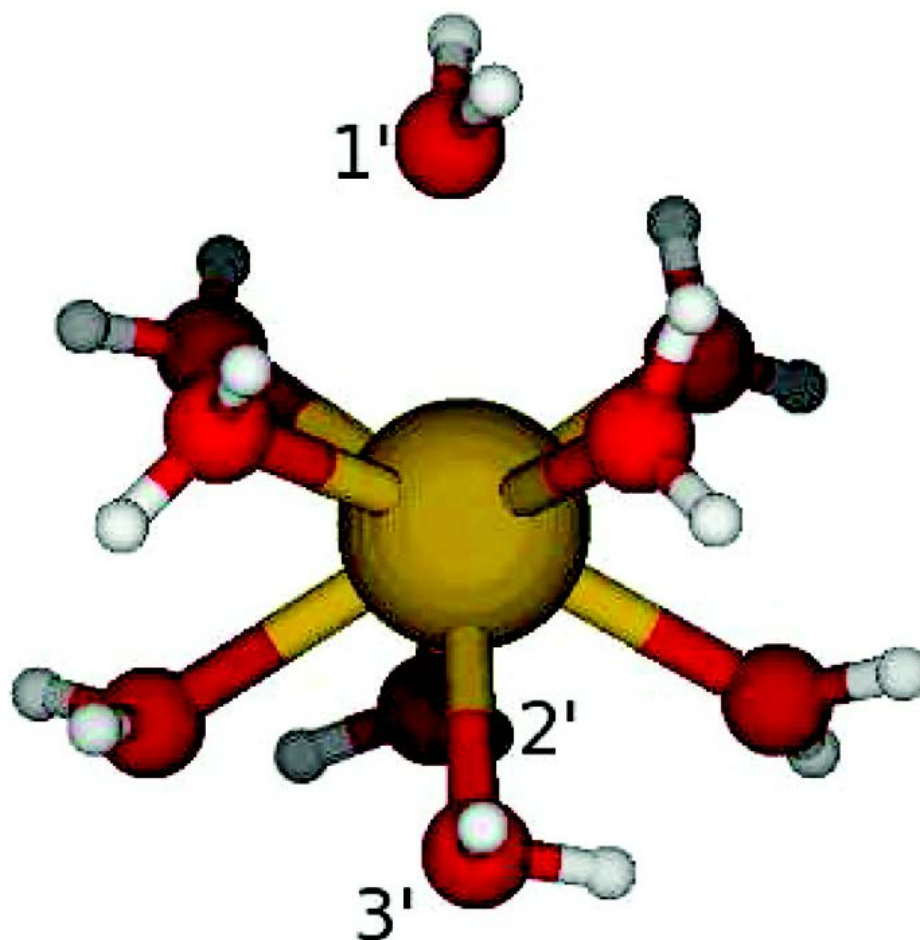
Figure 6.1: *This is the structure of a gadolinium (III) ion bound to nine water molecules. The ninth water molecule is more loosely associated with the metal ion than the others[7].*

Once bound, the relaxation rate of water can change dramatically. Since the exchange time is too long to affect the dipolar coupling between the water and the unpaired electrons, the two times to consider are the rotational correlation time and the relaxation time of the electronic spin[8,9]. In the case of a bare metal ion, the rotational correlation time will be very short, roughly 35 picoseconds[10]. Once the ion is chelated in a molecule like DOTA, the rotational correlation time of the unpaired electrons will increase to a few nanoseconds, depending on the size of the chelating agent[10]. This time can be further increased by tethering the DOTA to a large particle, as done in the quencher and enhancer experiments[11]. This will further increase the rotational correlation time of the water metal complex, leaving the electronic relaxation as the main correlation time.

It is important to carefully examine the relaxation of electrons if their relaxation time is responsible for the relaxivity of a paramagnetic contrast agent. Different ions have drastically different effects on the relaxation rate of water, due mostly to variations in their electronic relaxation times. Some dissolved ions, like gadolinium (III), have electronic T_1 times in the nanoseconds, making them especially suited for MRI contrast[12]. Other Lanthanides are not so

suitable because of their extremely short electronic T_1 times[13]. The electronic T_1 of a dissolved ion can get as low as a few picoseconds, making it much shorter than the rotational correlation time of a chelated metal ion. The overall correlation rate is the sum of the individual correlation rates of the dipolar coupling between the unpaired electrons on the metal ion and the water complexed to the ion. So a paramagnetic metal ion with a short electronic relaxation time will not relax water efficiently because the electronic relaxation rate will be much greater than the other correlation rates.
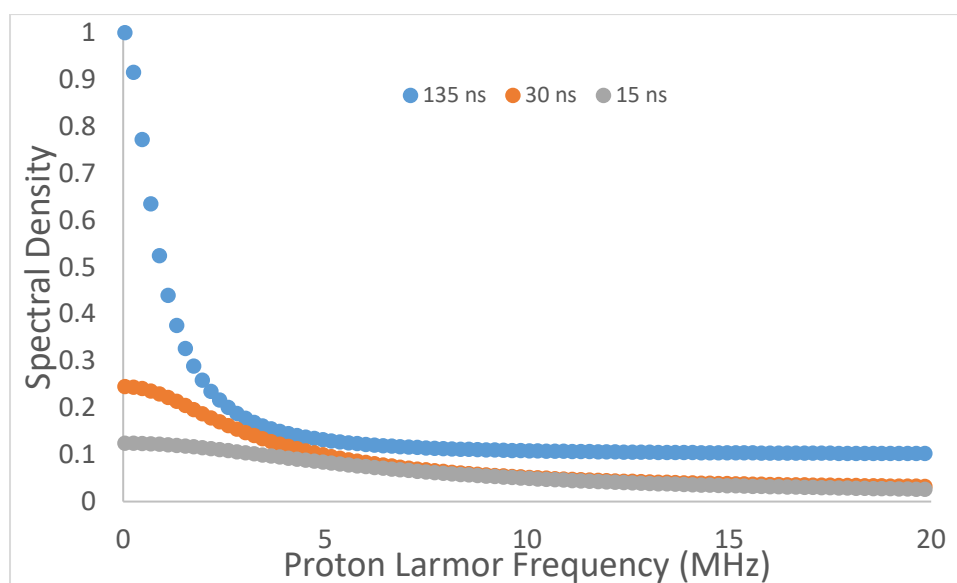
Figure 6.2: As the rotational correlation time increases, the spectral density function of the dipolar coupling between two spins becomes narrower. The effect of this narrowing depends on the strength of the external magnetic field. Notice how the lines intersect at various fields. At about 10 MHz, the 15 ns correlation time sample relaxes a little faster than the 30 ns correlation time sample. The three curves approach one another as the magnetic field gets larger. At low magnetic fields, the slow interaction relaxes best. More importantly, a difference in correlation time results in a bigger difference in relaxation at low magnetic fields. Extremely rapid interactions would result in essentially flat spectral density functions.

With this in mind, the relaxation of water bound to the enhancer is determined by the relaxation rate of the unpaired gadolinium (III) electrons. The other time constants are roughly a few microseconds, much longer than the nanosecond relaxation times expected for a metal ion dissolved in water. Rotational correlation times tend to be a few nanoseconds for small molecules, but are much longer in this case because the chelating agent is covalently attached to a large nanoparticle. The effect of changing rotational frequencies on the bound relaxation rate is shown in figure 6.2. However, this does not mean that changes in the exchange times are irrelevant. While the rate of exchange between the bound water and the free water does not affect the relaxation rate of the water on the metal, it does affect the relaxation of the entire solvent. The exchange rate determines how quickly the relaxed water mixes with the rest of the population, changing the overall observed relaxation rate.
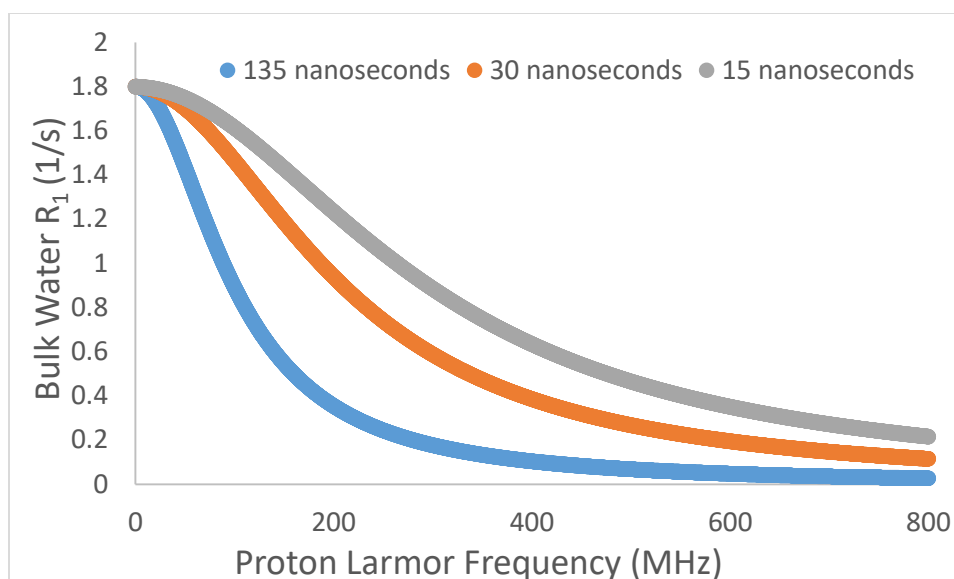
Figure 6.3: *It is important to remember that the relaxation of the water bound to the Gd ion cannot be directly observed. The effect of the paramagnetic ion is instead measured by monitoring changes in the bulk water relaxation. This has a few implications, shown in this plot of the bulk water relaxation rate for samples with different overall correlation rates, shown in the legend, and an exchange time of 10 μs. The first is that the rate of exchange limits the effect of the gadolinium on the water. If the rate of relaxation of water is much greater than the rate of exchange, then the parameter that determines the relaxivity of the gadolinium is the exchange rate. In this regime, the water relaxes and then stays on the gadolinium after relaxing. This means that the relaxed water cannot be observed until it leaves the ion. This decreases the effect of paramagnetic ions and also eliminates the cross overs seen in figure 6.2.*

With this in mind, there are two parameters to consider when discussing a quencher enhancer biosensor: the exchange time and the electronic relaxation time. Both of these times change when the enhancer is brought closer to the quencher. It is possible to distinguish between a change in the exchange time and a change in the electronic relaxation time by measuring the effect of the external magnetic field on the relaxation of water. The electronic relaxation time affects the shape of the spectral density function governing the relaxation of water. A sample with a different electronic relaxation time will have a different response to the field. If the relaxation time is very short, then the biosensor will be insensitive to changes in the magnetic field and if it is long it can be very sensitive to field changes. The same is not true for the exchange time. Changing the exchange time will not alter the sensor's sensitivity to the external magnetic field because the exchange time is much longer than the T_1 of the unpaired electrons. Therefore, if the exchange time of water changes when the enhancer approaches the quencher, then the spectral density of the water should remain the same. This approach works so long as the bound relaxation time is longer than the exchange time. If the exchange time is much longer than the bound relaxation time for all variations of the biosensor, then changes in the spectral density will be undetectable. Figure 6.3 gives as example of how the exchange time can mask changes in the spectral density function. These dynamic constants can be extracted from the data and then used to figure out how the quencher affects the enhancer.

The water relaxivity of various sensors was measured and fitted to the equations below. Only the overall correlation time and the exchange time were used as fit parameters, with the rest of the parameters treated as constants. All fitting was performed using a nonlinear least squares fitting algorithm bundled with matlab. The scalar contribution to relaxation was excluded from this fit because of its relatively small contribution to relaxation[14].

$$R_{1\ bound\ proton} = \frac{2}{15} * S(S+1) * b^2 * (\frac{\tau_{c2}}{1 + (\omega_S - \omega_I)^2 \tau_{c2}^2} + \frac{3\tau_{c1}}{1 + \omega_I^2\ \tau_{c1}^2} + \frac{6\tau_{c2}}{1 + (\omega_S + \omega_I)^2 \tau_{c2}^2})$$

$$\omega_S = Larmor\ Frequency\ of\ electron\ in \frac{rad}{s}$$

$$\omega_I = Larmor\ Frequency\ of\ proton\ in \frac{rad}{s}$$

$$\frac{1}{\tau_{c1,2}} = Summed\ Correlation\ rates\ in\ Hz.$$

$$\frac{1}{\tau_{c1,2}} = \frac{1}{T_{1,2e}} + \frac{1}{\tau_m} + \frac{1}{\tau_r}$$

$$\tau_m = proton\ exchange\ time\ when\ bound\ to\ Gd\ ion$$

$$\tau_r = proton\ rotational\ correlation\ time\ when\ bound\ to\ Gd\ ion$$

$$T_{1,2e} = Electronic\ relaxation\ time\ in\ seconds$$

$$b = dipolar\ coupling\ between\ bound\ water\ and\ unpaired\ electrons\ in\ 1/s$$

$$S = number\ of\ unpaired\ electrons\ on\ the\ metal\ ion$$

6.3 Silica Layer model system

In order to study how the distance between the quencher and enhancer affects the relaxivity of the sensor, several different types of nanoparticles were prepared as model systems. These nanoparticles had a zinc iron oxide core and a layer of silica surrounding it. Hundreds of gadolinium (III) ions chelated to DOTA are attached to the silica surface with a peptide chain. Several different batches of these nanoparticles were made, each with a different silica layer thickness. By altering the thickness of the silica layer, the distance between the gadolinium (III) DOTA and the super paramagnetic core could be controlled. A cartoon of this effect is shown in figure 6.4 and TEM images of the different model sensors are shown in figure 6.6. The relaxivity of these sensors was then measured at multiple fields so that the dynamics relevant to relaxation could be estimated.
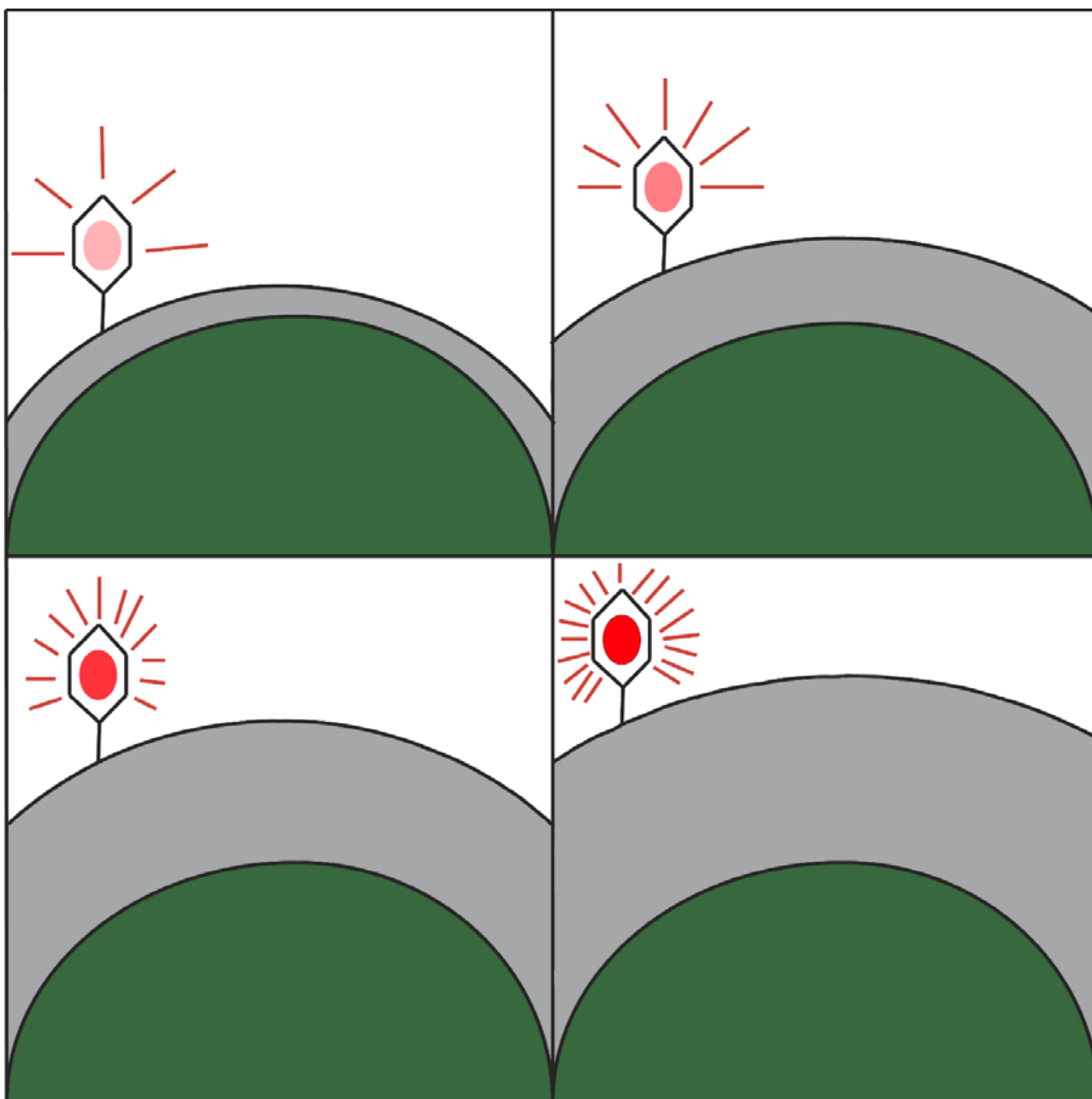
Figure 6.4: *A nanoparticle is coated with a layer of silica and a chelated metal ion is covalently attached to the silica layer. The relaxation effect of the ion can be tuned by changing the thickness of the silica layer. When the layer is thin, the relaxivity of the ion is quenched and when the layer is thick, the relaxivity returns. Therefore, the nanoparticle is called a quencher and the chelated metal ion is called an enhancer in D-MRET. The thickness of the silica layer ranged from 5 nm to 20 nm.*

These sensors with silica layers of varying thicknesses all had different proton relaxivities. As the silica layer got thinner, the relaxation rate of water got slower. The relaxation rate of each nanoparticle was then measured at multiple fields in order to understand why the thickness of the silica layer affected the relaxivity of the enhancer. There doesn't seem to be any obvious reason why getting closer to the nanoparticle core would affect the relaxivity of the gadolinium (III) DOTA. Many different explanations were explored. While increasing the thickness of the outer layer could drastically increase the rotational correlation time of the enhancer quencher pair, this increase would not affect the relaxation of the water bound to the enhancer. The

nanoparticles used, even with the thinnest silica layer were large enough to rotate with correlation times of a few microseconds. This rotation is far too slow to compete with the relaxation rate of the electron.
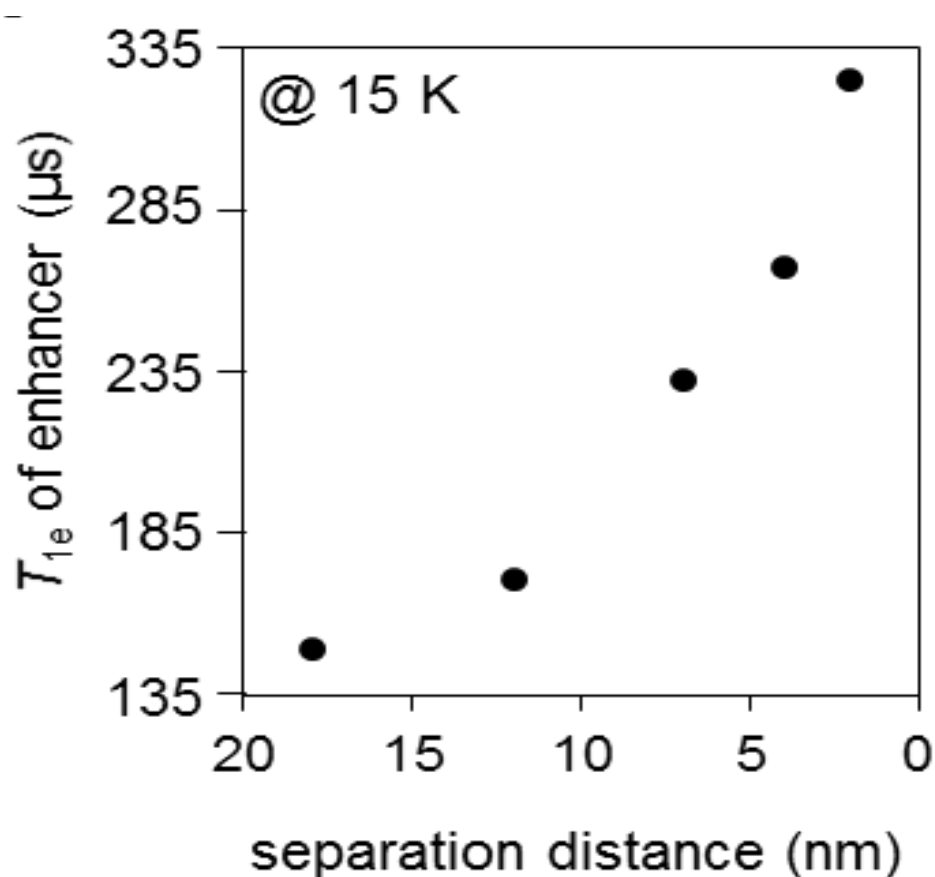
Figure 6.5: *These are the electronic relaxation times of the gadolinium (III) ions attached to the surface of the model nanoparticles studied in this experiment. The further the ion gets away from the nanoparticle, the longer its electronic relaxation time becomes. This distance between the nanoparticle and the ion is controlled by changing the thickness of the silica layer that separates the two. These experiments were conducted in the solid state at very low temperatures because the electronic relaxation times are too short to easily measure in the solution state. Reproduced with permission from Choi et al[3].*
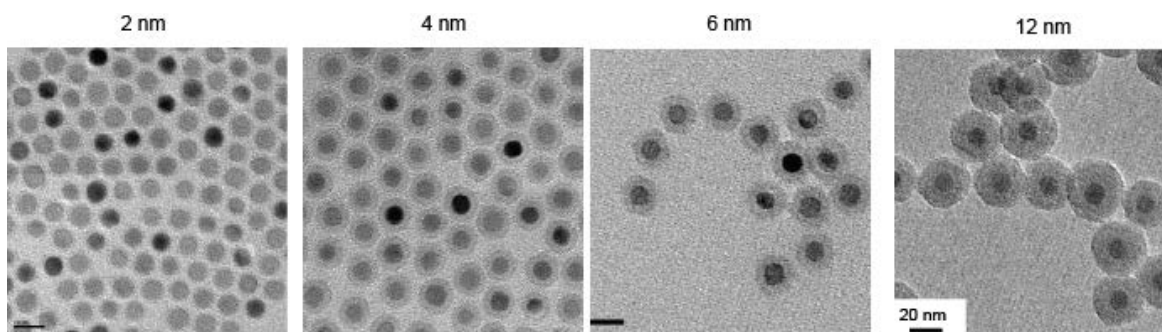
Figure 6.6: *TEM images of the nanoparticles made for this model system. The dark spots in these images are the superparamagnetic nanoparticle core and the lighter areas around the spots are the silica layer. These nanoparticles are made from a $Zn_{0.4}Fe_{2.6}O_4$ core with a layer of silica on the exterior. The core of these nanoparticles has a diameter of 12 nm. Reproduced with permission from Choi et al[3].*

The relaxation time of the electron is the smallest time constant involved in the relaxation of water, so changes in it are responsible for the differences in the sensors. These sensors were studied using a solid state EPR instrument in order to measure how the T_1 of the electron changed as the silica got thicker. The T_1 times of the gadolinium electrons were longer in samples with thinner silica layers, as seen in figure 6.5. While this indicated that changing the layer affected the relaxation of the electrons, it was difficult to extrapolate this to the solution state. So, the water relaxivity of the sensor was measured in solution at 3, 9.4 and 15.2 T. This data was then used to find the electronic relaxation time, as well as the water exchange time.
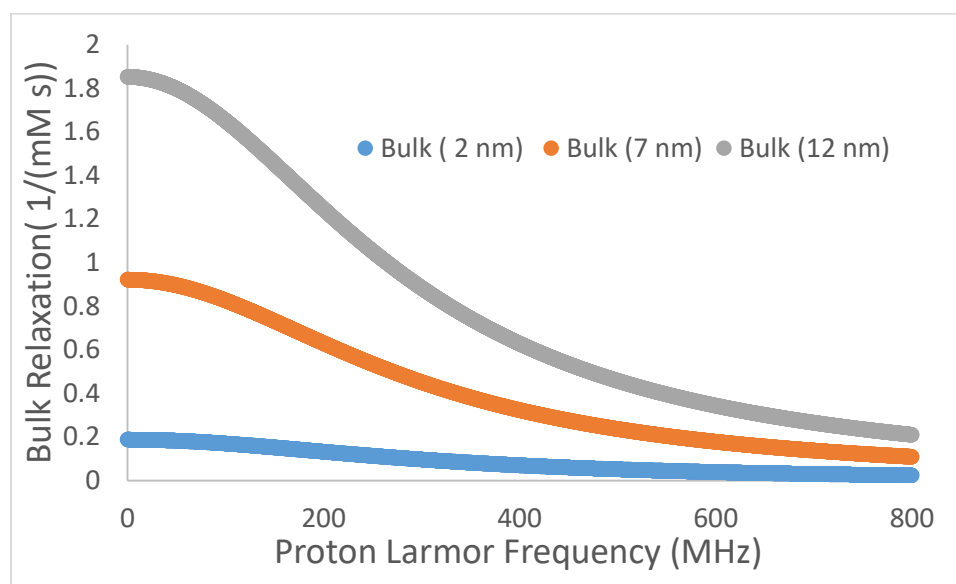
Figure 6.7: *There are several features to consider in the dispersion of these sensors, shown in these calculated curves. The first is that the 2 nm sample has the weakest response to changes in the external magnetic field. This is surprising because that sample has the longest electronic relaxation time, meaning that its bound relaxation rate has the steepest response to the magnetic field. However, the 2 nm sample also has the longest exchange time. Its rapid relaxation of water is quenched because the water takes too long to rejoin the bulk. The 12 nm sample, which has the shortest electronic T_1, has the steepest field response because it also has the shortest exchange time. If the exchange time of all samples were*

drastically shortened, then the bulk relaxation dispersion would resemble the bound relaxation dispersion.

A change in the relaxation of the electrons alone was not sufficient to explain the changes in relaxation observed. Fitting the multi-field data set with the assumption that a change in the electronic T_1 was responsible would not yield an adequate fit, regardless of the parameters chosen. What this means is that the spectral density of the interaction between the water and the unpaired electrons on the gadolinium (III) is not the only thing that changes when the silica layer changes. Adding another fit parameter, the exchange time, greatly improves the quality of the fit. The exchange time also increase as the silica layer gets thinner. Getting closer to the nanoparticle core quenches relaxation in two ways: by making the spectral density function narrower and by reducing the rate of exchange between the bound and free water. The expected relaxation dispersion of these sensors calculated from the fit parameters is shown in figure 6.7.

6.4 Sensor Varieties

With these model systems studied, it is now possible to design new sensors based on a change in distance between the enhancer and quencher. Several methods for changing the distance were tested by the IBS institute. The distance between the enhancer and quencher was changed by cleaving, binding and folding the linker between them. Results from tests conducted with sensors based on these methods agree well with the results from the silica model system. These sensors were then taken further with invitro and invivo experiments conducted with a sensor responsive to MMP2.

Two types of cleaving sensors were studied by the IBS institute. These sensors were similar to the model sensors studied before. A gadolinium (III) ion chelated to a DOTA was covalently attached to the surface of a superparamagnetic nanoparticle. Unlike before, there is no silica layer on the nanoparticle. Also, the molecule linking the DOTA and the nanoparticle was chosen to be easily cleaved and made short enough for the nanoparticle to quench the relaxivity of the gadolinium (III). Two linkers fitting this description were studied, a sulfonate linker that cleaves with peroxide and a peptide linker that cleaves with MMP, an enzyme[15,16]. These sensors were poor relaxation agents unless the linker was cleaved. Once freed from the quencher, the enhancer could efficiently relax water. Both sensors yielded similar results once their linkers were cleaved; the relaxation rate increased by 1.3 per second. Similar results were found when the other types of sensors were studied and are summarized in figure 6.8.

Sensors that work by binding were also studied. These sensors were similar to the ones used in the cleavage experiments; an enhancer and quencher pair were synthesized with the aim of bringing them together to reduce the proton relaxivity of the enhancer. Unlike before, the enhancer begins unbound to the quencher. This makes the T_1 of the solution without the target very short. Once the target is introduced into the sample, the quencher and the enhancer bind together and the T_1 rises. The linkers were split into two parts that joined together in the presence of a catalyst. One linker pair had an azide on the nanoparticle and the alkyne on the DOTA that would join together in the presence of copper (I)[17]. The other linker pairs were two

DNA segments that sandwich together in the presence of a third DNA segment, bringing the DOTA close enough to the nanoparticle to be quenched[18]. The results were the opposite of the cleavage experiments, as expected. Once the target was present, the relaxation rate decreased by about 1.3 per seconds. These changes fit the ones found in the cleaving experiments extremely well. With both cleaving and binding shown to work, our collaborators then studied linkers that change shape when they find their targets.

Sensors that depended on conformational changes in the linker between the quencher and enhancer were also studied. These sensors were especially interesting because the sensor response is reversible. Once the conditions responsible for the conformational change are removed, the sensor response changes back to what it was before. This implies that these types of sensors could be used to monitor changes over time in a sample because the sensor is not spent once it finds its target. The linkers used in this experiment were oligonucleotide linkers that folded in response to changes in solution[19]. One linker folded in acidic solutions and unfolded in basic solutions. The other folded when mercury (II) was in solution and then unfolded when the ions were removed with EDTA[20]. When the linker folded, the enhancer was quenched. The change in the T_1 of the solution was less drastic than the change found in the binding and cleaving experiments. The folding and unfolding changed the R_1 of the solution by about 1 per second, very close to the other experiments but a bit less. Nevertheless, these sensors, regardless of their linkers show tremendous promise. To prove how that these sensors can be used, the IBS institute conducted several invitro and invivo experiments.
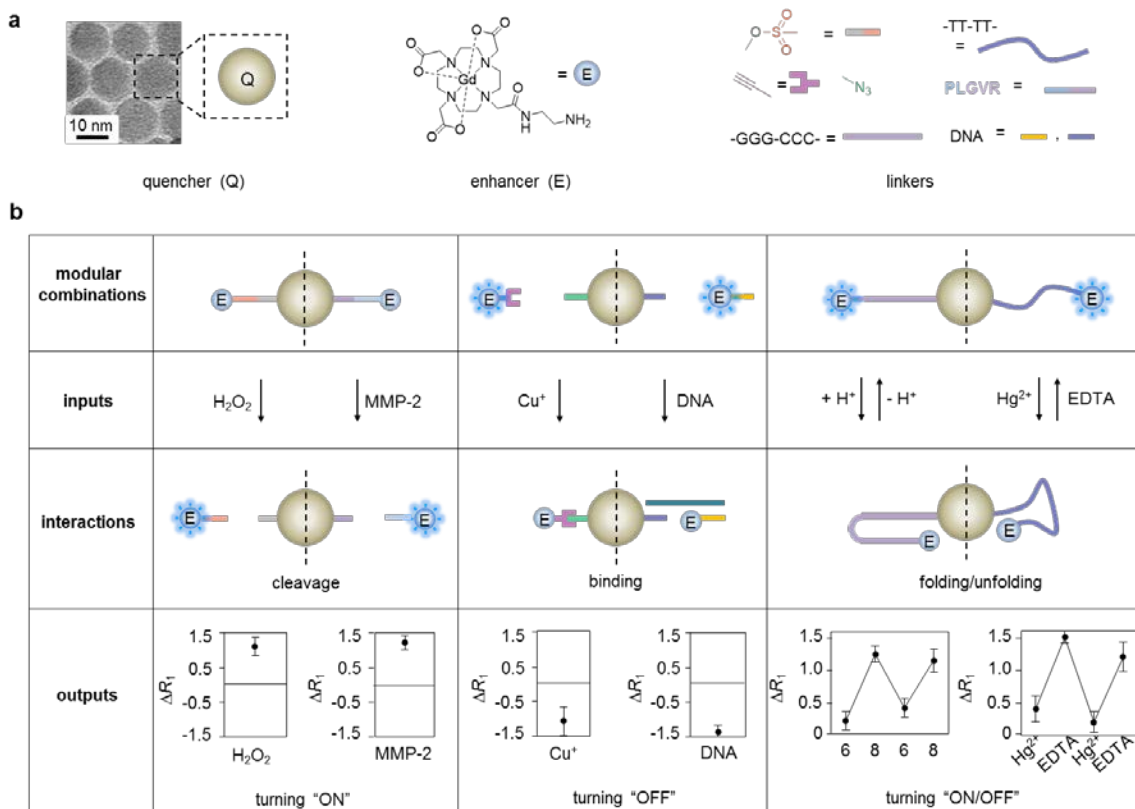
Figure 6.8: *Many varieties of sensors were tested. Sensors that responded to their targets by cleaving, binding, and folding were studied and all were shown to work. In section (a), the quencher and enhancer used in these experiments is shown, as well as the responsive linkers. The quencher used is a 12 nm diameter nanoparticle without a silica layer, as shown in the TEM image. The enhancer is a gadolinium (III) ion chelated to a DOTA, which is attached to the various active molecules used in this experiment with an amine group. Six linkers were used, two for each type of response. In (b), the responses of the sensors made from these three components are shown. These sensors behave much like the silica models mentioned before. Reproduced with permission from Choi et al[3].*

6.5 In vitro and In vivo experiments

The linker used in these practical experiment was a peptide chain sensitive to MMP2. Once the quencher enhancer pair was exposed to MMP2, the peptide connecting the two would cleave and the T_1 of the solution would decrease. Several experiments were conducted to determine if this sensor could be used to detect MMP2. First, the selectivity of the peptide linker was tested. The sensor was exposed to a few different enzymes besides MMP2. Adding the other enzymes to the solution did not affect the T_1 of the water. Only the MMP2 was able to cleave the peptide linking the enhancer and the quencher, suggesting that this sensor selectively responds to MMP2. The next test was to see if the sensor's response changed as a function of the concentration of MMP2. Several solutions containing a fixed amount of the sensor and differing amounts of the protein were made and their T_1 times measured. The R_1 of the solution increased roughly linearly with respect to the concentration of the protease. With both the

selectivity and concentration dependence proven, the next step was to conduct these experiments in biological environments.

There is no guarantee that a relaxation based biosensor that works in solution will work in a sample containing cells or inside a mouse. In such biological environments, there are many mechanisms contributing to the relaxation of water, making the T_1 of water in those samples shorter than the T_1 of neat water. It can therefore be difficult to notice a biosensor if its contribution is too small compared to the rapid background relaxation of water. Luckily, the change in T_1 induced by cleaving the peptide linker was drastic enough to be noticed despite the background relaxation. In the case of experiments done in cells, several different cell lines were studied. These different cell lines all expressed MMP2 in different concentrations[21]. The greater the concentration of MMP2 they expressed, the greater the change in T_1 when compared to a solution containing media and no cells. An independent assay of the MMP2 concentration in each cell culture was conducted to confirm their concentrations. Interestingly, the greatest change in R_1 in the cell experiments was only a little bit less than the greatest change in R_1 in the experiments conducted in solution. In the cell experiments, the greatest change was 1 per second, only 0.3 per second less than the greatest change in solution. After confirming that this sensor works in solutions containing cells, an invivo experiment done on mice was performed.

The experiments done on mice were done by xenografting a tumor onto the animal. The presence of the tumor with the sensor injected inside resulted in a brighter signal when compared to the surrounding tissue. This indicates that the T_1 inside the tumor is shorter. To confirm that this change was due to the presence of MMP2 inside the tumor, an MMP2 inhibitor was injected inside the tumor[22]. Once the inhibitor was introduced, the tumor becomes indistinguishable from the rest of the tissue, suggesting that the MMP2 was responsible for the change in relaxation. Next, different amounts of inhibitor were injected into tumors to determine if the sensor was responsive to different concentrations of MMP2. As one would expect, the less inhibitor used, the greater the T_1 contrast. Like the experiments conducted in solution, the change in R_1 is a roughly linear function of MMP2 concentration. The only obvious difference between these invivo experiments and the experiments conducted in solution is that the change in R_1 is much smaller. The greatest change in R_1 measured inside the mice was 0.27 per second, despite a very high concentration of MMP2 in the tumor. This is not too surprising because there are many other things inside the mouse tissue contributing to the relaxation of water, making it a little more difficult to notice the sensor's effects. These biological applications of this quencher enhancer biosensor are summarized in figure 6.9.
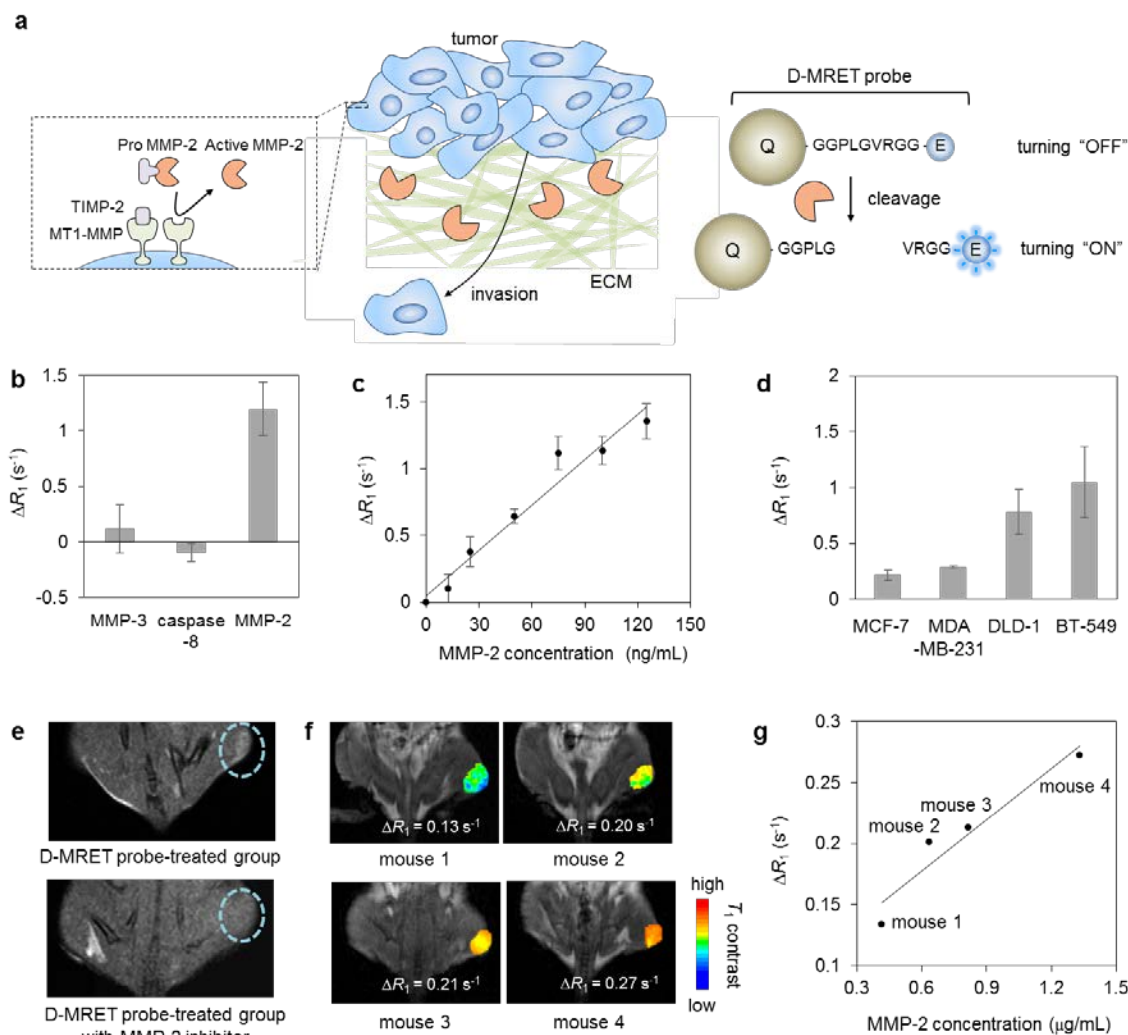
Figure 6.9: *Experiments conducted with MMP2. Part (a) of the figure shows the general idea behind this experiment. Tumors tend to release MMP2, meaning that areas around tumors will have an excess of the enzyme. So, a D-MRET biosensor with a linker that can be cleaved by MMP2 is introduced into the body. Once the sensor encounters the MMP2, the linker between the enhancer and the quencher is cleaved, drastically decreasing the T_1 of the nearby water. In part (b), the selectivity of the linker is tested by exposing it to other enzymes. Only MMP2 has a significant effect on the linker. Moving on to section (c), the biosensor's sensitivity to concentration is tested. As expected, the sensor responds more strongly to higher concentrations of the enzyme. With the sensitivity to the enzyme proven, the experiment now moves on to testing various cell lines in section (d). These cell lines are known to express differing amounts of MMP2, making them excellent test cases for this sensor. The relaxation responses seen in this cell line test match the amount of MMP2 they express, measured with an MMP2 assay kit. After proving that the sensor functions both in solution and in cell cultures, an invivo experiment was performed by xenografting a tumor onto a mouse (e). The sensor noticeably increases the T_1 contrast inside the tumor. To confirm that the sensor is responding to MMP2, an inhibitor was injected into the tumor. The inhibitor once again made the tumor invisible. A concentration study was also performed, as shown in section (f). These four images show tumors with different amounts of inhibitors added to them.*

As expected, the more inhibitor is added, the weaker the T_1 contrast. The results from this experiment are plotted in section (g). Reproduced with permission from Choi et al[3].

With the invivo experiments conducted, it is clear that these D-MRET sensors have a wide variety of applications. These nanoparticle metal ion pairs are extremely sensitive to changes in the distance between them. These changes in distance alter both the exchange rate of water bound to the ion and the relaxation rate of the unpaired electrons on the ion. These two parameters combine to give each sensor a unique response to changes in the external magnetic field. The distance between the ion and the nanoparticle can be changed in many ways. The linker between the two can be cleaved if they start attached, created if they start detached. It is even possible to make the linker bend, bringing the ion and the particle close together. Using a cleaving sensor, the IBS institute detected the enzyme MMP2 in many environments, including a tumor xenografted into a mouse. This both demonstrates that this sensor can detect relevant targets and that the contrast it produces is great enough to be detected inside a living organism. These sensors can be designed for arbitrary targets, they alter T_1 instead of T_2 and their contrast is greatest at low magnetic fields. These three properties make D-MRET sensors a very attractive choice for magnetic resonance imaging specialists looking for greater sensitivity in their analyses. Tests could potentially be done at low magnetic fields using cheap scanners, making MRI screening accessible to all.

6.6 Bibliography

1.   Tóth, É., Helm, L. & Merbach, A. E. Relaxivity of MRI Contrast Agents. *Top. Curr. Chem.* **221,** 61–101 (2002).

2.   Veiseh, O., Gunn, J. W. & Zhang, M. Design and fabrication of magnetic nanoparticles for targeted drug delivery and imaging. *Adv. Drug Deliv. Rev.* **62,** 284–304 (2010).

3.   Choi, J. *et al.* Distance-dependent magnetic resonance tuning as a versatile MRI sensing platform for biological targets. *Nat. Mater.* (2017). doi:10.1038/nmat4846

4.   Egeblad, M. & Werb, Z. New functions for the matrix metalloproteinases in cancer progression. *Nat. Rev. Cancer* **2,** 161–174 (2002).

5.   Lauffer, R. B. Paramagnetic metal complexes as water proton relaxation agents for NMR imaging: theory and design. *Chem. Rev.* **87,** 901–927 (1987).

6.   Botta, M. Second Coordination Sphere Water Molecules and Relaxivity of Gadolinium(III) Complexes: Implications for MRI Contrast Agents. *ChemInform* **31,** no-no (2010).

7.   Villa, A., Hess, B. & Saint-martin, H. Dynamics and Structure of Ln (III) - Aqua Ions : A Comparative Molecular Dynamics Study Using ab Initio Based Flexible and Polarizable Model Potentials. *J. Phys. Chem. B* 7270–7281 (2009).

8.   Micskei, K., Helm, L., Brucher, E. & Merbach, A. E. Oxygen-17 NMR study of water

exchange on gadolinium polyaminopolyacetates [Gd(DTPA)(H2O)]2- and [Gd(DOTA)(H2O)]- related to NMR imaging. *Inorg. Chem.* **32,** 3844–3850 (1993).

9.   Borel, A., Yerly, F., Helm, L. & Merbach, A. E. Multiexponential electronic spin relaxation and Redfield's limit in Gd(III) complexes in solution: Consequences for 17O/1H NMR and EPR simultaneous analysis. *J. Am. Chem. Soc.* **124,** 2042–2048 (2002).

10.   Borel, A., Helm, L. & Merbach, A. *Molecular Dynamics of Gd (III) Complexes in Aqueous Solution*. (2004).

11.   Pikkemaat, J. *et al.* Dendritic PARACEST contrast agents for magnetic resonance imaging. *Contrast Media Mol. Imaging* **2,** 229–239 (2007).

12.   Benmelouka, M., Borel, A., Moriggi, L., Helm, L. & Merbach, A. E. Design of Gd(III)-based magnetic resonance imaging contrast agents: Static and transient zero-field splitting contributions to the electronic relaxation and their impact on relaxivity. *J. Phys. Chem. B* **111,** 832–840 (2007).

13.   Alsaadi, B. B. M., Rossotti, C., Williams, R. J. P. & Road, S. P. Electronic Relaxation Rates of Lanthanide Aquo-cations. *Dalt. Transcations* 2147–2150 (1980).

14.   Kowalewski, Jozef, Maler, L. *Nuclear Spin Relaxation in Liquids: Theory, Experiments, and Applications*. (Taylor and Francis Group, 2006).

15.   Maeda, H. *et al.* Fluorescent probes for hydrogen peroxide based on a non-oxidative mechanism. *Angew. Chemie - Int. Ed.* **43,** 2389–2391 (2004).

16.   Wang, Y., Shen, P., Li, C., Wang, Y. & Liu, Z. Upconversion fluorescence resonance energy transfer based biosensor for ultrasensitive detection of matrix metalloproteinase-2 in blood. *Anal Chem* **84,** 1466–1473 (2012).

17.   Jańczewski, D., Tomczak, N., Liu, S., Han, M.-Y. & Vancso, G. J. Covalent assembly of functional inorganic nanoparticles by 'click' chemistry in water. *Chem. Commun.* **46,** 3253 (2010).

18.   Kang, T., Yoo, S. M., Yoon, I., Lee, S. Y. & Kim, B. Patterned multiplex pathogen DNA detection by Au Particle-on-wire SERS sensor. *Nano Lett.* **10,** 1189–1193 (2010).

19.   Kay, E. R., Lee, J., Nocera, D. G. & Bawendi, M. G. Conformational control of energy transfer: A mechanism for biocompatible nanocrystal-based sensors. *Angew. Chemie - Int. Ed.* **52,** 1165–1169 (2013).

20.   Lin, J.-H. & Tseng, W.-L. Design of two and three input molecular logic gates using non-Watson–Crick base pairing-based molecular beacons. *Analyst* **139,** 1436 (2014).

21.   Giambernardi, T. A. *et al.* Overview of Matrix Metattoproteinase Expression in Cuttured Human Ceils. *Matrix Biol.* **16,** 483–496 (1998).

22. Brown, S. *et al.* Potent and Selective Mechanism-Based Inhibition of Gelatinases. *J. Am. Chem. Soc.* **122,** 6799–6800 (2000).

CHAPTER 7: APPLICATION OF XENON RELAXOMETRY TO PROTEIN LIGAND INTERACTIONS

Xenon NMR has been used in a wide variety of systems thanks both to its wide chemical shift range and its tendency to occupy cage molecules. These cage molecules have been especially important in xenon NMR. By using these functionalized cages, it is possible to study molecules that have weak associations with xenon. The long-lived interactions between xenon and these cages allow one to monitor changes in chemical shift and also changes in relaxation. The experiments done with the relaxation-based sensors have shown that the short lived interactions between xenon and proteins also affect the bulk relaxation of xenon. This is in stark contrast to the effect of the protein on the xenon spectrum; due to the rapid exchange in and out of the protein, its presence only shifts the dissolved xenon peak by a few Hertz at low concentrations of protein. Large changes in the chemical shift can be observed if xenon is dissolved in highly concentrated solutions of proteins. This opens up a new possibility for xenon NMR, one that resembles the earlier experiments done with the gas. Instead of working with a functionalized sensor, the direct interactions between xenon and the target will be monitored by measuring changes in the bulk xenon relaxation.

7.1 Nonspecific Interactions between Xenon and Proteins

Interactions between xenon and proteins have been studied before[1,2,3,4,5,6]. In one early study, the effect of nine amino acids on the bulk xenon peak was studied[7]. Each of the amino acids studied shifted the bulk peak by a different amount. The change in ppm ranged from 0.009 ppm per mM of aspartic acid to 0.0039 ppm per mM of proline. None of the molecules studied yielded a separate amino acid xenon peak, which is expected given the small size of the molecules and the lack of any cage structure on them, making any interactions between the two likely short lived. A poly peptide, YPYDVPDYA, was also studied and found to change the chemical shift of bulk xenon by 0.038 ppm per mM. Building off their findings with these amino acids, Rubin *et al* began studying full proteins with xenon NMR[1].

Two proteins were examined in this early study, bovine serum albumin (BSA) and lysozyme. These two proteins were titrated in and their effect on the bulk peak was measured. BSA altered the chemical shift of the bulk peak much more than lysozyme. BSA changed the chemical shift of xenon by 3.48 ppm per mM, much more than lysozyme's 0.43 ppm per mM. In order to get some insight into this effect, these two proteins were denatured with urea. When the lysozyme was denatured, its effect on the bulk peak increased to 0.62 ppm per mM. This result may be due to an increase in the surface area of the protein after unfolding. Greater surface area would mean more contact between xenon and the amino acids of lysozyme and therefore a greater change in the bulk chemical shift. However, the same effect was not observed in the case of bovine serum albumin. Denaturing that protein decreases the change in chemical shift per mM of protein to 2.87 ppm per mM. This suggests that the effect one would expect from an increase in the surface area of the protein was overwhelmed by the loss of

another contribution to the change in the bulk xenon chemical shift. The paper suggests that the lost contribution was a weak binding between xenon and BSA. This is an important result because it shows that xenon interacts with proteins enough to change the chemical shift and that this interaction can be perturbed. This perturbation can then be detected by monitoring the xenon spectrum. A similar experiment was conducted on apomyoglobin and metmyoglobin[6].

However, proteins do not only change the frequency of the dissolved xenon peak. These proteins also affect the relaxation rate of the bulk xenon population. The effect of proteins on the relaxation of xenon was first seriously studied in an early experiment meant to test the viability of performing in vivo xenon NMR[1]. Xenon was dissolved in a wide variety of biologically relevant solutions: oxygenated blood, deoxygenated blood, plasma, etc. These solutions were found to have a strong effect on the T_1 of xenon.
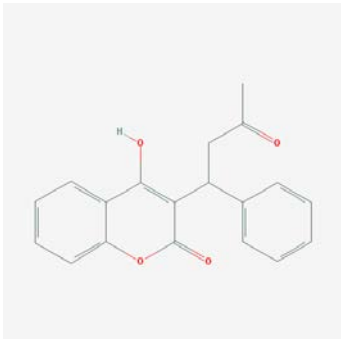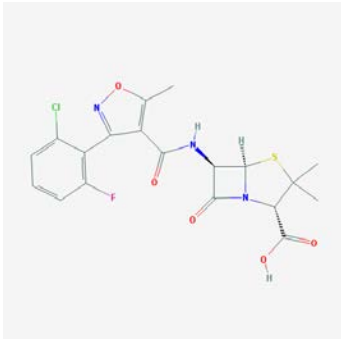
There was an early attempt by the Bifone group to discover what parts of the blood are responsible more rapidly relaxing xenon. The different components of the blood were studied under various conditions; leading to the discovery that blood serum had a strong effect on the T_1 of xenon. The interactions responsible for this change would have had to be between the xenon and the proteins in solution. To test this hypothesis, flucloxacillin, an antibiotic known to bind to blood proteins, was added to serum. Adding the antibiotic to the solution increased the T_1 of xenon, suggesting that there was some binding pocket that xenon bound to a pocket that flucloxacillin blocked. This results fits nicely with the one found in the study by *Rubin et al,* where albumin, which comprises half of the protein in the blood serum, has an unusually large effect on the bulk peak, suggesting some kind of binding.
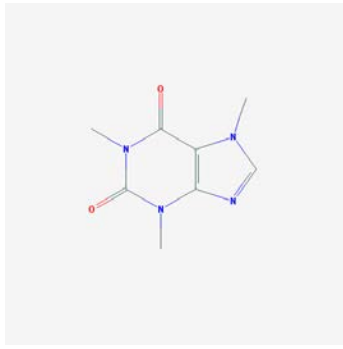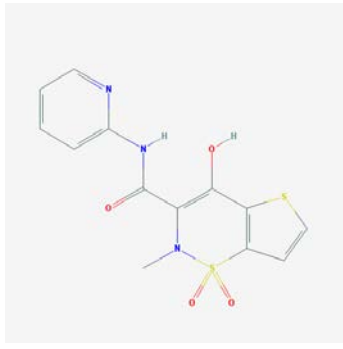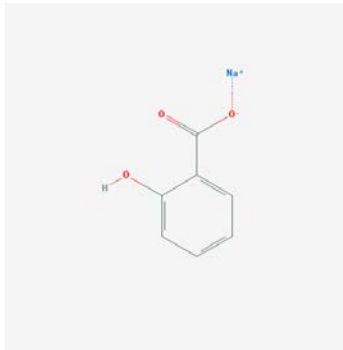
A similar effect was noticed in my work with avidin. As mentioned in previous chapters, avidin has a strong effect on the T_2 of xenon[8]. In fact, it relaxes xenon more efficiently than the biosensor used to detect it. This effect is interesting because there is no avidin-xenon peak, suggesting that the interactions between xenon and avidin are very short lived and weak. Nevertheless, these interactions are strong enough to drastically alter the T_2 of xenon, but not the T_1. The avidin had almost no effect on the T_1 of xenon at the concentration used in that study, which was 1.5 μM. This is in agreement with the results from the literature, where about 700 μM of albumin was needed to lower the T_1 of xenon to 12 seconds[1]. Neither protein has a strong effect on the T_1 of xenon, at least at high field. There was also another similarity between the avidin experiment and the albumin experiment; the interaction between xenon and avidin could be interrupted with a small molecule ligand. Adding biotin to an avidin solution, enough to completely bind the avidin, increased the T_2 of xenon. The effect on T_1 is unknown because not enough avidin was used to affect the bulk xenon T_1. This suggests that xenon enters the biotin binding pocket of avidin.

7.2 Experimental Overview of New Method

With these studies in mind, I propose a new application for hyperpolarized xenon. This new method hopes to find the binding affinity of a small molecule ligand for a protein by monitoring changes in the bulk xenon relaxation as the concentration of ligand changes. Instead of using a

sensor to functionalize xenon, its natural interactions with its environment are used. These interactions are strong enough to affect the relaxation of xenon but are either too fast or too weak yield a unique resonance. In this test case, bovine serum albumin is used as a model target. As previous studies have shown, the relaxivity of proteins can be altered by introducing certain ligands into solution. Biotin increased the T_2 of avidin solutions and flucloxacillin increased the T_1 of albumin solutions. These changes have also been shown to be dependent on the concentration of the ligand. So, with all these things in mind, several different drugs were titrated into solutions of bovine serum albumin. A structure of albumin is shown in figure 7.1. The drugs studied, their structure and their affinity for bovine serum albumin are listed in table 7.1. At each point in the titration curve, the bulk T_2 of xenon was measured, with the aim of using the change in xenon T_2 as proxy for the binding of the drug to the protein.

Drug	BSA Binding Affinity log$_{10}$(Ka)	Structure
Warfarin	6.8[9]	10
Flucloxacillin	4.6[11]	12

Caffeine	4.3[13]	
		14
Tenoxicam	5.4[15]	
		16
Sodium Salicylate	5.3[9]	
		17
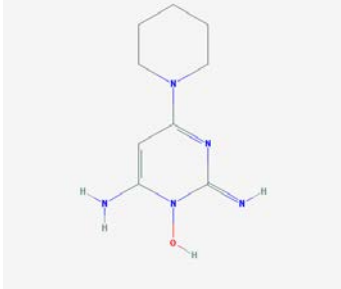
Minoxidil	0.7[18]	
		19

Table 7.1: *Structures and binding affinities of the six drugs studied in this chapter. The binding affinity of these drugs varied depending on whether bovine serum albumin or human serum albumin was used in the experiment. These affinities chosen for this table were for bovine serum albumin. For drugs with multiple binding affinities, only the highest association constant is listed in this table. All structures were taken from PubChem, the open chemistry database.*
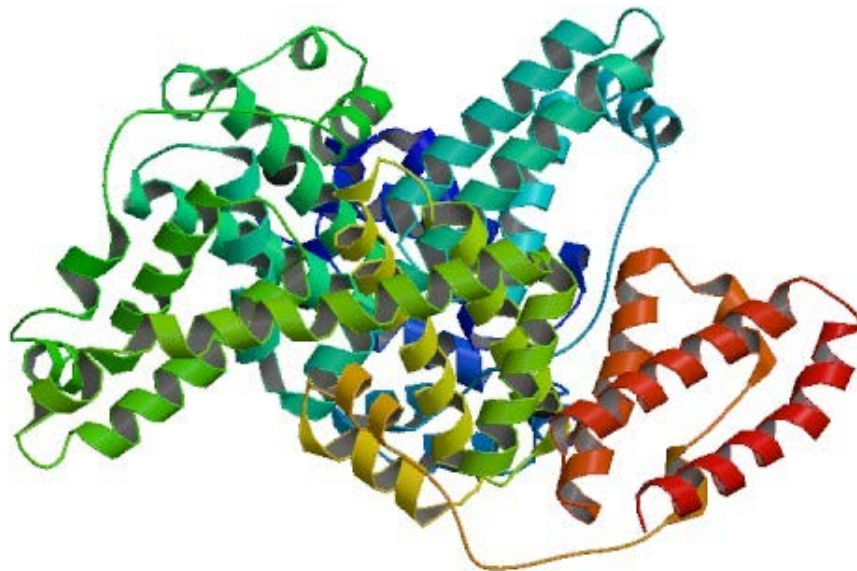
Figure 7.1: This is the structure of bovine serum albumin[20]. With a serum concentration of roughly 700 µM, albumin is the most abundant protein in the blood. It performs many functions in the body, including binding to various endogenous ligands, such as bilirubin, as well as drugs taken in by the blood stream.

These drug binding assays were chosen as a model experiment for this new xenon method because it is important to know a drug's affinity for serum albumin. When a drug is taken, some of it will be bound the albumin in the blood[21]. Depending on the affinity of a drug and its dosage, most of the drug in the serum might be taken up by the serum albumin. Binding strongly to albumin can affect the distribution of the drug in the body or even prevent the drug from binding to its target[22]. Therefore, the affinity of a drug for blood albumin must be known in order to predict alter the dosage of a drug and also to predict its pharmokinetics[23]. A way to rapidly measure the binding affinity of a drug for serum albumin would be useful to many researchers.

7.3 Brief Overview of Currently Used Methods for Probing Protein Ligand Interactions

There are currently several methods for measuring the binding affinity of drugs for serum proteins, including some using NMR[24]. Among the techniques used for this purpose, equilibrium dialysis is considered the gold standard[23]. Equilibrium dialysis is a relatively straightforward technique done with two chamber chips separated by a semipermeable membrane. A drug solution is placed in one chamber and a protein solution into the other. If the correct membrane is used, the drug from the first chamber will diffuse into the second chamber and then bind to the protein. The binding affinity of the drug for the protein can then be inferred from changes in free drug concentration. If the change in free drug concentration is simply halved after incubation, then that implies that the drug diffused through the membrane and then failed to bind to the protein. If it is less than half, then some of the drug is bound to the protein.

While this method is simple, it has some limitations. The most important one is that the sample must incubate for a long time. The membrane must have very fine openings in order to let the drug through but not the protein. This means that it can take a long time for the drug concentration to reach equilibrium. Some literature mentions incubation times lasting as long as sixteen hours[25]. There is also the problem of the membrane itself; some drugs bind to it[26]. This reduces the effective concentration of the drug, making its binding affinity for a protein seem higher. When performing equilibrium dialysis, it is therefore necessary to perform many control experiments to compensate for the effect of the membrane and also to learn how much time is needed for the concentration of drug to equilibrate. This makes this method labor intensive, a big problem for an area of research requiring that experiments be conducted under a wide variety of conditions[22].

Unlike equilibrium dialysis, xenon relaxation experiments do not require lengthy incubation. Drugs and protein are placed in the same chamber, making a membrane unnecessary. This makes the xenon experiment much faster. This increase in experiment speed is needed because many different sample conditions need to be tested to understand the affinity between a drug and a protein. The binding affinity of a drug can be affected by ionic strength, the presence of other drugs, the presence of fatty acids and the conformation of albumin [22,25,27]. This means that many experiments need to be performed in order to understand how a drug behaves in the serum. A method that allows one to perform these necessary tests quickly would therefore be welcome.

7.4 Discussion of Sample Preparation and Experimental Parameters of Protein Solutions for Xenon Experiments

While sample preparation for these xenon-based drug binding experiments can be done quickly, it is a bit more complicated than the procedure for other xenon experiments. It is necessary to spend some time discussing how to correctly prepare a protein solution for analysis with xenon NMR. Failure to properly prepare a protein solution will lead to inconsistent T_2 measurements and a clogged xenon flow system. All protein solutions discussed in this section were made with fatty acid free bovine serum albumin.

The problem is the protein's tendency to form foams in solution. Even at low concentrations, a solution of bovine serum albumin will foam after mild shaking. This foam will take several minutes to dissipate. At some concentrations, it can take hours for the foam to dissipate. These two properties make it difficult to study albumin with xenon because it is introduced into the sample by bubbling. Once xenon is bubbled into an albumin solution, a column of protein rich foam immediately forms in the NMR tube. This column is pushed through the flow system into the solenoid valve controlling the flow. This can disturb the flow control. Furthermore, this foaming can also affect the concentration of the remaining solution. If the concentration of protein in the liquid is low, then the formation of protein rich foam can alter the solution by removing a significant fraction of the protein from solution[28].

It is therefore necessary to find a way to prevent the sample from foaming. The industry standard for studying proteins in these conditions involves use of antifoaming agents. These antifoaming agents are proprietary mixtures of various surfactants that reduce the surface tension of the proteins and therefore reduce the stability of the foams. While these agents are extremely effective at stopping the foams, they also drastically shorten the T_2 of xenon. Small amounts of these agents bring the xenon T_2 below even what one would expect from the protein itself. Since the companies that produce these agents keep their components a secret, it is difficult to say why they reduce the T_2 of xenon so much. It is possible that the surfactants used in the mixture form micelles and other types of organized structures in solution. These structures, with their hydrophobic interiors, would easily bind xenon and therefore alter its relaxation properties.

It was necessary to find a surfactant that would prevent the protein solution from foaming during the bubbling while also leaving the xenon T_2 mostly unchanged. Proprietary antifoaming agents were not considered during this search because their properties would be difficult to predict due to their unknown composition. Instead, long chain alcohols were used. At first, 1-decanol was used as the antifoaming agent but it was found to be inadequate because solutions containing it do not have a stable T_2. Later on, 1-octanol and 1- hexanol were tested, with 1-octanol having the best results if used carefully.

The problem with decanol and hexanol was a lack of stability, as seen in figure 7.2 and 7.3. For example, a solution containing 1-decanol dissolved in 1 x PBS would not yield a steady xenon T_2. The T_2 of a solution would increase as new experiments were performed. At the concentrations used in the test, 5 μL of decanol per 10 mL of buffer, the T_2 of the solution would start at about 20 seconds, 40 seconds lower than the T_2 of xenon in the buffer alone. After every curve was collected, more xenon would be bubbled in and the next T_2 would be longer. The T_2 kept increasing with each experiment. The current hypothesis for this behavior is that decanol is easily separated from water due to its limited solubility. So, every time xenon is bubbled into a mixture of decanol and water, some of the decanol is forced out of the mix, increasing the xenon T_2 of the solution. Hexanol was more stable than decanol, provided the solution contained just water and the alcohol. But, a solution that also contained protein did not yield a steady T_2. The T_2 of a solution containing hexanol, albumin and buffer would steadily increase after each bubbling, as seen in figure 7.3. It may be that the hexanol was unable to prevent the formation of foam. More foam did form in the solution with hexanol compared to the ones

containing decanol and octanol. Only octanol yielded a steady T_2 in solutions both with and without protein.
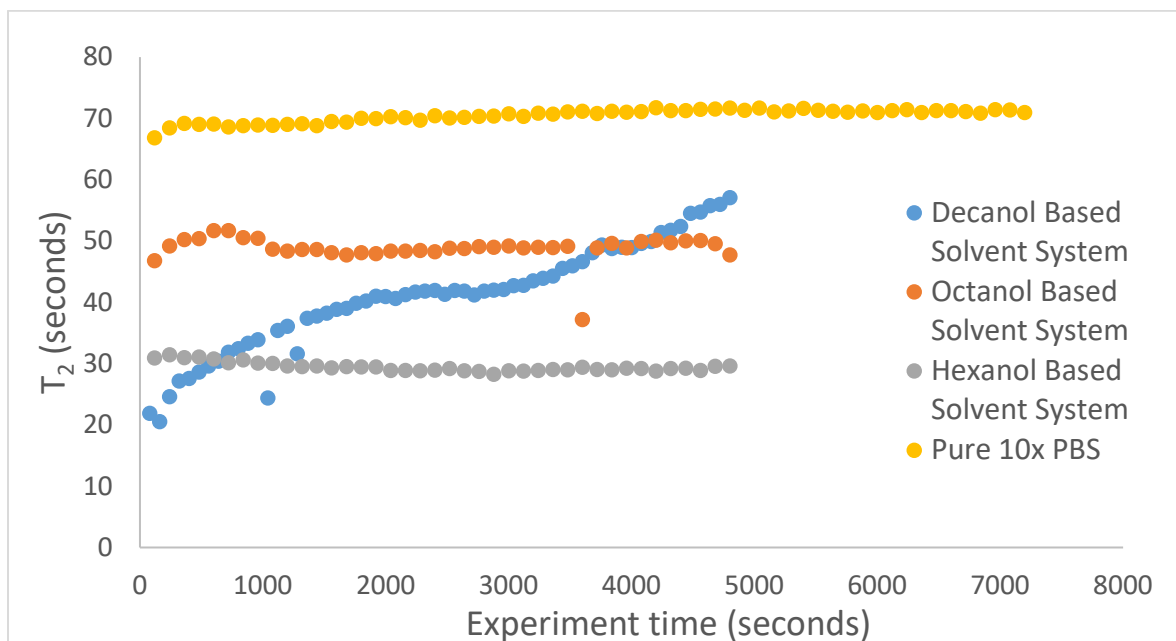
Figure 7.2: *T_2 times of the same sample over time were collected repeatedly by bubbling xenon into the same solution and then measuring the transverse decay with a CPMG. Three long chain alcohols, hexanol, octanol, and decanol were studied, as well as the solvent used to dissolve them for comparison. A solution containing decanol was clearly unstable.*
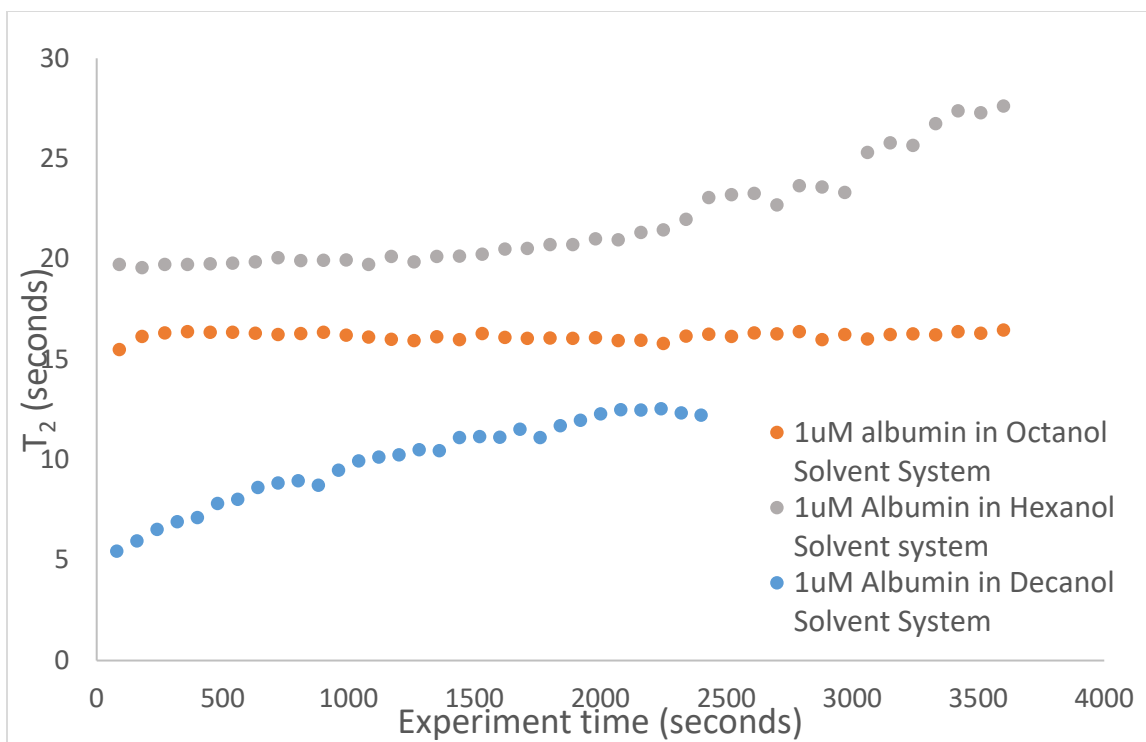
Figure 7.3: *Only the solution with octanol yielded a steady T_2 relaxation time. The rest saw a steady increase in the T_2 over time. It is important to remember that this effect can still occur with octanol if too much is used.*

Making the solutions containing octanol stable proved trickier than expected. The T_2 of the protein solution stayed constant for about an hour of repeated measurements but other solutions were not so stable. It was discovered that adding too much octanol to the solution lead to the gradual increase in T_2 as the experiment was conducted. This effect was attributed to the tendency of octanol to induce the precipitation of proteins. This introduces a tradeoff into the sample preparation procedure. The more octanol is added to a solution, the less likely it is to foam. Unfortunately, the more octanol is added to solution, the more likely it is to precipitate its protein.

A sample preparation procedure was developed and found to produce stable protein solutions. First, a needle is dipped in pure octanol. The needle is run across the mouth of the vessel containing octanol to remove any droplets. A drop of octanol can be enough to ruin the sample. Once the needle has had all drops removed from it, it is dipped into the protein solution. The solution is then shaken to see how much foam forms. If only a small layer of foam forms, a layer that quickly dissipates, then enough octanol has been added. Adding more risks precipitating the protein. There are several signs that one has added to much octanol. If the solution turns cloudy after shaking but doesn't turn clear after some time, then it is likely that too much octanol was added to the solution. A complete lack of foam after vigorous shaking is also a sign of too much octanol. But, the best way to test one's sample preparation is to collect the T_2 of xenon over many experiments. If the T_2 remains steady after thirty or so experiments, then it is safe to say that the protein is remaining in solution.

The samples in this study were prepared in the following manner. 10 mL of 10 µM albumin solutions were prepared from 100 µM stock solutions. Both the 100 µM and the 10 µM solutions were treated with octanol to prevent foaming. While the 100 µM solution was not going to be used in the xenon bubbling experiments, it was nevertheless treated so no protein was lost to the foam, keeping the concentration of the solution constant. Aliquots of highly concentrated drug solutions were added to the protein samples to bind to the avidin.

Since many drugs are only slightly soluble in water, it is recommended that one use a drug's salt if available. If a drug salt is not available, then it may be necessary to heat the drug stock solutions to increase their solubility. It is not recommended that you dilute the stock in order to dissolve the remaining solid drug because then more of the stock must be added to the original sample. This means that the protein is diluted more during the titration experiment, skewing the T_2 measurements. If even heating the solution is not enough, then one can try dissolving it in DMSO. It is generally not advisable to add other solvents to the aqueous protein solution. The problem with doing so is not that the solvent will affect the protein, although that is definitely a possibility. The problem is that these solvents can have an unpredictable effect on the T_2 of xenon. DMSO is luckily an exception, probably because it lacks a fatty tail with a polar end. Molecules like that are very likely to affect the T_2 of xenon. It is also important to make sure there are no solid drug particles in the protein solution. These solids tend to clog the flow system.

The NMR spectrometer and xenon polarizer were operated in the following manner. Hyperpolarized xenon was bubbled into the sample at a rate of about 0.2 standard liters per minute for about 20 seconds at a pressure of 60 psi. After bubbling, the sample was allowed to settle for ten or more seconds. More time than normal is needed for settling because sometimes foam will still form even with octanol added to the solution. It will quickly dissipate if given some time. A ten mm NMR tube was is preferred for this experiment because the foam tends to settle more quickly in tubes with wider diameters. It is also more difficult to force the foam up a wider tube. After settling, the T_2 of the sample is collected with a CPMG, with echo spacing set to 100 milliseconds. This time was chosen because it is short enough to remove contributions from diffusion to T_2 but long enough not to refocus chemical exchange. It is likely that part of the relaxation changes observed come from chemical exchange from sites with different chemical shifts. The timescale of this exchange is not known, so it is better to keep the echo spacing long. Five T_2 decay curves were collected for each sample. Several CPMG dispersion experiments were also performed, with no dispersion seen at the echo frequencies tested.

After the decay curves were collected, the sample was removed from the magnet and mixed with the rest of the sample. Ten mL of sample were prepared for each experiment but only about two mL were placed in the magnet. The two mL studied are mixed with the eight left behind and then an aliquot of drug solution is added to the mix. Then, the T_2 of the sample is studied again in the same way. It is very important to recalibrate the pulse width after reintroducing the sample into the magnet. Depending on the probe used and method for placing the sample inside it, it may be possible to put the sample in a place with a very different B_1 profile. For example, the pulse width needed for a 180 pulse using the ten mm probe varied

from 62 to 72 μs throughout a day. The pulse width is consistent after putting the sample inside the probe but it is not consistent when the sample is taken out and placed back in.

All experiments were performed with a Varian spectrometer and a 9.4 Tesla magnet. The xenon polarizer used was built in the lab. All experiments were performed at 25 degrees Celsius using the spectrometer's built in temperature control. All drugs and proteins were dissolved in 1x PBS, except tenoxicam, which was dissolved in DMSO.

Two sets of titration experiments were performed. The first set measured the change in bulk xenon T_2 as the concentration of the drug increased from 0 to 1 mM. Some of the drugs had a very small effect on the T_2 of xenon over this range, so another titration experiment was performed with drug concentrations ranging from 0 to 6 mM.

7.5 Results from Xenon Study of Protein Drug Interactions

Six drugs were studied with this new method. The drugs chosen were: warfarin, tenoxicam, flucloxacillin, caffeine, sodium salicylate, and minoxidil. These drugs bind with different strengths and they are also known to target different parts of albumin. In the literature, there are two drug binding pockets: site 1 and site 2. Site 1 is supposed to bind warfarin, tenoxicam and sodium salicylate and site 2 binds the other three drugs[29,11].

The effect of these drugs on the T_2 of xenon was surprising. Instead of blocking the binding site and increasing the relaxation time, like in the previous experiment[1], the T_2 dropped as more of the drugs were added. Warfarin, tenoxicam and sodium salicylate reduced the xenon T_2 of albumin, while minoxidil, flucloxacillin and caffeine had a much weaker effect on the T_2. None of the drugs consistently increased the T_2 of xenon. Unfortunately, their effect on T_1 was not measured because the protein concentrations used were too low and because the external magnetic field was too high. Experiments where proteins drastically lowered the T_1 of xenon were performed at clinical fields of 1.5 Tesla, much lower than the fields used in this experiment. Changes in T_1 are unlikely to be noticeable under such conditions.

The first thing to consider is that the drugs themselves are responsible for the drop in T_2. Many small molecules can affect the T_2 of xenon, usually by forming some kind of structure that binds the xenon. Long chain alcohols and cryptophane cages are good examples of small molecules that have a strong effect on the T_2 of xenon, as seen in figure 7.2. While the drugs used in this experiment do not resemble either of these examples, none of them have nonpolar tails with a polar end or a cage like cavity, it is still necessary to characterize the effect of these drugs on the T_2 of xenon. So, solutions containing high concentrations of the drug were prepared and then studied. At concentrations several times those used in the titration experiments, the T_2 of the solutions remained above 20 seconds. The concentrations chosen for the drug were those close to their saturation point. Results from this experiment are summarized in table 7.2.

Drug	concentration (mole per Liter)	T_2 (s)
tenoxicam	0.05	41±1
salicylate	0.0014	50±1
caffeine in buffer	0.057	25.8±0.2
flucloxacillin	0.0021	43±1
warfarin	0.00303	47±2
minoxidil	0.010	35.3±0.4

Table 7.2: *Table of the relaxation times of xenon in solutions with a high concentration of drugs. These solutions were made by dissolving the drugs in 1 x PBS, with the exception of the tenoxicam solution, which was made by mixing a tenoxicam stock solution made with DMSO with 1x PBS. There are two key results in this table. The most important result is that the drugs themselves have a weak effect on the T_2 of xenon even at high concentrations. This means that the drugs themselves are not bringing down the T_2 of xenon when they are introduced into a solution of albumin. The second important result is that DMSO does not bring down the T_2 of xenon significantly. For the tenoxicam solution, about 400 μL of DMSO was added to a 10 mL solution of 1x PBS. This only lowered the T_2 of the solution from 60 to 40 seconds. This means that, used sparingly, DMSO can be used to dissolve water insoluble drugs for this method.*

These data at least show that the decrease in T_2 is likely not due to the presence of the drug alone. This suggests that the interaction between the drug and the protein is responsible for the change in the xenon T_2. Since the T_2 of xenon doesn't increase with the addition of the drugs, this suggests that the gas can still access its binding pockets. This at least rules out competitive binding, at least at the conditions used in this experiment.

 It is possible that the drugs and xenon bind cooperatively to albumin. Such an effect has some precedence in the literature. Early work on protein binding noted that some drugs would increase the binding affinity of other drugs[30]. The various binding pockets found on albumin are coupled together, allowing for more types of interactions between drugs besides competitive binding. It could be that we are observing something similar with xenon, where the binding of one drug increases the affinity of xenon for albumin by altering the conformation of the xenon binding sites. This change in the xenon binding sites makes it more likely to accept xenon.

There are considerable differences in the behavior of the various drugs studied, as seen in figures 7.4 to 7.7. Drugs that were supposed to bind the site 1, warfarin, tenoxicam and sodium salicylate, showed more drastic changes than the other drugs. Of these three site one drugs, only the warfarin titration curve stopped changing after reaching a specific concentration. The other two site one drugs continued to affect the T_2 of xenon for the entire titration curve until reaching a concentration of 1 mM, the end of the titration. This experiment was repeated with higher concentrations of drug. In that experiment, warfarin once again plateaued quickly. Sodium salicylate showed little change during the experiment and tenoxicam continued to

decrease the xenon T_2 of the albumin solution until the end of the titration experiment. Perhaps the lack of a plateau is due to the presence of more binding sites. Flucloxacillin and minoxidil had almost no effect and caffeine had a mild effect.
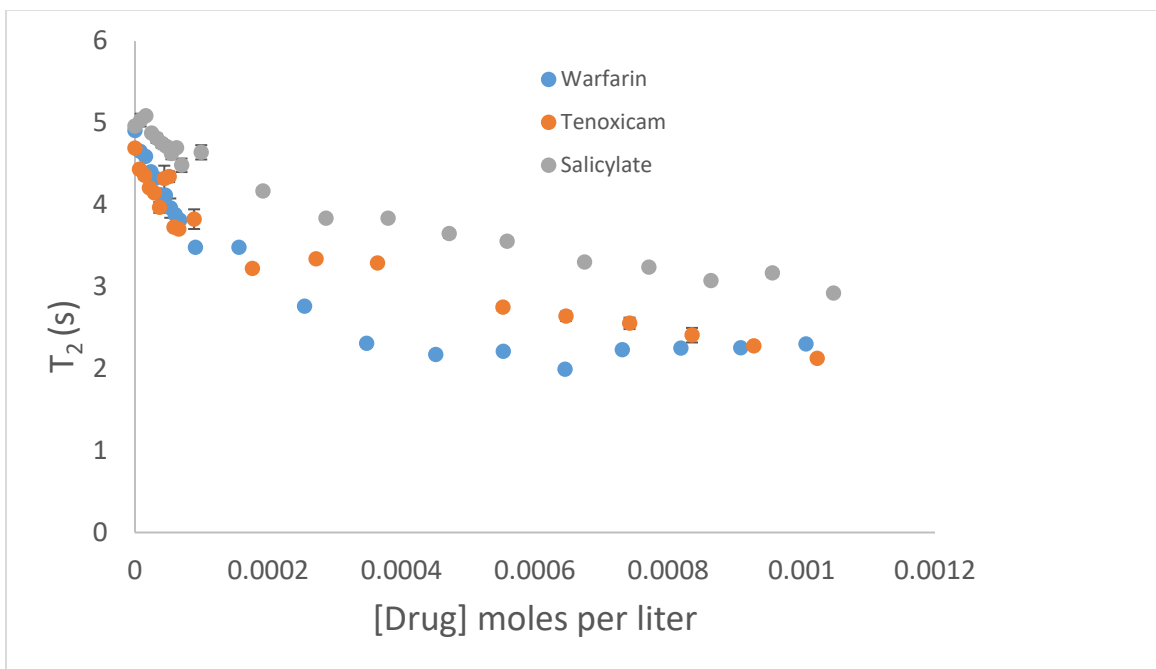
Figure 7.4: *This drug titration curve shows the change in xenon T_2 of a 10 μM solution of bovine serum albumin for three drugs. The three drugs chosen were sodium warfarin, sodium salicylate, and tenoxicam. These three drugs were chosen for this figure because they are the ones that most strongly affected the relaxation of xenon. Of the three, warfarin had the greatest effect, bringing the xenon T_2 of the albumin solution down to 2 seconds from about 5 seconds with only 300 μM of drug. However, the tenoxicam curve intersects the warfarin curve at 1 mM of drug. The warfarin curve stops decreasing after 400 μM, but the tenoxicam curve continues to drop. This continues far past 1 mM, as a later figure will show. Salicylate also had a strong effect on the T_2 of the solution, but much less than the other two. This result is similar to what one sees in the literature, which states that tenoxicam and warfarin have a strong affinity for albumin, with salicylate having a similar, but lesser, affinity.*
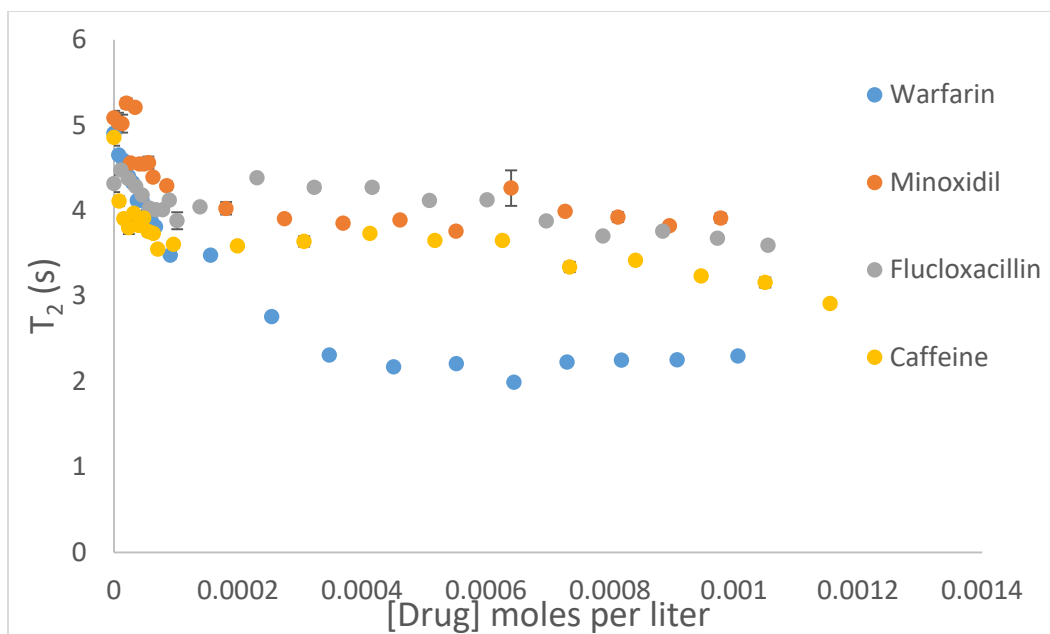
Figure 7.5: *These drug titration curves compare a strong binding drug, warfarin, to three drugs predicted to have lesser binding affinities in the literature. Drugs with weaker binding affinities show inconsistent results, and tend to quickly level off at relatively high T_2 relaxation times. It is also important to note that these three weakly binding drugs primarily bind to site 2, while the strongly binding drugs studied here bind to site 1.*

A difficulty in interpreting the data collected with this experiment is the strange non-monotonic behavior sometimes observed in the titration curve. This behavior is clearly seen in figures 7.5 and 6. This behavior is especially prevalent in drugs with lower binding affinity. This suggests that the change induced by the drug, if there is any, is less than the variation in the signal from taking the sample out of the magnet and putting it back in. While the variation in T_2 for a sample once placed inside the magnet is small, the variation of the same sample taken in and out of the sample is greater. This might explain the variation seen in the beginning of the titration curve. While the obvious solution to this would be to use drug stock solutions with very high concentrations, many drugs are not very soluble. The high concentration caffeine stock solution required heating to dissolve the sample; the minoxidil high concentration solution had to be diluted and also heated, and tenoxicam had to be dissolved in DMSO.
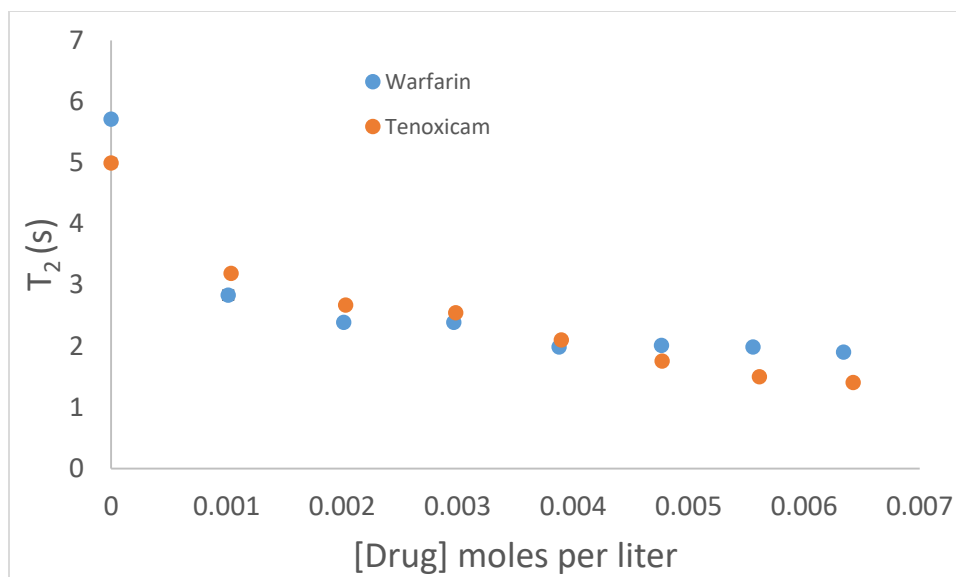
Figure 7.6: *Another drug titration curve comparing warfarin and tenoxicam. This curve goes beyond the concentrations in the previous experiment. Like before, the warfarin brings the T_2 of xenon down more rapidly but stops having much of an effect, while tenoxicam continues to lower the xenon T_2 for the entire experiment.*
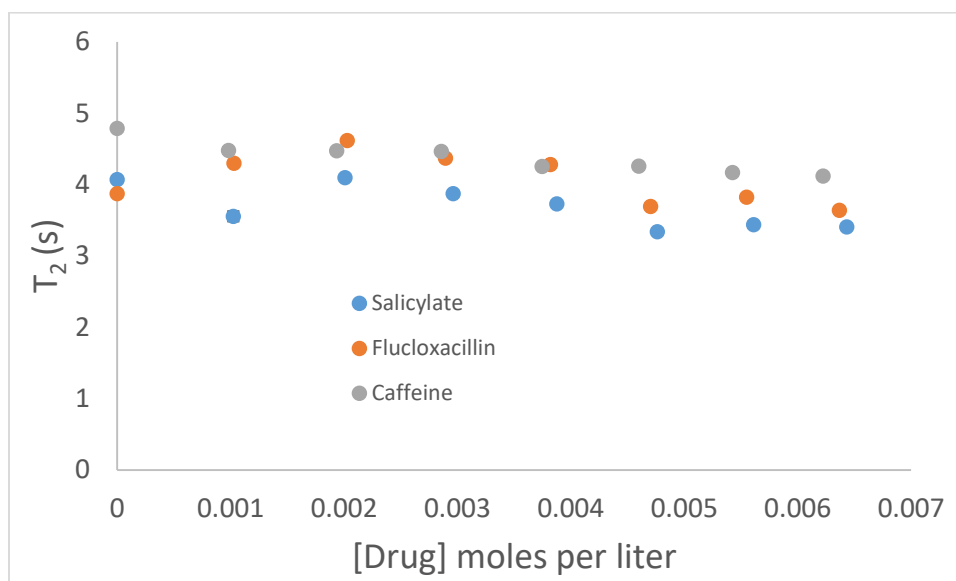
Figure 7.7: *These drug titration curves were collected using the same methods as the previous ones, with the one difference being that the concentrations used were much greater. Salicylate continues to have a small but noticeable effect by bringing the T_2 of xenon down from 4 to 3.4 seconds. This change is much less than the one measured before. Unfortunately, these high concentration experiments needed to be performed with a 5 mm probe instead of the desired 10 mm probe. This introduces considerable scatter to the dataset, making the effect of the weakly binding drugs less noticeable. The effect of using the 5 mm probe on the other drugs, sodium flucloxacillin and caffeine is even more striking. The small changes seen in previous experiments are absent entirely.*

The results from these experiments are promising. So far, the binding between drugs with strong affinities, such as tenoxicam and warfarin, has been shown to be detectable with xenon relaxometry. Drugs that bind more weakly, like flucloxacillin and caffeine, have also been shown to affect the T_2 of xenon, but not as consistently. These experiments would need to be made more reproducible to measure the effects of drugs that weakly interact with albumin. If developed further, this method could become a useful tool for probing the interactions between a wide variety of ligands and proteins.

7.6 Further Development of Xenon Studies of Protein Ligand Interactions

While this new method shows some promise there are still several questions that need to be answered. It is necessary to discover why the drugs lower the T_2 of xenon. It is strange that the effect of the drugs on T_2 is different from flucloxacillin's effect on T_1. If a drug blocks access to a binding pocket, one would expect that the pocket's contribution to T_2 would decease too. It is difficult to state what is responsible for the change in T_2 with the current data. It is possible that the allosteric coupling between binding sites is responsible for this change in the T_2 of xenon[26,30]. Previous experiments have shown that drugs binding to different pockets can affect the affinity of drugs that bind elsewhere. There is even some discussion of binding sites being created by the interactions between albumin and a drug. Discovering what is actually happening would require more experiments.

The first step to finding the mechanism for this change is to discover what contributions to T_2 change when the protein binds to a drug. There are several variables that contribute to T_2 and almost all of them could be changed by a drug binding to albumin. The most obvious one is the exchange rate. The exchange rate affects the bulk T_2 of xenon in two ways: by affecting how much the quickly relaxing bound xenon exchanges with the bulk and by affecting the chemical exchange contribution to T_2. If the exchange between the xenon associated with the protein and the free xenon were altered by the drug binding, then one could expect a change in the bulk xenon T_2.

Either an increase or a decrease in the exchange time could explain a drop in T_2. A slower exchange time can increase the chemical exchange contribution to R_2 because $R_{2\ exchange}$ increases linearly with exchange time in the fast exchanging regime. However, if the main contribution to the observed change in the bulk R_2 is the rapidly relaxing pool of xenon associated with the protein, then faster exchange could lead to faster relaxation because the quickly relaxing pool would mix more quickly with the slowly relaxing pool. This assumes that the relaxation rate of the xenon associated with the protein is fast relative to the exchange time.

There are several experiments that could be done to measure a possible change in exchange time. The first and easiest experiment to perform would be a CPMG dispersion. A change in the exchange time would alter how T_2 responds to a change in the echo spacing. Unfortunately, this requires unusually rapid echo trains. Xenon is almost certainly exchanging very rapidly from the various pockets on the protein. If the exchange were slow, then there would be a protein pocket resonance. Instead, the different resonances are averaged into a single solvent peak.

One can also consider the case of water. Like xenon, water molecules will frequently bind to pockets in proteins, including albumin. Unlike xenon, water's interactions with albumin and other proteins are well studied. In those experiments, it has been shown that the exchange time between bulk water and the water buried inside the protein can range from nanoseconds to microseconds[31,32]. If xenon exchanges at a similar timescale, then there should not be a CPMG dispersion within the echo frequencies accessible to this lab. The difficult of performing a CPMG dispersion on a sample undergoing exchange on the microsecond time scale can be seen in figure 7.8, which shows how little T_2 responds to a change in the echo frequency until that frequency approaches the exchange rate.
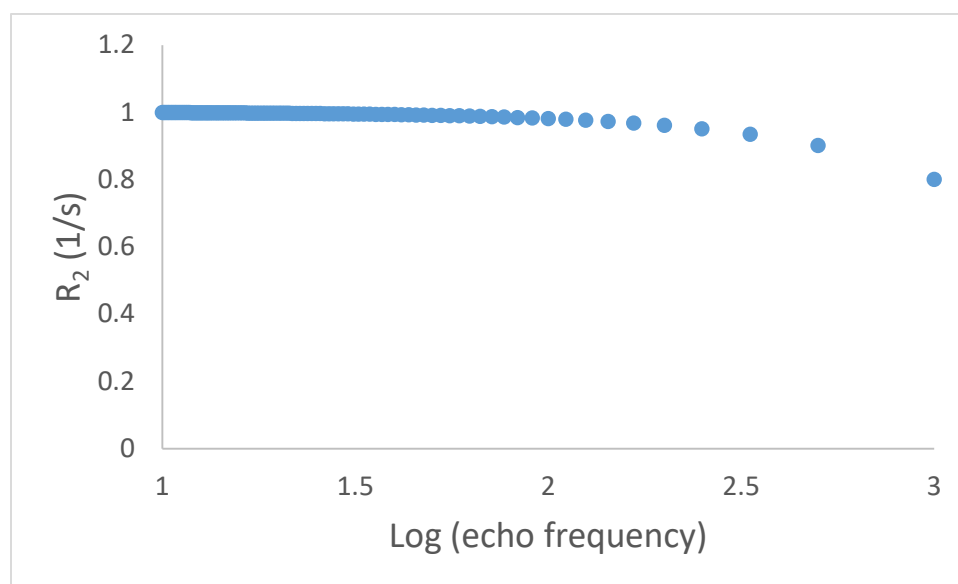
Figure 7.8: *This figure shows how the exchange contribution to R_2 scales with the frequency of 180 degree refocusing pulses assuming an exchange rate of 10000 Hz. R_2 begins to plateau at echo frequencies below 10^2. Unfortunately, echo frequencies greater than 10^2 are difficult to reliably achieve with this lab's equipment.*

A relaxation dispersion curve would be more useful for discovering what is happening to the xenon when it interacts with albumin. It is possible to extract an exchange time from a T_1 relaxation dispersion curve by fitting the data collected to a simple model. A brief explanation of the fitting procedure can be found in the MRET chapter. One could collect a dispersion curve from a solution containing unbound albumin and then one with drug saturated albumin and then compare the exchange times extracted from the fit. This procedure would also reveal any changes to the overall rotational correlation time of the xenon associated with the protein. While the drugs are too small to affect the overall rotational dynamics of albumin, they still might be able to affect the dynamics of xenon by changing the pockets it occupies. The effect on the pockets could also be inferred from a series of relaxation dispersion experiments. It would also be helpful to collect T_2 dispersion curves. By performing a fit on the T_1 data, and then using the results as constants in a T_2 fit, one should be able to extract changes in chemical shift as well. With all this data, the spin physics of this drug binding experiment would be well

known, making the experiment more quantitative. Knowing these parameters would also make it possible to design an experiment that increases the contrast upon binding, allowing one to study drugs with weaker binding affinities.

7.7 Bibliography

1.   Wolber, J., Cherubini, a, Dzik-Jurasz, a S., Leach, M. O. & Bifone, a. Spin-lattice relaxation of laser-polarized xenon in human blood. *Proc. Natl. Acad. Sci. U. S. A.* **96,** 3664–3669 (1999).

2.   Wołoszyn, Ł., Ilczyszyn, M. & Ilczyszyn, M. M. Experimental evidence on interaction between xenon and bovine serum albumin. *Spectrochim. Acta - Part A Mol. Biomol. Spectrosc.* **125,** 449–452 (2014).

3.   Ewing, G. J. & Maestas, S. The thermodynamics of absorption of xenon by myoglobin. *J. Phys. Chem.* **74,** 2341–2344 (1970).

4.   Tilton, R. F. & Kuntz, I. D. Nuclear Magnetic-resonance Studies of Xe-129 With Myoglobin and Hemoglobin. *Biochemistry* **21,** 6850–6857 (1982).

5.   Rubin, S. M., Lee, S. Y., Ruiz, E. J., Pines, A. & Wemmer, D. E. Detection and characterization of xenon-binding sites in proteins by 129Xe NMR spectroscopy. *J. Mol. Biol.* **322,** 425–440 (2002).

6.   Rubin, S. M., Spence, M. M., Goodson, B. M., Wemmer, D. E. & Pines, A. Evidence of nonspecific surface interactions between laser-polarized xenon and myoglobin in solution. *Proc. Natl. Acad. Sci. U. S. A.* **97,** 9472–9475 (2000).

7.   Rubin, S. M., Spence, M. M., Pines, a & Wemmer, D. E. Characterization of the effects of nonspecific xenon-protein interactions on (129)Xe chemical shifts in aqueous solution: further development of xenon as a biomolecular probe. *J. Magn. Reson.* **152,** 79–86 (2001).

8.   Gomes, M. D. *et al.* 129Xe NMR Relaxation-Based Macromolecular Sensing. *J. Am. Chem. Soc.* **138,** 9747–9750 (2016).

9.   Meyer, M. & Guttman, D. Dynamic dialysis as a method for studying protein binding II: Evaluation of the method with a number of binding systems. *J. Pharm. Sci.* **59,** 39–48 (1970).

10.   National Center for Biotechnology Information. Warfarin. *PubChem Compound Database* doi:54678486

11.   Seedher, N. & Agarwal, P. Interaction of some isoxazolyl penicillins with human serum albumin. *J. Biol. Sci.* **6,** 167–172 (2006).

12.   National Center for Biotechnology Information. Flucloxacillin. *PubChem Compound Database* doi:21319

13.   Zhang, H. M., Chen, T. T., Zhou, Q. H. & Wang, Y. Q. Binding of caffeine, theophylline, and theobromine with human serum albumin: A spectroscopic study. *J. Mol. Struct.* **938,** 221–228 (2009).

14.   National Center for Biotechnology Information. Caffeine. *PubChem Compound Database* doi:2519

15.   Punith, R., Katrahalli, U., Kalanur, S. S. & Jaldappagari, S. Mechanistic and conformational studies on the interaction of anti-inflammatory drugs, isoxicam and tenoxicam with bovine serum albumin. *J. Lumin.* **130,** 2052–2058 (2010).

16.   National Center for Biotechnology Information. Tenoxicam. *PubChem Compound Database* doi:54677971

17.   National Center for Biotechnology Information. Sodium Salicylate. *PubChem Compound Database* doi:16760658

18.   Nidhi, K., Indrajeet, S., Khushboo, M., Gauri, K. & Sen, D. J. Estimating unbound volume of distribution and tissue binding by in vitro HPLC-based human serum albumin and immobilised artificial membrane-binding measurements. *Int. J. Drug Dev. Res.* **3,** 26–33 (2011).

19.   National Center for Biotechnology Information. Minoxidil. *PubChem Compound Database* doi:4201

20.   Majorek, K. A. *et al.* Structural and immunologic characterization of bovine, horse, and rabbit serum albumins. *Mol. Immunol.* **52,** 174–182 (2012).

21.   Vallner, J. J. Binding of drugs by albumin and plasma protein. *J. Pharm. Sci.* **66,** 447–465 (1977).

22.   Zeitlinger, M. a. *et al.* Protein binding: Do we ever learn? *Antimicrob. Agents Chemother.* **55,** 3067–3074 (2011).

23.   Zhivkova, Z. D. Studies on Drug – Human Serum Albumin Binding : The Current State of the Matter. *Curr. Pharm. Des.* **21,** 1817–1830 (2015).

24.   Oida, T. Proton Nuclear Magnetic Resonance Study on the Multimode Interactions of Human Serum Albumin with Drug Molecules. *J. Biochem.* **100,** 99–113 (1986).

25.   Wilting, J., Giesen, W. van der, Janssen, L. H. M., Weideman, M. M. & Otagiri, M. The Effect of Albumin Conformation on the Binding of Warfarin to Human Serum Albumin. *J. Biol. Chem.* **255,** 3032–3037 (1980).

26.   Honoré, B. & Brodersen, R. Albumin Binding of Anti-Inflammatory Drugs. *Mol. Pharmacol.* **25,** 137–150 (1984).

27.   Ahmad, B., Parveen, S. & Khan, R. H. Effect of albumin conformation on the binding of

ciprofloxacin to human serum albumin: A novel approach directly assigning binding site. *Biomacromolecules* **7,** 1350–1356 (2006).

28. Schnepf, R. W. & Gaden, E. L. Foam fractionation of proteins: Concentration of aqueous solutions of bovine serum albumin. *J. Biochem. Microbiol. Technol. Eng.* **1,** 1–11 (1959).

29. Kragh-Hansen, U., Chuang, V. T. G. & Otagiri, M. Practical aspects of the ligand-binding and enzymatic properties of human serum albumin. *Biol. Pharm. Bull.* **25,** 695–704 (2002).

30. Sjoholm, Ingvar Ekman, Bo Ljungstedt-Pahlman, Ingrid Seiving, Birgitta, Sjodin, T. Binding of Drugs to Human Serum Albumin: XI. *Mol. Pharmacol.* **16,** 767–777 (1979).

31. Persson, E. & Halle, B. Nanosecond to microsecond protein dynamics probed by magnetic relaxation_Supporting Information. *J. Am. Chem. Soc.* **130,** 1774–1787 (2008).

32. Mattos, C. Protein-water interactions in a dynamic world. *Trends Biochem. Sci.* **27,** 203–208 (2002).

CHAPTER 8: CONCLUSION

With the end of the chapter on xenon based analyses of protein ligand interactions, my dissertation is now over. I have explained my work on xenon relaxometry and how it can be applied. I have also discussed similar proton based methods, which have already been applied. While much work has already been completed, there is still much more to do. Making this method ready for general applications require that the mechanisms of relaxation become better understood and also that it be brought to lower fields, where it would be of greater use. With these two changes, xenon relaxometry can become an established and useful method.

While much time has been spent trying to understand the relaxation of xenon in this dissertation, many mysteries remain, which make it difficult to understand some of the results. The changes in the dynamics of xenon when it encounters a target molecule, either directly or indirectly with a sensor, are not well characterized. For example, it is known that the rotational correlation time of bound xenon changes when a functionalized cryptophane cage binds to avidin. This conclusion is reached because the cage peak is extremely broad and because the relaxation of xenon quickens once the sensor binds to avidin. Both these changes indicate a significant slowing of the xenon motions. It is also generally expected that a small molecule tethered to a protein will move more slowly than one not tethered to a protein. However, the degree of this change is not known nor is it known if other types of motion changed too. As the D-MRET chapter has shown, multiple changes in dynamics can be responsible for a change in relaxation. Getting a complete understanding of the change in the rotational correlation time and the chemical exchange time is necessary for using these xenon biosensors efficiently. Gaining a similar understanding for the dynamics of the direct interactions between xenon and various proteins would also be useful. Doing so would allow one to extract quantitative information from the titration experiments discussed in chapter 7, as well as possibly gaining some insight into the changes the drugs induced in the protein itself. Collecting the data needed for this would require taking xenon NMR to multiple fields, especially low fields.

In addition to making it possible to get a better understanding of the parameters affecting xenon relaxation, going to lower fields would also make the methods discussed in this dissertation more effective and widely applicable. I have mentioned that T_1 changes much more drastically at lower magnetic fields in this dissertation several times. In addition to changing more at lower fields, relaxation is also generally faster at those fields too. Both of these facts make low field xenon relaxometry attractive by both making it more sensitive to changes in the environment and also lowering the detection limit of a given target. Low field analyses are also attractive because of their relatively low cost. By not doing these experiments with a high field NMR spectrometer, one could potentially lower one's costs by an order of magnitude while getting better results. This is the main point of this work. The experiments discussed in this dissertation can be done at many fields, something that is true for few other xenon experiments.

If this work is continued, then going to low fields and characterizing xenon relaxation would be the best tasks to take. Doing so would allow for better designed experiments that could then be taken out of the research lab and into industry and clinics. A unique and interesting approach would be brought into the wider world.

Appendix Section 1: Data Extraction Code

Matlab was used to both process data and to simulate spin dynamics. The code used for these tasks is shown below.

Relaxation Data Processing:

The first scripts are the ones used to extract data from the Varian files. This code has been in the lab for a long time. These functions were not written by me. They are all listed in the order in which they are called, culminating in a script that loads an FID.

A 1.1 Data reading script:

_____Getnextline_____

```matlab
function line = getNextLine(fid)
line = fgetl(fid);
while(line(1) == '#')
line = fgetl(fid);
end
end
```

_____Getnextline_____

_____Fid Path_____

```matlab
% FIDPATH gets the path of Varian FID data

% Note that the filename one chooses in the path doesn't really
% matter since the Varian *.fid directory contains 4 files,
% and they are always named "fid" (FID data), "procpar" (MR
% parameters), "log" (acquisition on/off), and text (PSD name).

function fpath = fidpath(fpath, checkfid, title)

if nargin < 3
  title = 'Select Varian FID/PAR Directory';
```

```matlab
  if nargin < 2
    checkfid = false;
    if nargin < 1
      fpath = cd;
    end
  end
end

if isempty(fpath)
  fpath = cd;
end
if isempty(checkfid)
  checkfid = false;
end
if isempty(title)
  title = 'Select Varian FID/PAR Directory';
end

if fileexist(fpath, checkfid)
  return
end

% Check if the user forgot to add .fid extension
fpathnew = [fpath '.fid'];
if fileexist(fpathnew, checkfid)
  fpath = fpathnew;
  return
end

% Check if the user forgot to add .par extension
fpathnew = [fpath '.par'];
if fileexist(fpathnew, false)
  fpath = fpathnew;
```

```matlab
        return
    end


    % Get FID file path/name
    contflag = 1;
    while (contflag == 1),
        fpath = uigetdir(fpath, title);

        % Make sure "fid" and "procpar" files exist
        if isequal(fpath, 0)
            error('No directory selected.')
        elseif ~fileexist(fpath, checkfid)
            disp('GETPATH unable to locate fid and/or procpar file in selected directory. Try again.')
        else
            contflag = 0;
        end
    end

    drawnow;
    return




    % LOCAL FUNCTION
    function res = fileexist(fpath, checkfid)

    if checkfid
        if (exist([fpath '/fid'], 'file') ~= 2)
            res = 0;
            return
        end
    end
```

```matlab
if exist([fpath '/procpar'], 'file') == 2
   res = 1;
else
   res = 0;
end


return
```

_____**Fid Path**_____

_____**Getblock**_____

```matlab
function [dta,bheader]=getblock(file,np,n)

  %file: file to read block from
  %dta: returned block
  %bheader: returned fid block header information for the last block that
  %was read


bheader=struct('scale',{0},'status',{0},'index',{0},'mode',{0},'ctcount',{0},'lpval',{0},'rpval',{0},'lvl',
{0},'tlt',{0});

  %Read vnmr file
  dta=[];

  bheader.scale=fread(file,1,'short');
  bheader.status=fread(file,1,'short');
  bheader.index=fread(file,1,'short');
  bheader.mode=fread(file,1,'short');
  bheader.ctcount=fread(file,1,'long');
   bheader.lpval=fread(file,1,'float');
   bheader.rpval=fread(file,1,'float');
   bheader.lvl=fread(file,1,'float');
   bheader.tlt=fread(file,1,'float');
```

```matlab
    d=fread(file,np,'int32');


    d=transpose(reshape(d,2,size(d,1)/2));
    d=complex(d(:,1),d(:,2));
    if n>=0
      d=d-mean(d(end-n:end));
      dta=[dta,d];
    end


end
```

_____**Getblock**_____

_____**Readprocpar**_____

```matlab
function [par] = readprocpar(fpath, ext)


% READPROCPAR reads in parameter used in FID acquisition
%
%   PAR = READPROCPAR(FPATH) reads the parameters in the the
%   procpar file in the FID directory FPATH
%
% see also WRITEPROCPAR, READFID, WRITEFID



% Written by L Martyn Klassen
% Copyright 2003 Robarts Research Institute

if nargin < 1
  error('READPROCPAR requires one input argument.');
end

if nargin < 2
  ext = [];
```

```matlab
end

% Check for validity of file
fp = fopen([fpath '/procpar' ext], 'r', 'ieee-be');
if fp == -1
  fp = fopen([fpath '.fid/procpar' ext], 'r', 'ieee-be');
  if fp == -1
    fp = fopen([fpath '.par/procpar' ext], 'r', 'ieee-be');
    if fp == -1
      error(['READPROCPAR unable to open ' fpath ' for reading.']);
    else
      fpath = [fpath '.par'];
    end
  else
    fpath = [fpath '.fid'];
  end
end

% Initialize outputs
par.path    = fpath;
par.dp      = [];
par.seqfil  = [];
par.nf      = [];
par.ni      = [];
par.sw      = [];
par.ns      = [];
par.ne1     = [];
par.ne2     = [];
par.rfspoil = [];
par.rfphase = [];
par.nt      = [];
par.np      = [];
par.nv      = [];
```

```
par.nv2     = [];
par.nv3     = [];
par.ne      = [];
par.polarity = [];
par.evenecho = [];
par.tr      = [];
par.te      = [];
par.esp     = [];
par.espincr  = [];
par.nprof   = [];
par.tproj   = [];
par.phi     = [];
par.psi     = [];
par.theta   = [];
par.vpsi    = [];
par.vphi    = [];
par.vtheta  = [];
par.array{1} = [];
par.arraydim = [];
par.seqcon  = [];
par.lro     = [];
par.lpe     = [];
par.lpe2    = [];
par.pro     = [];
par.ppe     = [];
par.ppe2    = [];
par.pss     = [];
par.thk     = [];
par.thk2    = [];
par.pos1    = [];
par.pos2    = [];
par.pos3    = [];
par.vox1    = [];
```

```
par.vox2    = [];
par.vox3    = [];
par.nD      = [];
par.cntr    = [];
par.gain    = [];
par.shimset = [];
par.z1      = [];
par.z2      = [];
par.z3      = [];
par.z4      = [];
par.z5      = [];
par.z6      = [];
par.z7      = [];
par.z8      = [];
par.x1      = [];
par.y1      = [];
par.xz      = [];
par.yz      = [];
par.xy      = [];
par.x3      = [];
par.y3      = [];
par.x4      = [];
par.y4      = [];
par.z1c     = [];
par.z2c     = [];
par.z3c     = [];
par.z4c     = [];
par.xz2     = [];
par.yz2     = [];
par.xz2     = [];
par.yz2     = [];
par.zxy     = [];
par.z3x     = [];
```

```
par.z3y      = [];
par.zx3      = [];
par.zy3      = [];
par.z4x      = [];
par.z4y      = [];
par.z5x      = [];
par.z5y      = [];
par.x2y2     = [];
par.z2xy     = [];
par.z3xy     = [];
par.z2x3     = [];
par.z2y3     = [];
par.z3x3     = [];
par.z3y3     = [];
par.z4xy     = [];
par.zx2y2    = [];
par.z2x2y2   = [];
par.z3x2y2   = [];
par.z4x2y2   = [];
par.petable  = [];
par.nrcvrs   = [];
par.trise    = [];
par.at       = [];
par.gro      = [];
par.gmax     = [];
par.intlv    = [];
par.rcvrs    = [];
par.celem    = [];
par.arrayelemts = [];
par.contrast = [];
par.tep      = [];
par.date     = [];
par.ti       = [];
```

```
par.gss2     = [];
par.gss      = [];
par.tpwri    = [];
par.tpwr1    = [];
par.tpwr2    = [];
par.orient   = [];
par.tof      = [];
par.resto    = [];
par.grox     = [];
par.groy     = [];
par.fov      = [];
par.res      = [];
par.npix     = [];
par.nseg     = [];
par.nzseg    = [];
par.waveform = [];
par.SR       = [];
par.gradfrac = [];
par.sfrq     = [];
par.B0       = [];
par.dtmap    = [];
par.nnav     = [];
par.tnav     = [];
par.fast     = [];
par.bt       = [];
par.nhomo    = [];
par.fpmult   = [];
par.d1       = [];
par.ss       = [];
par.ssc      = [];
par.r1       = [];
par.r2       = [];
par.ps_coils = [];
```

```
par.coil_array = [];
par.nav        = [];
par.fliplist   = [];
par.varflip    = [];
par.nfreq      = [];
par.flip       = [];
par.flip1      = [];
par.flipprep   = [];
par.seg        = [];
par.state      = [];
par.rfdelay    = [];
par.gro        = [];
par.gimp       = [];
par.SR         = [];
par.readaxis   = [];
par.timescale  = [];
par.etl        = [];
par.grof       = [];
par.Po         = [];
par.Psl        = [];
par.console    = [];
par.shimcoils  = [];
par.spiral_gmax     = [];
par.spiral_gamma    = [];
par.spiral_delay    = [];
par.spiral_tep      = [];
par.dtg            = [];
par.nturns         = [];
par.direction      = [];
par.ninterleave    = [];
par.tn            = [];
par.randomseed      = [];
par.interleave_order = [];
```

```
par.profile        = [];
par.image          = [];
par.spiral_version  = [];
par.spiral_filter   = [];
par.spiral_alpha    = [];
par.spiral_density  = [];
par.navigator       = [];
par.tfirst          = [];
par.tpe             = [];
par.ky_order        = [];
par.alternate       = [];
par.offlineAverages = [];
par.satpwr          = [];
par.sattof          = [];
par.satfreq         = [];
par.settle          = [];
par.satdly          = [];
par.bubble          = [];
par.wait            = [];
par.exchange        = [];
par.exchange1       = [];
par.exchange2       = [];
par.rfdelay         = [];
par.gamp            = [];
par.gwidth          = [];
par.gaxis           = [];
par.pw              = [];
par.tpwr            = [];
par.p1              = [];
par.temp            = [];
par.rof1            = [];
par.rof2            = [];
par.satmod          = [];
```

```
par.samplename    = [];
par.page        = [];
par.notebook      = [];
par.satcycle     = [];
par.echo2      =[];
par.width      =[];
par.idelay      =[];
par.nscan       =[];
par.sl_n       = [];
par.tpwr_sl     =[];
par.p2      =[];
par.d2       =[];
par.p1pat       =[];
par.p2pat      =[];
par.idelay     =[];
par.g1      =[];
par.g2 =      [];
par.lg1   =[];
par.lg2 =  [];
par.tcp =[];
par.RG1 =[];
par.RG2 = [];
par.pa = [];
par.read=[];
par.pre = [];
par.sat=[];
par.tof1=[];
par.tof2=[];
par.d3=[];
par.d4=[];
% The structure par MUST use parameter names which match the
% parameter names used by VNMR or it will not read correctly
```

```matlab
% This function extracts the first letter of each field name
% in order to quickly discard any line which does not being
% with one of the parameters of interest.
names = fieldnames(par);
value = char(zeros(1,size(names,1)));
m     = 1;
value(m) = names{1}(1);
for n = 2:size(names,1)
   if isempty(strfind(value, names{n}(1)))
     m = m + 1;
     value(m) = names{n}(1);
   end
end
value = value(1:m);
clear n names;

buffer = fgets(fp);

% Parse the ASCII procpar file
while ( buffer ~= -1 )
  % Check to see if the first letter in the buffer matches
  % the first character of any parameter of interest
  % This provides a 3 to 4 fold speed up.
  if (strfind(value, buffer(1)))

    % Get only the first word of the buffer, the parameter name
    ind = strfind(buffer, ' ');
    lenb = ind(1)-1;
    buffer = buffer(1:lenb);

    % Read in required parameters
    if (lenb == 2)
      if any(strcmp(buffer, {'z1','z2','z3','z4','z5','z6','z7','z8', ...
```

```matlab
                'x1','y1','xz','yz','xy','x3','y3','x4','y4','nD', ...
                'nf','ni','np','ns','nv','ne','ss','nt','ti','te', ...
                'tr','sw','at','bt','d1','SR','r1','r2','B0','SR', ...
                'Po','pw','p1','p2','d2','g1','g2','pa','d3','d4'}))
            val = sscanf(fgets(fp), '%f');
            par.(buffer) = val(2:end).';
            fgets(fp);
        elseif any(strcmp(buffer, {'dp','tn'}))
            tmpbuffer = fgets(fp);
            ind = strfind(tmpbuffer, '"');
            par.(buffer) = tmpbuffer(ind(1)+1:ind(2)-1);
            fgets(fp);
        end
    elseif (lenb == 3),
        if any(strcmp(buffer, {'z1c','z2c','z3c','z4c','xz2','yz2', ...
                'zxy','z3x','z3y','zx3','zy3','z4x','z4y','z5x', ...
                'z5y','ssc','nv2','nv3','ne2','tep','esp','lro', ...
                'pro','lpe','ppe','pss','phi','psi','thk','gro', ...
                'gss','tof','fov','res','gro','etl','Psl','dtg', ...
                'tpe','ne1','lg1','lg2','RG1','RG2','tcp','pre','sat'}))
            val = sscanf(fgets(fp), '%f');
            par.(buffer) = val(2:end).';
            fgets(fp);
        elseif any(strcmp(buffer, {'nav','seg'}))
            tmpbuffer = fgets(fp);
            ind = strfind(tmpbuffer, '"');
            par.(buffer) = tmpbuffer(ind(1)+1:ind(2)-1);
            fgets(fp);
        end
    elseif (lenb == 4)
        if any(strcmp(buffer, {'x2y2','z2xy','z3xy','z2x3','z2y3', ...
                'z3x3','z3y3','z4xy','lpe2','ppe2','thk2','pos1', ...
                'pos2','pos3','thk2','vox1','vox2','vox3','vpsi', ...
```

```matlab
        'vphi','gmax','flip','gss2','sfrq','nnav','tnav', ...
        'grox','groy','nseg','npix','gain','cntr','gimp', ...
        'grof','gamp','rof1','rof2','wait','tpwr','temp','sl_n','read','tof1','tof2'}))
        val = sscanf(fgets(fp), '%f');
        par.(buffer) = val(2:end).';
        fgets(fp);
    elseif any(strcmp(buffer,{'date','fast','page'}))
        tmpbuffer = fgets(fp);
        ind = strfind(tmpbuffer, '"');
        par.(buffer) = tmpbuffer(ind(1)+1:ind(2)-1);
        fgets(fp);
    end
elseif (lenb == 5)
    if any(strcmp(buffer, {'zx2y2','celem','tproj','trise', ...
        'tpwr1','tpwr2','tpwri','theta','resto','nhomo', ...
        'nfreq','dtmap','nzseg','nproj','state','flip1', ...
        'image','gaxis','echo2','width','nscan','p1pat','p2pat','idelay'}))
        val = sscanf(fgets(fp), '%f');
        par.(buffer) = val(2:end).';
        fgets(fp);
    elseif (strcmp(buffer, 'rcvrs'))
        buffer = fgets(fp);
        % Count the number of 'y' values to find number of receivers
        ind = strfind(buffer, '"');
        buffer = buffer(ind(1)+1:ind(2)-1);
        par.rcvrs = buffer;
        par.nrcvrs = sum(double(buffer) == 121);
        fgets(fp);
    elseif (strcmp(buffer, 'intlv'))
        buffer = fgets(fp);
        ind = strfind(buffer, '"');
        par.intlv = buffer(ind(1)+1:ind(2)-1);
        fgets(fp);
```

```matlab
elseif (strcmp(buffer, 'array'))
  buffer = fgets(fp);
  % Strip the buffer down to the core data
  ind = strfind(buffer, '"');
  buffer = buffer((ind(1)+1):(ind(2)-1));

  % Parse the data string
  index1 = 1;
  index2 = 1;
  incr = 0;
  par.array{1}{1} = [];
  for o = 1:length(buffer)
    switch buffer(o)
    case '('
      incr = incr + 1;
      if incr > 1
        error('invalid coupling in array paramater.');
      end
    case ')'
      incr = incr - 1;
      if incr == 0
        index2 = 1;
      elseif incr < 0
        error('invalid coupling in array paramater.');
      end
    case ','
      if incr > 0
        index2 = index2 + 1;
      else
        index1 = index1 + 1;
      end
      par.array{index1}{index2} = [];
    otherwise
```

```matlab
                par.array{index1}{index2} = [par.array{index1}{index2} buffer(o)];
            end
        end
        fgets(fp);
    end
elseif (lenb == 6)
    if any(strcmp(buffer, {'z2x2y2','z3x2y2','z4x2y2','vtheta', ...
        'fpmult','nturns', 'tfirst','satpwr','sattof','gwidth','settle','satdly','bubble','idelay'}))
        val = sscanf(fgets(fp), '%f');
        par.(buffer) = val(2:end).';
        fgets(fp);
    elseif any(strcmp(buffer, {'seqfil','seqcon','orient','satmod'}))
        tmpbuffer = fgets(fp);
        ind = strfind(tmpbuffer, '"');
        par.(buffer) = tmpbuffer(ind(1)+1:ind(2)-1);
        fgets(fp);
    end
elseif (lenb == 7)
    if any(strcmp(buffer, {'espincr','rfphase','shimset','rfdelay','satfreq','tpwr_sl'}))
        val = sscanf(fgets(fp), '%f');
        par.(buffer) = val(2:end).';
        fgets(fp);
    elseif any(strcmp(buffer, {'rfspoil','varflip','petable', ...
        'console','profile'}))
        tmpbuffer= fgets(fp);
        ind = strfind(tmpbuffer, '"');
        par.(buffer) = tmpbuffer(ind(1)+1:ind(2)-1);
        fgets(fp);
    end
elseif (lenb == 8)
    if any(strcmp(buffer, {'evenecho','polarity','arraydim', ...
        'fliplist','gradfrac','exchange','satcycle'}))
        val = sscanf(fgets(fp), '%f');
```

```matlab
      par.(buffer) = val(2:end).';
      fgets(fp);
    elseif any(strcmp(buffer, {'waveform','contrast', ...
        'flipprep','readaxis','ky_order','notebook'}))
      tmpbuffer = fgets(fp);
      ind = strfind(tmpbuffer, '"');
      par.(buffer) = tmpbuffer(ind(1)+1:ind(2)-1);
      fgets(fp);
    elseif (strcmp(buffer, 'ps_coils'))
      tmpbuffer = fgets(fp);
      n = sscanf(tmpbuffer, '%f', 1);
      for m = 1:n
        ind = strfind(tmpbuffer, '"');
        par.(buffer){m} = tmpbuffer(ind(1)+1:ind(2)-1);
        tmpbuffer = fgets(fp);
      end
    end
  elseif (lenb == 9)
    if any(strcmp(buffer, {'direction','exchange1','exchange2'}))
      val = sscanf(fgets(fp), '%f');
      par.(buffer) = val(2:end).';
      fgets(fp);
    elseif any(strcmp(buffer, {'timescale','navigator','alternate'}))
      tmpbuffer = fgets(fp);
      ind = strfind(tmpbuffer, '"');
      par.(buffer) = tmpbuffer(ind(1)+1:ind(2)-1);
      fgets(fp);
    elseif (strcmp(buffer, 'shimcoils'))
      tmpbuffer = fgets(fp);
      n = sscanf(tmpbuffer, '%f', 1);
      for m = 1:n
        ind = strfind(tmpbuffer, '"');
        par.(buffer){m} = tmpbuffer(ind(1)+1:ind(2)-1);
```

```matlab
        tmpbuffer = fgets(fp);
      end
    end
  elseif (lenb == 10)
    if any(strcmp(buffer, {'spiral_tep','randomseed'}))
      val = sscanf(fgets(fp), '%f');
      par.(buffer) = val(2:end).';
      fgets(fp);
    elseif any(strcmp(buffer, {'samplename'}))
      tmpbuffer = fgets(fp);
      ind = strfind(tmpbuffer, '"');
      par.(buffer) = tmpbuffer(ind(1)+1:ind(2)-1);
      fgets(fp);
    elseif any(strcmp(buffer, {'coil_array'}))
      tmpbuffer = fgets(fp);
      n = sscanf(tmpbuffer, '%f', 1);
      for m = 1:n
        ind = strfind(tmpbuffer, '"');
        par.(buffer){m} = tmpbuffer(ind(1)+1:ind(2)-1);
        tmpbuffer = fgets(fp);
      end
    end
  elseif (lenb == 11)
    if any(strcmp(buffer, {'arrayelemts','spiral_gmax','ninterleave'}))
      val = sscanf(fgets(fp), '%f');
      par.(buffer) = val(2:end).';
      fgets(fp);
    end
  elseif (lenb == 12)
    if any(strcmp(buffer, {'spiral_gamma', 'spiral_delay', 'spiral_alpha'}))
      val = sscanf(fgets(fp), '%f');
      par.(buffer) = val(2:end).';
      fgets(fp);
```

```matlab
        end
    elseif (lenb == 13)
      if any(strcmp(buffer, {'spiral_filter'}))
        val = sscanf(fgets(fp), '%f');
        par.(buffer) = val(2:end).';
        fgets(fp);
      end
    elseif (lenb == 14)
      if any(strcmp(buffer, {'spiral_version','spiral_density'}))
        val = sscanf(fgets(fp), '%f');
        par.(buffer) = val(2:end).';
        fgets(fp);
      end
    elseif (lenb == 15)
      if any(strcmp(buffer, {'offlineAverages'}))
        val = sscanf(fgets(fp), '%f');
        par.(buffer) = val(2:end).';
        fgets(fp);
      end
    elseif (lenb == 16)
      if any(strcmp(buffer, {'interleave_order'}))
        tmpbuffer = fgets(fp);
        ind = strfind(tmpbuffer, '"');
        par.(buffer) = tmpbuffer(ind(1)+1:ind(2)-1);
        fgets(fp);
      end
    end
  end

  buffer = fgets(fp);
end  % End of while loop

% Close file
```

fclose(fp);

return

_____**Readprocpar**_____

_____**GetParam**_____

function [par] = getparam(fpath)

% GETPARAM reads in parameter used in FID acquisition

%

%   PAR = GETPARAM(FPATH) reads the parameters in the FID directory

%   specified by FPATH and stores them in the structure PAR.

%

% see also FIDREAD, SETPARAM

%

% History

% 2003/03/14 Written by L Martyn Klassen

%

if nargin < 1

   error('GETPARAM requires one input argument.');

end

par = readprocpar(fpath);

% Calculate the number of complex pairs as a favor since it is an often required

par.nc = par.np/2;

% Some variables are sometimes set to zero when they really should be one

```matlab
% Even VNMR does this for reasons it never fully explains. It basically treats
% zeros values as implied one values, so we just have to make that explicit so
% that downstream user don't have to be continually checking for zero values
if par.ni < 1, par.ni = 1; end;
if par.nv < 1, par.nv = 1; end;
if par.nv2 < 1, par.nv2 = 1; end;
if par.nv3 < 1, par.nv3 = 1; end;
if par.ne < 1, par.ne = 1; end;
if par.ne1 < 1, par.ne1 = par.ne; end;



% Check that the slice info is consistent. People seem to like to change
% this without ensuring they stick to VNMR specification.
if length(par.pss) ~= par.ns & par.ns ~= 1
    warning('VNMR:parameters','PROCPAR contains invalid slice information. Assuming
uncompressed slices')
    par.seqcon(2) = 's';
    par.ns = 1;
end


% It makes no sense to have par.ns > 1 without compression of slice
% assume somehow the procpar got corrupted
if par.ns > 1
    par.seqcon(2) = 'c';
end


% Calculate some sequence specific information
if length(par.seqfil) >= 5
    if strcmp(par.seqfil(1:5), 'gedse')
        par.ne1 = par.ne - par.ne2;
        timespin = par.te/2 + (-par.esp*(par.ne2-1)/2:par.esp:par.esp*(par.ne2-1)/2);
        par.time = par.te/2 + [-1*timespin(par.ne1:-1:1) timespin];
    end
```

```matlab
end

return
```

_____**GetParam**_____

_____**Readreconheader**_____

```matlab
function dims = readReconHeader(filenameBase)
    filename = strcat(filenameBase,'.hdr');
    fid = fopen(filename);

    line = getNextLine(fid);
    dims = str2num(line);

    fclose(fid);
end
```

_____**Readreconheader**_____

_____**Readcfl**_____

```matlab
function data = readcfl(filenameBase)
% function data = readcfl(filenameBase)
%
% Read in recon data stored in filenameBase.cfl (complex float)
% based on dimensions stored in filenameBase.hdr.
```

```
    dims = readReconHeader(filenameBase);


    filename = strcat(filenameBase,'.cfl');
    fid = fopen(filename);


    data_r_i = fread(fid, prod([2 dims]), 'float32');
    data_r_i = reshape(data_r_i, [2 dims]);
    data = zeros(dims);
    data(:) = data_r_i(1:2:end) + 1i*data_r_i(2:2:end);


    fclose(fid);
end
```

_____**Readcfl**_____

_____**ReadFID**_____


```
% readfid allows one to read in the Varian 4T FID data acquired with:
%
% [K, HDR, BLOCK_HDR] = READFID(FPATH, PAR, DC_CORRECT) reads k-space data
% from fid file if the FID directory FPATH. DC correction based on level
% and tilt can be can be suppressed by setting DC_CORRECT to false. If DC
% correction is applied, the level and tilt are set to zero. PAR is the
% parameters as read by getparam. The main header is returned in HDR and
% the block headers are returned in BLOCK_HDR
%
% see also WRITEFID, READPROCPAR, WRITEPROCPAR

function [k, hdr, block_hdr, par] = readfid(fpath, par, dc_correct, tfisp, ext)

if nargin < 1
```

```matlab
    error('READFID requires fid file name');
end

if nargin < 5
  ext = [];
end

% Read procpar if not already provided
if nargin < 2 || isempty(par)
  par = readprocpar(fpath, ext);
end

% Turn on DC correction by default
if nargin < 3 || isempty(dc_correct)
  dc_correct = true;
end
% Turn off tfisp by default
if nargin < 4 || isempty(tfisp)
  tfisp = false;
end

% Check for validity of fid file
if exist([fpath '/fid' ext], 'file') ~= 2
  if exist([fpath '.fid/fid'], 'file') ~= 2
    error('Unable to open FID file: %s', fpath);
  else
    fpath = [fpath '.fid'];
  end
end

infid = fopen([fpath '/fid' ext],'r', 'ieee-be');
if infid == -1
  error('Unable to open FID file: %s', fpath);
```

```matlab
end

% Read in all the information from the FID file
try
  hdr.nblocks   = fread(infid, 1, 'int32');
  hdr.ntraces   = fread(infid, 1, 'int32');
  hdr.np        = fread(infid, 1, 'int32');
  hdr.ebytes    = fread(infid, 1, 'int32');
  hdr.tbytes    = fread(infid, 1, 'int32');
  hdr.bbytes    = fread(infid, 1, 'int32');
  hdr.vers_id   = fread(infid, 1, 'int16');
  hdr.status    = fread(infid, 1, 'int16');
  hdr.nbheaders = fread(infid, 1, 'int32');

  m = hdr.bbytes/hdr.ebytes;
  n = hdr.nblocks;

  % Read in the block headers
  % Imaging data all has only one block header and VERY BAD people use
  % nbheaders as their own spare field. Therefore we ignore the nbheaders
  % and treat everything as having one block header.
  if nargout > 2
    % Create the block_hdr structure
    block_hdr.scale   = 0;
    block_hdr.status  = 0;
    block_hdr.index   = 0;
    block_hdr.mode    = 0;
    block_hdr.ctcount = 0;
    block_hdr.lpval   = 0;
    block_hdr.rpval   = 0;
    block_hdr.lvl     = 0;
    block_hdr.tlt     = 0;
    block_hdr = block_hdr(ones(n, 1));
```

```matlab
  % Read in the block header values
  for i = 1:n
    block_hdr(i).scale   = fread(infid, 1, 'short');
    block_hdr(i).status  = fread(infid, 1, 'short');
    block_hdr(i).index   = fread(infid, 1, 'short');
    block_hdr(i).mode    = fread(infid, 1, 'short');
    block_hdr(i).ctcount = fread(infid, 1, 'long');
    block_hdr(i).lpval   = fread(infid, 1, 'float');
    block_hdr(i).rpval   = fread(infid, 1, 'float');
    block_hdr(i).lvl     = fread(infid, 1, 'float');
    block_hdr(i).tlt     = fread(infid, 1, 'float');
    fseek(infid, hdr.bbytes-28*hdr.nbheaders, 'cof');
  end
end

% Get the data format from the header
if bitand(hdr.status, 8)
  % Floating
  format = 'float32';
  if hdr.ebytes ~= 4
    error('Inconsistent Format: %d-bytes and %s.', hdr.ebytes, format);
  end
else
  % Integer
  if bitand(hdr.status, 4)
    % 32-bit integer
    format = 'int32';
    if hdr.ebytes ~= 4
      error('Inconsistent Format: %d-bytes and %s.', hdr.ebytes, format);
    end
  else
    % 16-bit integer
```

```matlab
        format = 'int16';
        if hdr.ebytes ~= 2
            error('Inconsistent Format: %d-bytes and %s.', hdr.ebytes, format);
        end
    end
end

% Read in all the data
fseek(infid, 32, 'bof');
k = fread(infid, [m,n], format);

% Strip block header and reorganize into complex values
k = complex(k(28/hdr.ebytes+1:2:m,:), k(28/hdr.ebytes+2:2:m,:));

% Apply the lvl and tlt correction
if dc_correct && rem(par.nt(1),2)
    % Read in the lvl and tlt correction
    fseek(infid, 52, 'bof');
    cor = fread(infid, [2, n], '2*float32', (hdr.bbytes) - 8);

    % Set the block header values to zero after correcting
    if (nargout > 1)
        for i = 1:n
            block_hdr(i).lvl    = 0;
            block_hdr(i).tlt    = 0;
        end
    end

    % nt = 3,7,11,... have DC rotated by 90 degrees
    if rem(par.nt,4) == 3
        cor = complex(-cor(2,:), cor(1,:));
    else
        cor = complex(cor(1,:), cor(2,:));
```

```
end
if tfisp
  % tfisp switches detection direction on each phase encode
  % acquisition is always compressed phase encodes
  [m, n] = size(k);
  nro = par.np / 2;
  if par.nv == 0
    nv = 1;
  else
    nv = par.nv;
  end
  r = m / (nro * nv);
  k = reshape(k, [nro nv r n]);
  if any(cor ~= cor(1))
    cor = reshape(cor, [1 1 1 n]);
    nv_1 = ceil(nv / 2);
    nv_2 = floor(nv / 2);
    if rem(par.ssc, 2) == 0
      k(:,1:2:end,:,:) = k(:,1:2:end,:,:) + cor(ones(1,nro), ones(1,nv_1), ones(1,r),:);
      k(:,2:2:end,:,:) = k(:,2:2:end,:,:) - cor(ones(1,nro), ones(1,nv_2), ones(1,r),:);
    else
      k(:,2:2:end,:,:) = k(:,2:2:end,:,:) + cor(ones(1,nro), ones(1,nv_2), ones(1,r),:);
      k(:,1:2:end,:,:) = k(:,1:2:end,:,:) - cor(ones(1,nro), ones(1,nv_1), ones(1,r),:);
    end
    % cor = reshape(cor, [1 n]);
  else
    if rem(par.ssc, 2) == 0
      k(:,1:2:end,:) = k(:,1:2:end,:) + cor(1);
      k(:,2:2:end,:) = k(:,2:2:end,:) - cor(1);
    else
      k(:,2:2:end,:) = k(:,2:2:end,:) + cor(1);
      k(:,1:2:end,:) = k(:,1:2:end,:) - cor(1);
    end
```

```
        end
      k = reshape(k, [m n]);
    else
      if any(cor ~= cor(1))
        k = k - cor(ones(1,size(k,1)),:);
      else
        k = k - cor(1);
      end
    end
  end


catch
    fclose(infid);
    rethrow(lasterror);
end
fclose(infid);
```

_____**ReadFID**_____
_____**ReadHeader**_____

```
function [fheader]=readheader(f,n)


  %f: file pointer to read from
  %n: number of points at the end of fid to use for baseline correction
  %(-1 = no correction)
  %fheader: returned fid file header information



fheader=struct('nblocks',{0},'ntraces',{0},'np',{0},'ebytes',{0},'tbytes',{0},'bbytes',{0},'vers_id',{0},
'status',{0},'nb_headers',{0});

bheader=struct('scale',{0},'status',{0},'index',{0},'mode',{0},'ctcount',{0},'lpval',{0},'rpval',{0},'lvl',
{0},'tlt',{0});
```

```matlab
%Read vnmr file

    fheader.nblocks=fread(f,1,'long');
    fheader.ntraces=fread(f,1,'long');
    fheader.np=fread(f,1,'long');
    fheader.ebytes=fread(f,1,'long');
    fheader.tbytes=fread(f,1,'long');
    fheader.bbytes=fread(f,1,'long');
    fheader.vers_id=fread(f,1,'short');
    fheader.status=fread(f,1,'short');
    fheader.nb_headers=fread(f,1,'long');


end
```

_____ReadHeader_____

_____ReadPar_____

```matlab
function p=readpar(filename,parname)

  %reads a parameter from vnmr parameter file
  %filename= path to vnmr procpar file
  %parname= name of parameter to read
  %p= returned parameter value

  f=fopen(filename,'r','b');
  line=fgetl(f);
  while (~strncmp(line,parname,length(parname)))&&(~feof(f))
     line=fgetl(f);
  end
  line=fgetl(f);
  fclose(f);

  if line == -1
```

```
        p=1;
    else
        param = str2num(line);
        param = param(2:(size(param,2)));
        p=param';
    end


end
```

_____**ReadPar**_____

_____**FID Read**_____

```
% FIDREAD allows one to read in the Varian 4T FID data acquired with:
%
% [par, img, k, kraw] = fidread(fpath, nodc)
%
% par      - important parameters as read by GETPARAM
% img      - complex image data
% k        - k-space data
% kraw     - raw k-space data (2D matrix of one column per block)
%
% Input (optional)
% fpath    - name of FID directory to read
% nodc     - do not apply DC correction

function [par, img, k, kraw] = fidread(fpath,nodc)

% Get the FID directory to read
if nargin < 1
   fpath = fidpath;
else
   fpath = fidpath(fpath, 1);
end
```

```matlab
% Turn on DC correction by default
if nargin < 2
  nodc = false;
end


% Get MR parameters from procpar file and place in par structure
par = getparam(fpath);
[kraw, hdr] = readfid(fpath,par,~nodc);


[m,n] =size(kraw);
ntraces = hdr.ntraces;
clear hdr;


if par.ni > 1
  nimage = par.arraydim/par.ni;
  k = permute(reshape(kraw, [m/ntraces, ntraces, nimage, n/nimage]), [1 4 3 2]);
else
  k = reshape(kraw, [m/ntraces, ntraces, n]);
end


% Preform the Fourier Transform into complex image space
[m,n,o] = size(k);
img = k;
r1 = floor(m/2);
r2 = floor(n/2);
img(:,:,:) = fft2(k([r1+1:m 1:r1], [r2+1:n 1:r2],:));
r1 = ceil(m/2);
r2 = ceil(n/2);
img(:,:,:) = img([r1+1:m 1:r1], [r2+1:n 1:r2],:);
```

_____**FID Read**_____

This is the script that allows one to load an FID with parameters into matlab.

_____**FID_Extractor**_____

filename=''; %Just click the file you want

[parameters,spectrum,fid,d] = fidread(filename);

fid = squeeze(fid);

_____**FID_Extractor**_____

Appendix Section 2: Data Fitting Code

This section contains the code used to fit the data extracted by the functions shown in the previous section. Like the previous section, this section is organized such that the functions called first are listed first. This section ends with a sample script. The script one uses to process data depends on the relaxation time one is trying to measure.

_____**T1process**_____

```
function [fitresult, gof] = T1process(exchangetime, data)
[xData, yData] = prepareCurveData( exchangetime, abs(data) );
ft = fittype( 'exp1' );
opts = fitoptions( ft );
opts.Display = 'iter';
opts.maxIter = 5000;
opts.maxFunEvals = 5000000;
opts.TolX = 1e-12;
opts.TolFun = 1e-12;
opts.DiffMaxChange = 1e-6;
opts.Lower = [-Inf -Inf];
opts.StartPoint = [-0.966222858727536 -0.0149556526770078];
opts.Upper = [Inf Inf];
[fitresult, gof] = fit( xData, yData, ft, opts );
T1=(-1)/fitresult.b;
T1string = num2str(T1);
figure(2)
h = plot( fitresult, xData, yData );
legend( h, 'data',T1string , 'Location', 'NorthEast' );
xlabel( 'exchange time (s)' );
ylabel( 'normalized signal' );


end
```

_____**T1process**_____

```matlab
%This code allows one to fit T2 data collected with a CPMG.
%The pulse sequence assumed by this script contains two echo trains. This
%script takes that into account.
clear;
clc;

filename='';
[par,b,c1,d] = fidread(filename);
fid = squeeze(c1);
sl_field = par.tpwr_sl;
sl_time = (par.p2 * 10^-6 +2* (par.tcp-par.RG1))* par.sl_n;
tcp = par.at;
echo_time = (par.at+par.pa) * 2 + par.pw* 10^-6;
total_time = sl_time + echo_time;
time_array = 0:1:par.nf-1;

time_array = time_array * total_time;
mean_amp = max(fid);
amplitude = abs(mean_amp);
amplitude = squeeze(amplitude);
intRange=[0.5];
lim =par.nscan;
curves = size(par.d1,2);
for j = 1:size(intRange,2)
    for i =1:curves
        fid_test=fid(:,:,i);
        spectra = fft(fid_test);
        spectra = fftshift(spectra,1);   %FT FID file


        [C,I] = max(abs(spectra(:,1)));
```

```matlab
        sfid(:,i)=sum(spectra((I-intRange(j)):(I+intRange(j)),1:lim));    %Taking integral of peaks


        hold all
        figure(1)
        plot(time_array(1:lim),abs(sfid(:,i)));
        [coeff,goodness] = T1process(time_array(1:lim),abs(sfid(:,i)));
        T2(i,j)=-1/coeff.b;
        T2_norm(i,j) = coeff.a;
    end
end
sl_field= sl_field';
rel_pwr= par.p2*10^-6/(par.tcp*2);
Avg_T2= mean(T2);
std_dev = std(T2);
Result(:,1) =Avg_T2;
Result(:,2) = std_dev;
R2 = 1./T2;
Avg_R2 = mean(R2);
std_dev_R2 = std(R2);
Result (:,3) = Avg_R2;
Result (:,4) = std_dev_R2;
```

Appendix Section 3: Relaxation Dispersion Code

This section of the appendix contains the code used to fit the data in the D-MRET chapter.

Code: The functions are listed in the order in which they are called. This ends with the script that executes the fit.

_____**sdf**_____

```
function y = sdf (w,t)
%Standard spectral density function. This is a typical Lorentzian with a
%single correlation time and Larmor frequency.
y = 2/5 * (t/(1+(w*t)^2));
```

_____**sdf**_____
_____**PRE_T1_KRE**_____

```
function [ R1,R1_e,R2_e,tau_c1,tau_c2,amp] = PRE_T1_KRE( B,g, tau_r,r,S,tau_m,R1_e)
% This function calculates relaxation of a nucleus next to one or more
% unpaired electrons. This function does not calculate the bulk relaxation
% rate. This function assumes that the R1 of the electron is known.
% To use this function, input the variables with the following units:
% B in Tesla, g in radians per second per Tesla, r in meters, tau_m in seconds
% and R1_e in Hertz.
% Tau_r is the rotational correlation time. Tau_m is the spin's exchange
% time. r is the distance between the electrons and the nucleus. R1_e is
% the relaxation rate of the electron. S is the number of unpaired
% electrons. g is the gyromagnetic ratio of the nucleus bound to the
% electrons.
h_b = 1.054 * 10^-34;% Plank's Constant
g_e = 28024 * 10^6; %Gyromagnetic ratio of an unpaired electron
g_e = g_e * 2 * pi; %Converts the gyromagnetic ratio to rad/(s T)
amp = 10^-14*h_b^2 *g^2*g_e^2/(4*r^6); %The magnitude of the dipolar coupling is calculated here
w = g * B;  % The Larmor frequency of the nucleus
w_e = g_e * B; %The Larmor frequency of the electron
```

R2_e = R1_e*2; % This is just a rough estimate of the electronic R2.

tau_c1 = tau_r^-1 + tau_m^-1 + R1_e; %The overall correlation time is calculated here

tau_c1 = tau_c1^-1;

tau_c2 = tau_r^-1 + tau_m^-1 + R2_e;

tau_c2 = tau_c2^-1;

R1 = sdf((w_e -w),tau_c2) + 3 * sdf(w,tau_c1) + 6 * sdf((w_e+w),tau_c2); % This calculates the spectral density contribution to relaxation

R1 = R1 * amp; % The dipolar coupling is multiplied in

R1 = R1 * S*(S+1); % And lastly, the amount of unpaired electrons are considered.

End

_____PRE_T1_KRE_____

_____R1_p_KRE_____

function [R1_p , R1m,R1_e,R2_e] = R1_p_KRE(B,g, tau_r,r,S,Pm,tm,R1_e)

%This function just calculates the bulk relaxation rate. The parameters are

%the same as the function that calculates the bound relaxation rate.

[R1m,R1_e,R2_e] = PRE_T1_KRE (B,g,tau_r,r,S,tm,R1_e);

T1m = 1/R1m;

R1_p = Pm/(tm + T1m);

_____R1_p_KRE_____

_____Relax_np_sd_____

function r = relax_np_sd (x,p)

%R1_p_KRE(B,g, tau_r,r,S,Pm,tm,R1_e)

%This function is used in the fitting procedure. The fitting procedure

%treats the 3 field data as the 3 outputs of this function. Notice that the

%first parameter in the three functions below changes. That is the field.

r(1) = R1_p_KRE(p(5),p(1), p(2),x(1),p(3),p(4),x(2),x(3));

r(2) = R1_p_KRE(p(6),p(1), p(2),x(1),p(3),p(4),x(2),x(3));

r(3) = R1_p_KRE(p(7),p(1), p(2),x(1),p(3),p(4),x(2),x(3));

_____Relax_np_sd_____

This is the script that calls the fitting code.

```
clear
comp_conc= 0.001; %This is the concentration of the Gd-DOTA
water = 55.55; %Molar concentration of water
q = 1; %Amount of water bound to each Gd
pm = comp_conc*q/water; %Fraction of water bound to Gd
r = 3.05*10^-10; %Distance between electron and water in Gd DOTA
tr =7* 10^-6; %Rotational Correlation time. Kept fixed. This parameter is calculated separately.
g = 42.576*10^6; %Gyromagnetic ratio of Hydrogen 1
g= g * 2  *pi;
S =7;  %Amount of unpaired electrons in Gd+3
%R1_p_KRE( B,g, tau_r,tau_v, dt,r,S,Pm,tm,R1_e)
p = [g,tr,S,pm,3,9.4,15.2]; %Parameter vector. The last three numbers are the external fields
s1=10^-10; %Step size for distance
s2=10^-6; %Step size for exchange
s3=100; %Step size for electronic relaxation rate
opt = optimoptions(@lsqcurvefit,'MaxFunEvals',1000,'TolX', 10^-9, 'TolFun',10^-9,'MaxIter',
1000,'Algorithm', 'trust-region-reflective','TypicalX', [s1,s2,s3]);
%opt is just the variables for the curve fitting software
lb = [3.05*10^-10 10^-9 1/10^-4];%Lower bound.
ub = [3.05*10^-10 10^-4 1/10^-13];%Upper bound
m=10; % This is the amount of steps taken in the initial guess matrix
R =[0.7754,0.3216,0.1597]; %7nm data
% R= [0.1596,0.0764,0.0243]; %2 nm data
% R = [1.5409,0.682,0.218]; % 12 nm data
%This loop creates a 10 x 10 matrix of initial guesses. These fitting
%programs tend to get stuck in local minima. To avoid this, initial guesses
%across most plausible values were tried. This gives us information about
%all of the probably local minima and allows us to find the global minimum
%or at least the minimum within a physically meaningful parameter space.
```

```matlab
%Also, this function does not sweep over any internuclear distances. This
%fitting code was retrofitted for this situation.
for j =1:m
    x_0(:,1) = linspace(log(lb(1)),log(ub(1)),m);
    x_0(:,2) = linspace(log(lb(2)),log(ub(2)),m);
    x_0(:,3) = linspace(log(lb(3)),log(ub(3)),m);
    x_0(:,1) = exp(x_0(:,1));
    x_0(:,2) = exp(x_0(:,2));
    x_0(:,3) = exp(x_0(:,3));
end
%This part begins the fitting procedure.
for i =1: 1
    for k = 1:size(x_0,1)
        for j= 1:size(x_0,1)
            [y(:,i,k,j),n(i,k,j)] = lsqcurvefit(@relax_np_sd,[x_0(i,1),x_0(k,2),x_0(j,3)],p,R,lb,ub,opt);
        end
    end
end
[Best,index] = min(n(:));%This finds the smallest square of the sum of residuals and its index
[I_row, I_col,I_Z] = ind2sub(size(n),index);
fit_param = y(:,I_row,I_col,I_Z);%With the index collected above, we collect the relaxation
%value with the smallest square of the sum of residuals.
R_calc = relax_np_sd(fit_param,p); %This calculates the bulk R1 given the parameters extracted
from the fit.
fit_param(3) = 1/fit_param(3);
y= squeeze(y);
%These three next lines extract all the fit parameters. This allows us to
%see how much the fit parameters change within solutions that have similar
%residuals.
r_array = y(1,:,:);
tm_array = y(2,:,:);
R1_e_array = y(3,:,:);
```

```
r_array=squeeze(r_array);
tm_array=squeeze(tm_array);
R1_e_array = squeeze(R1_e_array);

r_mean = mean(r_array(:));
tm_mean = mean(tm_array(:));
R1_mean = mean(R1_e_array(:));
R1_std = std(R1_e_array(:));
r_std =  std(r_array(:));
tm_std =std(tm_array(:));
```

%This is the residual array. This can be matched up to the variable arrays
%shown above. It's important to check this array to see if there are
%multiple initial guesses that lead to the same residuals. If there are,
%then this should be compared to the variable array to make sure that
%answers with similar residuals don't differ much. If they do differ, then
%that implies that there are several equally good answers, implying that
%one of the variables does not affect the solution.

```
n= squeeze(n);
```

Appendix Section 4: Xenon Cage Simulation Code

Matlab was used to get a better understanding of the relaxation dynamics of xenon cage systems. The functions used in these studies are listed here. This section of the appendix is divided into six sections: T_1, T_2, Paramagnetic T_1, Paramagnetic T_2, Carver Richards Equation, Spinach CPMG simulation. The functions take a model free approach to the dynamics of cage xenon[1].

_____**Cage_T1**_____

```
function [ R1] = Cage_T1( B,g, tau_r,r,tm,tl,S)
%S is the local order parameter and tl is the local correlation time
h_b = 1.054 * 10^-34;
tau_m = tm;
g_h = 267.5 * 10^6;%Proton gyromagnetic ratio


amp = 10^-14*h_b^2 *g^2*g_h^2/(4*r^6);
w = g * B;
w_h = g_h * B;
tau_c1 = tau_r^-1 + tau_m^-1;
tau_c1 = tau_c1^-1;
tau_c2 = tau_r^-1 + tau_m^-1;
tau_c2 = tau_c2^-1;
R1  = iso_sdf((w_h -w),S,tau_c2,tl) + 3 * iso_sdf(w,S,tau_c1,tl) + 6 *
iso_sdf((w_h+w),S,tau_c2,tl);
R1 = R1 * amp;
end
```

_____**Cage_T1**_____

_____R1_Cage_____

```
function [ R1_cage , R1m] = R1_cage( B,g, tau_r,r,tm,tl,S,Pm)
R1m = Cage_T1( B,g, tau_r,r,tm,tl,S);
T1m = 1/R1m;
R1_cage = Pm/(tm + T1m);
R1_cage = 1/200 + R1_cage;
```

_____R1_Cage_____

_____Cage_T2_____

```
function [ R2] = Cage_T2( B,g, tau_r,r,tm,tl,S)
%S is the local order parameter and tl is the local correlation time
h_b = 1.054 * 10^-34;
tau_m = tm;
g_h = 267.5 * 10^6;%Proton gyromagnetic ratio

amp = 10^-14*h_b^2 *g^2*g_h^2/(4*r^6);
w = g * B;
w_h = g_h * B;
tau_c1 = tau_r^-1 + tau_m^-1;
tau_c1 = tau_c1^-1;
tau_c2 = tau_r^-1 + tau_m^-1;
tau_c2 = tau_c2^-1;
R1  = iso_sdf((w_h -w),S,tau_c2,tl) + 3 * iso_sdf(w,S,tau_c1,tl) + 6 *
iso_sdf((w_h+w),S,tau_c2,tl);
R2 = R1 + 4 *iso_sdf(0,S,tau_c2,tl) + +6 * iso_sdf(w_h,S,tau_c2,tl);
R2 = R2 * amp/2;
end
```

_____Cage_T2_____

_____R2_cage_____

```
function [ R2_cage, R2m,R2_ex] = R2_cage( B,g, tau_r,r,tm,tl,S,ds,Pm)
R2m = Cage_T2( B,g, tau_r,r,tm,tl,S);
T2m = 1/R2m;
dw = B * g *ds/(10^6)*Pm;
% R2_cage = T2m^-2 + (T2m*tm)^-1 + dw^2;
% R2_cage = R2_cage /( (T2m^-1 + tm^-1)^2 +dw^2);
% R2_cage = R2_cage * (Pm/tm);
% R2_cage = R2_cage + 1/50;
R2_cage = Pm/(tm + T2m);
R2_cage = 1/50 + R2_cage+dw^2*Pm*(1-Pm)*tm;
R2_ex = dw^2*Pm*(1-Pm)*tm;
```

_____R2_cage_____

```matlab
function [ R1,R1_e,R2_e] = PRE_T1( B,g, tau_r,tau_v, dt,r,S,tm)
%Input dt in wavenumbers, B in tesla, tau_r in seconds and tau_v in
%seconds.
dt = dt^-1;
dt = dt/100;
dt = 3*10^8/dt;
dt = dt * 2 * pi;
h_b = 1.054 * 10^-34;
tau_m = tm;
g_e = 28024 * 10^6;
g_e = g_e * 2 * pi;
amp = 10^-14*h_b^2 *g^2*g_e^2/(4*r^6);
w = g * B;
w_e = g_e * B;
R1_e = (dt^2)/5 * sdf(w_e,tau_v) + 4* sdf(2*w_e, tau_v);
T1_e = R1_e^-1;
R2_e =  R1_e + (dt^2)/5 * 3*tau_v;
R2_e = R2_e/2;
T2_e = R2_e ^-1;
tau_c1 = tau_r^-1 + tau_m^-1 + T1_e^-1;
tau_c1 = tau_c1^-1;
tau_c2 = tau_r^-1 + tau_m^-1 + T2_e^-1;
tau_c2 = tau_c2^-1;
R1  = sdf((w_e -w),tau_c2) + 3 * sdf(w,tau_c1) + 6 * sdf((w_e+w),tau_c2);
R1 = R1 * amp;
R1 = R1 * S*(S+1);
end
```

_____**R1_P**_____

```
function [ R1_p , R1m,R1_e,R2_e] = R1_p( B,g, tau_r,tau_v, dt,r,S,Pm,tm)
[R1m,R1_e,R2_e] = PRE_T1 (B,g,tau_r,tau_v,dt,r,S,tm);
T1m = 1/R1m;
R1_p = Pm/(tm + T1m);
R1_p = R1_p;
```

_____**R1_P**_____

```matlab
function [ R2 ] = PRE_T2( B,g, tau_r,tau_v,dt,r,S,tm)
%Input dt in wavenumbers, B in tesla, tau_r in seconds and tau_v in
%seconds.
dt = dt^-1;
dt = dt/100;
dt = 3*10^8/dt;
dt = dt * 2 * pi;
h_b = 1.054 * 10^-34;
tau_m = tm;
g_e = 28024 * 10^6;
g_e = g_e * 2 * pi;
amp = 10^-14*h_b^2 *g^2*g_e^2/(4*r^6);
w = g * B;
w_e = g_e * B;
R1_e = (dt^2)/5 * sdf(w_e,tau_v) + 4* sdf(2*w_e, tau_v);
T1_e = R1_e^-1;
R2_e =  R1_e + (dt^2)/5 * 3*tau_v;
R2_e = R2_e/2;
T2_e = R2_e ^-1;
tau_c1 = tau_r^-1 + tau_m^-1 + T1_e^-1;
tau_c1 = tau_c1^-1;
tau_c2 = tau_r^-1 + tau_m^-1 + T2_e^-1;
tau_c2 = tau_c2^-1;
R1  = sdf((w_e -w),tau_c2) + 3 * sdf(w,tau_c1) + 6 * sdf((w_e+w),tau_c2);
R2 = R1 + 4 * tau_c1 + +6 * sdf(w_e,tau_c2);
R2 = R2/2;
R2 = R2 * amp;
R2 = R2 * S*(S+1);
end
```

_____**Cpmg_baldwin**_____

```
function R2 = cpmg_baldwin(kex, pb, dw, ncyc, Trel, R2g, R2e)

pa=(1-pb);
keg=kex*(1-pb);
 kge=kex*pb;
  deltaR2=R2e-R2g;
nu_cpmg=ncyc/Trel;
tcp=Trel/(4.0*ncyc);




 g1=2*dw*(deltaR2+keg-kge);
g2=(deltaR2+keg-kge)^2+4*keg*kge-dw*dw;
g3=cos(0.5*atan2(g1,g2))*(g1*g1+g2*g2)^0.25;
g4=sin(0.5*atan2(g1,g2))*(g1*g1+g2*g2)^0.25;

N=(kge+g3-kge+1i*g4);
NNc=(g3*g3+g4*g4);
 f0=(dw*dw+g3*g3)/(NNc);
f2=(dw*dw-g4*g4)/(NNc);
t2=(dw+g4)*((dw-g3*1i))/(NNc);
t1pt2=(2*dw*dw-g1*1i)/(NNc);
oGt2=((deltaR2+keg-kge-g3)+1i*(dw-g4))*t2;

Rpre=(R2g+R2e+kex)/2.0;


 E0= 2.0*tcp*g3;
E2= 2.0*tcp*g4;
E1=((g3-g4*1i))*tcp;
```

```
ex0b=(f0*cosh(E0)-f2*cos(E2));

ex0c=(f0*sinh(E0)-f2*sin(E2)*1i);

ex1c=sinh(E1);

v3=(ex0b*ex0b-1)^0.5;

y=((ex0b-v3)/(ex0b+v3))^ncyc;

v2pPdN=(( (deltaR2+kex+1i*dw) )*ex0c+(-oGt2-kge*t1pt2)*2*ex1c);

Tog=(((1+y)/2+(1-y)/(2*v3)*(v2pPdN)/N));

R2=Rpre-ncyc/(Trel)*acosh(real(ex0b))-1/Trel*log((real(Tog)));
```

_____**Cpmg_baldwin**_____

This function allows one to simulate a CPMG using the spinach spin dynamics software package. The default package did not allow one to simulate T_2 relaxation using default functions. So, I coded the function below.

_____**CPMG_cage_spinach**_____

```
function R2 = CPMG_cage_spinach(kex,pb,dis,dv,B,B1,tcp,echo_number,tr)

%This function calculates the R2 of xenon exchanging into and out of a cage.

%The cage is dv ppm away from the solvent.


%The following units must be used

% kex = exchange rate in per s. It is equal to k1 + k2

%pb = fraction of bound cage (not bound xenon!)

%dis = estimated xenon proton distance in cage in angstroms.

% B = the strength of the external field in Tesla

%B1 = the strength of the echo pulse in T

% tcp = the length of time between echoes in seconds

% echo_number = the amount of echoes.

% tr = the rotational correlation time in seconds.


sys.isotopes={'129Xe','129Xe','1H','1H'};

inter.zeeman.scalar={0, dv,0,0};

k1 =kex*(pb);

k2 = kex*(1-pb);
```

```matlab
inter.coordinates={[0.0 0.0 0.0]; [0.0 0.0 0]; [0.0 0.0 10]; [0.0 0.0 dis];};
inter.chem.parts={[1,3],[2,4]};
inter.chem.rates=[-k1 k2;
                  k1 -k2];


% Magnet field
sys.magnet=B;
sys.tols.prox_cutoff=inf;
% Basis set
bas.formalism='sphten-liouv';
bas.approximation='none';


% Relaxation theory parameters
inter.relaxation='redfield';
inter.rlx_keep='kite';
inter.temperature=298;
inter.tau_c=tr;


% Spinach housekeeping
spin_system=create(sys,inter);
spin_system=basis(spin_system,bas);


% Build the relaxation superoperator
R=relaxation(spin_system);
H = hamiltonian(assume(spin_system,'nmr'));
Lp=operator(spin_system,'L+','129Xe');
Lx=(Lp+Lp')/2; Ly=(Lp-Lp')/2*1i;
Lz = operator(spin_system,'Lz','129Xe');
gamma = 11.777 * 10^6;
K = kinetics(spin_system);


Pa =100;
```

```
Pb = 1;


rho1=Pa*(state(spin_system,{'L+'},{1})+state(spin_system,{'L-'},{1}))/2;
rho2=Pb*(state(spin_system,{'L+'},{2})+state(spin_system,{'L-'},{2}))/2;



rho  = rho1 + rho2;
rhoin=evolution(spin_system,1i*K,[],rho,100,1000,'final');
%       rhoin = state(spin_system,'Lz','129Xe');
rho = rhoin;




coilx = (state(spin_system,'L+','129Xe')+state(spin_system,'L-','129Xe'))/2;
coily =  (state(spin_system,'L+','129Xe')-state(spin_system,'L-','129Xe'))/2*1i;
coilz = state(spin_system,'Lz','129Xe');
coilm = state(spin_system,'L-','129Xe');
coilm = coilm/norm(coilm);


pulse_duration=pi/(gamma*B1*2*pi);
ss=0.0001;
sn = tcp/ss;
sn = round(sn);
ss_echo = 0.0000001;
sn_echo=pulse_duration/ss_echo;
```

```matlab
sn_echo=round(sn_echo);
L  = H +1i*K + 1i*R;
L_echo =   H + 1i*K+1i*R+B1*gamma*2*pi*1*Ly;

for i = 1:echo_number
    rho1(:,i)=evolution(spin_system,L,[coilx],rho(:,i),ss,sn,'final');
    rho2(:,i)=evolution(spin_system,L_echo,[coilx],rho1(:,i),ss_echo,sn_echo,'final');
    rho(:,(i+1))=evolution(spin_system,L,[coilx],rho2(:,i),ss,sn,'final');
end
%     ss=0.001;
%     sn=1000;
%     rho_ev1=evolution(spin_system,L,[coilm],rho,ss,sn,'final');
%     rho_ev2=evolution(spin_system,L_echo,[coilm],rho_ev1,ss_echo,sn_echo,'final');
%     rho_ev3=evolution(spin_system,L,[coilm],rho_ev2,ss,sn,'multichannel');
%     plot(real(rho_ev3));

time = 0:1:echo_number;
time = time * tcp;
time = time';
mag = abs(rho);
mag = sum(mag,1);
mag = full(mag);
mag = mag';
plot (time,mag);

fit2=coeffvalues(fit(time,mag,'exp1'));
R2 = -1*fit2(2);
end
```

_____CPMG_cage_spinach_____

1.   Lipari, G. & Szabo, A. Model-free approach to the interpretation of nuclear magnetic resonance relaxation in macromolecules. 1. Theory and range of validity. *J. Am. Chem. Soc.* **104,** 4546–4559 (1982).

Appendix Section 5: Xenon Polarizer Simulation Code

A xenon polarizer was simulated using the following code. This code was written to predict how changing various parameters affected the polarization of xenon. Like the previous section, the functions are listed in the order in which they are called. The theory for this code is described in the xenon chapter.

_____OP_Rate_Find_____

```
function
[OP_Rate,Rb_Absorption_line,Rb_OP_Rate,photon_flux]=OP_Rate_Find(P,MaxPwr,PBC,LW,v0,
beam_r,Temp,frac_N,frac_Xe)

%This function calculates the rate of optical pumping, along with some

%other useful plots for comparisons. This simulation assumes that the Rb is

%in a high pressure cell, with a pressure high enough that its D1

%absorption cross section can be modeled as a Lorentzian instead of a

%Voigt function. This simulation also assumes that the laser profile is a

%Gaussian

%Reference: Developments in Alkali-Metal Atomic Magnetometry by Scott

%Seltzer


c = (3 .* 10.^8); %Speed of Light in meters per second

He_PS = 3.26 * 10^9; %Pressure shift for Helium Hz per amagat

N2_PS = -8.256 * 10^9; %Pressure shift for N2 Hz per amagat

Rb_Abs = 795 * 10^-9; %Rubidium center absorption in vacuum

lm= 780:0.001:800; %Creates wavelength interval. It is unnecessary to sample wavelenghts
beyond the 700 to 800 nm range

lm = lm .*10^-9;

AN = 6.02*10^23; % atoms per mole

r = 0.08216; %atm L per mole Kelvin

v = c./lm;

lamda = v0;

lamda = lamda .* (10^-9);

PBC = PBC .* 10^9; %PBC is entered in GHz/amagalm. This converts it to Hz/Amagalm

max_pwr = 5.916.*10.^-9; %From laser specs
```

v0 = c/lamda; %Converts center wavelength to Hertz

h = (6.626.*10.^-34); %Plank's Constant in Joule seconds

num_to_amg = 2.687 * 10^19;

n = P.*AN./(r.*Temp.*1000*num_to_amg); % Uses pressure and temperature to calculate number density (atoms per cm^3).

PB = PBC.*n; %Calculates pressure broadening based on gas number density of cell and the pressure broadening constant. Typical PBCs are 17.8 GHz per amagalm

re = (2.82.*10.^-15); % radius of an electron in meters

hml = lamda + LW.*10.^-9; %This converts the wavelength based bandwidth into frequency

hmr = lamda - LW.*10.^-9;

hmlv = c ./hml;

hmrv = c./hmr;

lw = hmrv-hmlv;

sigma = lw./2.355; % This gives the standard deviation of a Gaussian given a full width half max.

w = sym('w');

power_g=(1./(2.*pi.*sigma.^2).^(0.5)).*exp(-(v-v0).^2/(2*(sigma.^2))); %Calculates area of laser profile for normalization

g_max = max(power_g);

Area = double(int((max_pwr/g_max)*(1/(2.*pi.*sigma.^2).^(0.5)).*exp(-(w-v0).^2/(2*(sigma.^2))),w,0,inf));

f = (1/3);

power_v = power_g.*(max_pwr./g_max)*(MaxPwr./Area); %Normalizes laser profile so it has a area of 150 Watts

photon_flux = power_v./(h .* v); %Converts power to photons per second

constants = (re.*f.*c.*pi/(pi.*beam_r.^2)); % These are the frequency independent parameters in the Rb optical pumping rate equation

e = c/(Rb_Abs) + He_PS * n*(1-frac_N-frac_Xe) + N2_PS * (frac_N)*n; %Calculates new center frequency based on gas composition and pressure

Rb_Absorption_line = PB.*1./((v-e).^2+(0.5.*PB).^2); %This is the D1 Rb absorption cross section

Rb_Absorption_Area = trapz(v,Rb_Absorption_line)*-1;%This gets the area of the Rb D1 cross section

Rb_Absorption_line = Rb_Absorption_line/Rb_Absorption_Area; % And this normalizes the cross section to have an area of one.

Rb_OP_Rate= photon_flux.*constants.*Rb_Absorption_line;

OP_Rate = trapz(v,Rb_OP_Rate); % And then integrated over all frequencies, giving an answer in atoms per second

_____**OP_Rate_Find**_____

_____**SD_calculator**_____

function [SD,Rb_C,Xe_C] = SD_calculator(Temp,Xe_f,N2_f,Total_P)

%This function calculates the spin destruction rate of Rb given certain

%parameters.

%Reference: Developments in Alkali-Metal Atomic Magnetometry by Scott

%Seltzer

RbCs = 1.6 * 10^-17; %This is the Rb-Rb Spin destruction Cross Section (cm^2)

HeCs = 9 * 10^-24; % This is the Rb-He spin destruction cross section (cm^2)

XeCs = 2.0 * 10^-19; % This is the Xe-Rb spin destruction cross section (cm^2)

N2Cs = 1 * 10^-22; % This is the N2-Rb spin destruction cross section (cm^2)

Rad = 2; %Radius of spherical cell in centimeters

DN2 = 0.19; % Diffusion coefficient at 1Amg and 273K (cm^2/s)

DHe = 0.50; % Diffusion coefficient at 1Amg and 273K (cm^2/s)

DXe = 0.136; % Diffusion coefficient at 1Amg and 273K (cm^2/s)

Rb_aw = 85.47; %Grams per mole

RbSECS = 1.9 * 10^-14; %This is the spin exchange cross section (cm^2)

num_to_amg = 2.687 * 10^19;%Conversion constant between number density to amagats.

AN = 6.02*10^23; % atoms per mole

Rb_mass = Rb_aw/(1000*AN); %Kilograms

Xe_aw = 131.29;

Xe_mass = Xe_aw/(1000*AN);

He_aw = 4.0026;

He_mass = He_aw/(1000*AN);

N2_mw = 14.07 *2;

N2_mass = N2_mw/(1000*AN); %All of the masses are converted to kilograms here

A = 4.312; %From Scott's Dissertation

B = 4040; %From Scott's Dissertation

Kb = 1.3806488 * 10^-23; %Joule per Kelvin

r = 0.08216; %atm L per mole Kelvin

Gas_C = Total_P.*AN./(r.*Temp.*1000); % Atoms per mL

He_f = 1-Xe_f - N2_f;

Xe_C= Gas_C *Xe_f;

He_C = Gas_C * He_f;

N2_C = Gas_C * N2_f; % The amount is calculated with the fraction of each gas

Rb_C = (1./Temp).*10.^(21.866+A-(B./Temp)); % This calculates the Rb concentration in the cell

RM_Rb_Rb =(2.*(1./Rb_mass)).^-1; %Reduced mass in kilograms

RM_Rb_Xe = ((1./Rb_mass) +(1./Xe_mass)).^-1;

RM_Rb_N2 =((1./Rb_mass) + (1./N2_mass)).^-1;

RM_Rb_He = ((1./Rb_mass) + (1./He_mass)).^-1;% The reduced masses of the Rb-Gas collisions are calculated here for the sake of the velocity calculation

Rb_vel =100.*(8.*Kb.*Temp./(pi.*RM_Rb_Rb)).^0.5; % Velocity in cm/s

Xe_vel =100.*(8.*Kb.*Temp./(pi.*RM_Rb_Xe)).^0.5;

N2_vel =100.* (8.*Kb.*Temp./(pi.*RM_Rb_N2)).^0.5;

He_vel =100.*(8.*Kb.*Temp./(pi.*RM_Rb_He)).^0.5; % Here, the average velocities of the collisons are calculated

Xe_SD = XeCs .* Xe_vel .* Xe_C; %Spin destruction rate in Hz.

He_SD = HeCs.* He_vel .* He_C;

N2_SD = N2Cs .* N2_vel .* N2_C;

Rb_SE = RbSECS .*Rb_vel .*Rb_C; %Spin exchange rate in Hz

Wall_SD = num_to_amg*(DN2 * (1/N2_C) + DHe*(1/He_C)+DXe * (1/Xe_C))*(Temp^1.5/273^1.5)*(pi/Rad)^2; %Wall relaxation equation taken from Scott's dissertation (assumes spherical cell)

Rb_SD = RbCs .* Rb_vel .* Rb_C; %The spin destruction rate is calculated with the spin destruction cross sections, the average velcocities and number concentrations.

SD = He_SD+N2_SD+Rb_SD+Xe_SD+Wall_SD+Rb_SE;

end

_____**SD_calculator**_____

_____**Rb_Pol_Find**_____

```
function [ Rb_Pol, OP,SD ] = Rb_Pol_Find(Temp,Xe_f,N2_f,Total_P,MaxPwr,PBC,LW,v0,beam_r)
%This function calculates the rubidium polarization and it also gives the
%optical pumping rate and spin destruction rate. Check out the source code
%of the functions below for more info. Note: This code assumes that the
%system is in a regime where gas collisions are the major source of Rb
%relaxation.
OP = (-1).*OP_Rate_Find(Total_P,MaxPwr,PBC,LW,v0,beam_r,Temp,N2_f,Xe_f); %The OP is
negative because the array used for integrating goes from low wavelengths to high wavelenghts
(high v to low v)
SD = SD_calculator(Temp,Xe_f,N2_f,Total_P);
Rb_Pol = OP./(SD+OP);
end
```

_____**Rb_Pol_Find**_____
_____**Xe_SE_Calc**_____

```
function [ Xe_SE_R ] = Xe_SE_Calc( Temp,Total_P,Xe_f )
%This function calculates the spin exchange rate. This function assumes
%that the xenon concentration is much greater than the rubidium
%concentration.
%Reference: Rubidium–xenon spin exchange and relaxation rates measured
%at high pressure and high magnetic field by Daniel Raftery
%Efficiency of Spin Exchange between Rubidium Spins and 129Xe Nuclei in a
%Gas by W. Happer
Xe_SE_CS = 7.3 .* 10.^-21; % The xenon rubidium spin exchange cross section (cm^2)
Rb_aw = 85.47; %Grams per mole
AN = 6.02.*10^23; % atoms per mole
Rb_mass = Rb_aw./(1000*AN); %kilograms
Xe_aw = 129; %grams per mole
Xe_mass = Xe_aw./(1000*AN); %kilograms
A = 4.312;% Constants from Scott's dissertation
B = 4040;
```

Kb = 1.3806488 .* 10^-23; %Joules per Kelvin

k = 5230; %Constant from paper by Raftery

r = 0.08216;%Atm Liter per mole Kelvin

Gas_C = Total_P.*AN./(r.*Temp*1000); %Atoms per cubic centimeter

Rb_C = (1./Temp).*10.^(21.866+A-(B./Temp)); %Atoms per cubic centimeter

RM_Rb_Xe = ((1./Rb_mass) +(1./Xe_mass)).^-1; % Reduced mass of Rb Xenon Van der Waals molecule

Xe_C= Gas_C .*Xe_f; %Fraction of xenon in atoms per milliter

mmHg_p_atm = 760; % Conversion from millimeters of mercury to atmopheres

Xe_P = Xe_f * Total_P*mmHg_p_atm;

N2_P = (1-Xe_f)* Total_P*mmHg_p_atm;

Xe_vel =100*(8.*Kb.*Temp./(pi.*RM_Rb_Xe)).^0.5; %centimeters per second

Xe_SE_Constant = Xe_SE_CS.*Xe_vel+(k./Xe_C)*(1/(1+0.275*Xe_P*N2_P)); %This includes both binary collisions and van der Waal complexes. Compensates for presence of N2.

Xe_SE_R = Xe_SE_Constant .* Rb_C; % Then the whole thing is multiplies by the Rubidium number concentration because Rb is the limiting reagent.

end

_____**Xe_SE_Calc**_____

_____**Xe_P_Find**_____

function [Xe_P] = Xe_P_Find(Xe_T1,Temp,Total_P,Xe_f,N2_f,Max_pwr,PBC,lw,v0,beam_r)

%This calculates the polarization of xenon given a variety of parameters.

%The following units are used. All pressures are in atmospheres. All

%temperatures are in Kelvin. All powers are in Watts. All line widths are

%in nanometers. All laser line centers are in nanometers. All pressure broadening

%constants are in giga hertz per amagalm and all beam radii are in millimeters. The xenon T1 is in minutes.

Xe_T1 = Xe_T1 * 60; %Given in the literature in minutes. This converts it to seconds.

beam_r = beam_r * 10^-3; %This converts the beam radius from millimeters to meters.

Xe_R1 = 1./(Xe_T1);

Xe_SE = Xe_SE_Calc(Temp,Total_P,Xe_f);

Rb_Pol = Rb_Pol_Find(Temp,Xe_f,N2_f,Total_P,Max_pwr,PBC,lw,v0,beam_r);

```
Xe_P= Xe_SE .* Rb_Pol/(Xe_SE+Xe_R1);
end
```

_____**Xe_P_Find**_____